

INTRODUCTION

Lung injury and inflammation resulting from exposure to environmental pollutants involves multiple molecular mechanisms regulated at various levels of cellular organization. Identifying the possible role of key regulatory molecules in this process will help to predict the mechanism(s) of air pollutant-induced cardiopulmonary injury in normal and predisposed conditions. Advances in molecular biology has led to the development of numerous methods to screen for expression profile of multiple genes in a single sample, such as differential display (Liang and Pardee, 1992), high density filter hybridization (Zhao et al., 1996), SAGE (Velculescu et al., 1995) and cDNA and oligonucleotide-based microarray chip hybridization (Schena et al., 1995; DeRisi et al., 1996; Wodicka et al., 1997). Gene Array technology gained considerable attention due to its potential to generate large volume of data on thousands of genes in a single hybridization experiment. Most of the currently available microarray slides and filters are for use with human samples and only a few commercial filters are available for animal toxicological studies. Cost associated with commercial microarrays and data handling of thousands of genes which may not be critical to one's interest, pose limitations on their use.

Based on our understanding of the cell signaling processes during inflammatory reactions and tissue repair/proliferation, it is conceivable that expression of hundreds of genes is altered. Most mechanistic studies, evaluate roles of the very few genes involved in one or two signaling pathways, and often the complexities associated with the interplay of multi genetic components in regulating expression of one another are poorly understood. It is further complicated when studies are carried out in predisposed hosts where many pathobiological events are readily apparent and injury to this host will bring in an entirely new cascade of regulation. High throughput screening of gene expression in such cases may lead to identification of candidate genes of signaling events that underlie the mechanism of tissue injury and repair. Further, screening genes which are known to be involved in a specific disease process and organ system will allow prediction of the mechanism of tissue injury from exposure to toxicants. Often humans are exposed to

environmental toxicants and pollutants as a complex mixture of many components, e.g., particulate matter (PM). In such cases many of its components exert toxicities through a complex interplay between different mechanisms and the expression of the injury and repair processes may culminate into a disease or exacerbated disease. With this understanding, we aimed at developing an array filter to monitor the gene expression profile in rat cardiopulmonary system. In this report we present the development of an array which includes 30 genes of interest in pulmonary and cardiac injury, and its use in studying the expression profile of rat lungs exposed to residual fly ash (ROFA) and its metallic constituents, nickel (Ni) and vanadium (V).

METHODS

Animals:

Sixty-day old, male Sprague Dawley (SD) rats weighing 250-300 g were obtained from Charles River Laboratories (Raleigh, NC) and housed in an AAALAC approved animal facility ($21 \pm 1^\circ\text{C}$, $50 \pm 5\%$ RH, 12:12 h light/dark cycle). All animals received standard Purina rat chow (Richmond, IN) and water *ad libitum*.

Intratracheal (IT) Instillation:

Residual oil fly ash (ROFA) previously used in our studies (Kodavanti et al., 1997a, b; 1999) was suspended in pyrogen-free bacteriostatic saline at concentrations of 0.0 (control) or 3.33 mg/ml and mixed gently for 20 min. V and Ni concentrations (predominant toxic metals of ROFA) in one milliliter of ROFA instillate were calculated based on our previous study (Kodavanti et al., 1997b) and accordingly nickel sulfate (NiSO_4 ; $1.3 \mu\text{mol/ml}$) and vanadium sulfate (VSO_4 ; $2.2 \mu\text{mol/ml}$) solutions were prepared in acidified saline, since ROFA suspension in saline resulted in pH of ~ 2.5 . These saline, ROFA or metal suspensions were IT instilled in rats (1 ml/kg body weight) under halothane anesthesia (Costa et al., 1986).

Tissue Isolation and Bronchoalveolar Lavage Fluid (BALF) Analysis for Determining Lung Injury:

Three or 24 hours following IT instillation, rats were anesthetized with sodium phenobarbital (Nembutal, Abbott Lab., Chicago; 50-100 mg/kg body weight, i.p.) and exsanguinated via the abdominal aorta. Tracheas were cannulated, the right lung lobes were immediately frozen in liquid nitrogen and stored at -80°C for RNA analysis. RNA was isolated from frozen right lung lobes using Ultraspec reagent (Biotex Laboratories Inc., Houston, TX). Left lungs were lavaged with phosphate buffered saline (pH 7.4) at a volume of 28 ml/kg body weight (approximately 75% total lung capacity). Three in-and-out washes were performed using the same fluid. One aliquot of whole lavage fluid was used for determining total cells using a Coulter Counter (Coulter, Inc., Miami FL), and a second aliquot was centrifuged using a Shandon 3 Cytospin (Shandon) for preparing cell differential slides. The slides were dried at room temperature and

stained with LeukoStat (Fisher Scientific Co., Pittsburgh, PA). Macrophages, neutrophils, eosinophils and lymphocytes were quantitated using light microscopy (200 cells/slide).

The remaining BALF was centrifuged at 1500 x g to remove cells, and the supernatant fluid was analyzed for protein and lactate dehydrogenase (LDH) activity. Assays for protein, and LDH activity were modified and adapted for use on a Hoffmann-La Roche Cobas Fara II clinical analyzer (Roche Diagnostics, Branchburg, NJ). Total protein content was determined using a Coomassie Plus Protein Assay Kit (Pierce, Rockford, IL) and bovine serum albumin as a standard. LDH activity was determined using a Kit 228 and standards from Sigma Chemical Co. (St. Louis, MO).

Cloning of PCR-derived cDNAs:

A selected group of genes involved in pulmonary and cardiac pathologies were identified based on the literature information and their PCR primers were designed using an on-line software program (Table 1). RT-PCR was performed using total RNA isolated from rat lungs intratracheally instilled with lipopolysaccharide (LPS; 200 µg/~400g rat in saline; 6 or 24 h later) or bleomycin (1 U/rat in saline; 48 or 96 h later) since injuries with LPS and bleomycin are known to involve most gene markers that are included in the array (Table 1). PCR products (~100 to 700 bp in size representing the coding region of respective genes) were cloned into the TA cloning vector (TA cloning kit, Invitrogen, CA) according to the manufacturer's recommendations with slight modifications. Briefly, bacterial colonies with cDNA inserts were isolated and propagated in the LB medium. Plasmid DNA was isolated from liquid cultures using Qiagen Plasmid DNA kit according to manufacturer's recommended procedures (Quagen, Valencia, CA). The size and the authenticity of cDNA inserts were confirmed by restriction digestion analysis and DNA sequencing. The steps involved in developing and screening the array blot are depicted in figure 1.

Array Blotting:

Plasmid DNA (1 µg) with cDNA inserts for respective clones was denatured by alkali treatment and blotted onto GeneScreen plus membrane (NEN-Dupont, Boston, MA) using BioRad Dot blot apparatus according to the manufacturer's recommendations. The membranes were then baked at 80°C for 2 h under

vacuum and stored at room temperature until used.

Lung total RNA (20 µg) from control, ROFA, Ni or V exposed rats was reverse transcribed using Superscript II reverse transcriptase in a reaction mix containing ³²P-dATP and random hexamers as detailed by Schummer et. al. (1997). The labeled cDNA produced in this reverse transcription reaction was hybridized to the array blots using standard Southern hybridization protocol (Sambrook et al., 1989) and the blots were washed in buffers of different stringencies until the background radioactivity was minimal. The washed blots were then exposed to X-ray film for 36 - 45 h and autoradiogram were developed using Kodak X-OMAT M 35 processor (Estaman Kodak, Rochester, NY).

Northern blotting:

Total RNA (15 µg) from control, ROFA, Ni or V-exposed rat lung lobes was separated by electrophoresis through 1.2 % formaldehyde-agarose gel suspended in 1 X MOPS buffer (20 mM MOPS, pH 7.0, containing 8 mM sodium acetate and 1 mM EDTA). The RNA was then transferred to GeneScreen plus membrane (NEN-Dupont, Boston, MA) by capillary transfer. Blots were dried under vacuum at 80°C for 2 hours and then prehybridized for 4 hours. Hybridization was carried out as described earlier (Nadadur et al., 1997). Briefly, blots were hybridized overnight with the ³²P-labeled cDNA probe generated in a nick translation reaction (Promega, Madison, WI) at 42 °C in 50% formamide and 5X Denherds reagent (5 Prime-3 Prime Inc., Boulder, CO) using VCAM-1 cDNA insert. The RNA blots were washed to a final high stringency condition of 0.1XSSC and 1% SDS at 65°C for 30 min. The blots were exposed to X-ray film for 20-30 hours and the films were developed as detailed above. X-ray films of gene array and northern blots were scanned and relative dot/band densities were read using AlphaImager version 3.3 (Alpha Innotech Corp., San Leandro, CA).

RESULTS

In an effort to develop a cardiopulmonary rat gene array, we initially cloned 30 genes representing inflammatory and anti-inflammatory cytokines, growth factors, adhesion molecules, metalloproteinases, vascular tone regulatory molecules, transcription factors, stress proteins, surfactant proteins and antioxidant enzymes (Table 1). The gene array blots were prepared as detailed in the methods section and spot locations on the array are depicted in figure 2.

Expression profile of these genes in saline, ROFA, Ni and V-exposed animals was compared and the lung injury and inflammation as determined by BALF analysis were evaluated to establish the relationship between the kinetics of injury and gene expression. Since our previous study indicated a role of ROFA-associated Ni and V in *in vivo* lung injury, differences in the kinetics of induced effects between metals (Kodavanti et al., 1997b) were also compared with the gene array blots derived from metal exposed rats at two different time points.

The array blots hybridized with the ³²P-labeled cDNA derived from rat lungs exposed to ROFA, Ni or V for 3 and 24 h are shown in figure 3. Densitometric scanning of the array blots indicated that out of the 30 genes included in the blot, half of them appeared to be increased following ROFA, Ni, or V exposure in the lung. A ~2-3 fold increased expression of IL-1 β , cellular fibronectin-EIIIA (cFn-EIIIA), PDGF-A chain, VCAM-1, ICAM-1 and MIP-1a and ~2 fold increase in the expression of TIMP-1 and TGF- β was observed in the rat lung, 3 h post ROFA exposure. Of the two metal constituents of ROFA studied, V induced a 2-3 fold increase in the expression of IL-1b, cFn-EIIIA, PDGF-A and ~1.5 fold increase in VCAM-1 expression. While Ni treatment induced ~1.5 fold increase in the expression of cFn-EIIIA, PDGF-A chain, and VCAM-1. Most of the genes found induced at 3h post exposure returned to basal levels by 24h especially in V or ROFA exposed animals. Negative controls with no plasmid, and plasmid with no cDNA insert showed no signals, whereas a positive control such as β -actin gave dark stained spots on all blots examined indicating that hybridization was specific to cDNA inserts present in each sample spots. Densitometric data on selected spots is presented in table 2.

To confirm the observations made with the gene array blot analysis we carried out northern blot analysis using cDNA probes for VCAM-1 and SP-A. As presented in Fig. 4, northern blot analysis indicated ~2 fold increase in the expression of VCAM-1, 3 h post exposure to ROFA, Ni or V-exposed rat lungs. VCAM-1 expression at 24 h post ROFA or metal exposure appeared to have decreased. To confirm equal loading of RNA, the blots were stripped and reprobed with SP-A cDNA insert. Densitometric scan of the autoradiogram indicated a minimal increase in the expression of SP-A 3h post ROFA or metal exposure (Table 3). This is consistent with equal loading of RNA as band densities for 28S and 18S RNA appeared to be similar in all exposure groups (Fig. 4; lower panel, Table 3).

BALF from same animals in all treatment groups were analyzed for lung injury markers to determine consistency between increased expression of inflammatory as well as other tissue injury-related genes and the expression of these changes in the lung. BALF protein and neutrophilic inflammation were increased as early as 3 h post ROFA, V and Ni exposure. ROFA and Ni-associated increase in protein was apparent at a later time point (24 h) whereas that of V was induced at earlier time point (3 h). Neutrophilic inflammatory response was readily apparent at 3 h and was largely reversed at 24 h following all exposures. This early inflammatory response is consistent with early induction of many inflammatory and other injury/repair-related genes.

DISCUSSION

DNA sequence information available from the genome databases along with advancements in technology has led from the screening a cDNA library for one specific gene to screening for expression pattern of multiple genes in a single hybridization experiment (Goffeau et al., 1996). Most commercially available microarray filters and chips are developed using randomly primed oligos of the human or mouse genome within stretches of DNA, which may or may not include genes of specific pathology or injury and repair. We chose to develop a gene array blot which includes rat genes involved in cardiopulmonary injury and pathology. The blot development and use included standard molecular approaches such as cloning of RT-PCR-derived cDNAs of interest, isolating and purifying plasmids with inserts and blotting them onto nylon membranes in a 96-well format. Hybridizing these membranes with ³²P-labeled RNA sample of pulmonary tissue resulted in expression profile that is consistent with previously observed increase in expression of IL-1 β , MIP-2, cFn-EIII α and VCAM-1 following lung injury caused by ROFA or metals (Kodavanti et al., 1997b). This screening also indicated an increase in the expression of PDGF-A chain by ROFA and V. This observation supports the previously reported involvement and induction of PDGF- α receptor by PM (Bonner et al., 1998). Northern analysis for VCAM-1 expression indicated more than ~ 1.5 fold induction compared to 2 fold increased expression observed in the array blot. Thus, such an array developed within the lab can be customized to a single or multiple disease conditions and used to determine expression profile of genes located at diverse sites or gene clusters within a segment of chromosome.

In general, toxicant-induced tissue injury involves activation of signaling pathways and expression of multiple genes of inflammation and tissue repair processes. Our study showed that expression of genes observed in the array blot following ROFA, Ni or V exposure were consistent with the associated lung injury and inflammation. Although, the dosage of ROFA or metals used in this study was 1/3 of what was used in our previous study, the increased expression of inflammatory and other genes was readily apparent, and was associated with inflammation. Recently, we have shown that ROFA, at lower IT dosage induces pulmonary injury and inflammation (Kodavanti et al., 1999), and we showed earlier (Kodavanti et al.,

1997b, 1998), ROFA-associated injury was almost entirely accountable to constituent transition metals such as Ni and V. These metals appear to exert *in vitro* and *in vivo* effects by different mechanisms and also express interactions (Kodavanti et al., 1997b). As ROFA represents a minor fraction of a more complex ambient PM, other components of ambient PM may exert or influence injury by varied mechanisms in an exposed host. The complexities of these biological effects may be more evident in models of susceptible hosts exhibiting one or more preexistent pathologies. Thus screening of multiple genes encompassing diverse aspects provide valuable information on potential mechanisms of injury and provide insight into further characterization of unique mechanisms.

Evaluating data derived from array chips containing thousands of genes and the validity of observed changes is challenging, and thus far, computer software is limited for such applications (Bittner et al., 1999; Nuwaysir et al., 1999). Use of commercial arrays offer an unique approach to identifying novel genes in understanding basic biology. However, most toxicologists are often interested in evaluating changes in expression of genes or pathways that are more specific or well characterized. Cloning of cDNAs of interest allow their potential usefulness in screening for *in situ* mRNA expression in the tissues, or assist in specific antibody development for usage in protein expression. In addition, it is relatively simple to develop multiple blots for future usage in a cost- effective manner.

In summary, the utility of our initial array blot containing 30 genes in comparing mRNA expression from ROFA and metal exposed rat lungs is consistent with those observed using RT-PCR and northern blotting. We are currently upgrading this array blot by including more genes involved in oxidative burden, cardiovascular contractility components, inflammatory/repair-related cytokines, transcription factors, kinases, cell proliferation and apoptosis-related markers. Such an array will provide important toxicological information and will contribute to the basic mechanism of tissue injury and repair.

REFERENCES

- Bitner, M., Meltzer, P., and Trent, J. 1999. Data analysis and integration: of steps and arrows. *Nat. Genet.* 22:213-215.
- Bonner, J. C., Rice, A. B., Lindroos, P. M., O'Brien, P. O., Dreher, K. L., Rosas, I., Alfaro-Moreno, E. and Osornio-Vargas, A. 1998. Induction of the lung myofibroblast PDGF receptor system by urban ambient particles from Mexico City. *Am. J. Respir. Cell. Mol. Biol.* 19: 672-680.
- Costa, D. L., Lehmann, J. R., Harold, W. M., and Drew, R. T. 1986. Transoral tracheal intubation of rodents using a fiberoptic laryngoscope. *Lab. Anim. Sci.* 36:256-261.
- DeRisi, J., Penland, L., Brown, P. O., Bitner, M. L., Meltzer, P. S., Ray, M., Chen, Y., Su, Y. A., and Trent, J. M.. 1996. Use of a cDNA microarray to analyze gene expression patterns in human cancer. *Nat. Genet.* 14:457-460.
- Goffeau, A., Barrell, B. G., Bussey, H., Davis, R. W., Dujon, B., Feldmann, H., Galibert, F., Hoheisel, J. D., Jaq, C., Johnson, M., Louis, E. J., Mewes, H. W., Murakami, Y., Phillipsen, P., Tettelin, H. and Oliver, S. G. 1996. Life with 6000 genes. *Science.* 274:563-567.
- Kodavanti, U. P., Jaskot, R. H., Su, W. Y., Costa, D. L., Ghio, A. J., and Dreher, K. L. 1997a. Genetic variability in combustion particle-induced chronic lung injury. *Am. J. Physiol.* 272:L521-L532.
- Kodavanti, U. P., Jackson, M. C., Ledbetter, A., Richards, J., Gardner, S. Y., Watkinson W. P., Campen, M. J., and Costa, D.L. 1999. Lung injury from intratracheal and inhalation exposures to residual oil fly ash

in a rat model of monocrotaline-induced pulmonary hypertension. *J. Toxicol. Environ. Health* 57:101-121.

Kodavanti, U. P., Hauser, R., Christiani, D. C., Meng, Z. H., McGee, J., Ledbetter, A., Richards, J., and Costa, D.L. 1998. Pulmonary responses to oil fly ash particles in the rat differ by virtue of their specific soluble metals. *Toxicol. Sci.* 43:204-212.

Kodavanti, U. P., Jaskot, R. H., Costa, D. L., and Dreher, K. L. 1997b. Pulmonary proinflammatory gene induction following acute exposure to residual oil fly ash: roles of particle-associated metals. *Inh. Toxicol.* 9:679-701.

Liang, P. and Pardee, A. B. 1992. Differential display of eukaryotic messenger RNA by means of polymerase chain reaction. *Science* 257:967-971.

Nadadur, S. S., Lisciandro, K., Mudipalli, A., Maccubbin, A. E., Faletto, M. B. and Gurtoo, H. L. 1997. Altered biochemical profile and gene expression in aflatoxinB1-transformed C3H10T1/2 cells. *Int. J. Oncol.* 10:1265-1275.

Nuwaysir, E. F., Bittner, M., Trent, J., Barrett, J. C., and Afshari, C. A. 1999. Microarray and toxicology: the advent of toxicogenomics. *Mol. Carcinog.* 24:153-159.

Sambrook, J., Fritsch, E. F. and Maniatis, T. 1989. *Molecular Cloning. A laboratory Manual*. CSH Laboratory Press, Cold Spring Harbor, NY.

Schena, M., Shalon, D., Davis, R. W., Brown, P. O. 1995. Quantitative monitoring of gene-expression patterns with a complementary DNA microarray. *Science* 270:467-470.

Schummer, M., Ng, W. I., Nelson, P. S., Bumgarner, R. E. and Hood, L. 1997. Inexpensive handheld device for the construction of high-density nucleic acid arrays. *Biotechniques* 23:1087-1092.

Velculescu, V. E., Zhang, L., Vogelstein, B., Kinzler, K. W. Serial analysis of gene expression. *Science* 270:484-487, 1995.

Wodicka, L., Dong, H. L., Mittmann, M., Ho, M. H., Lockhart, D. J. 1997. Genome-wide expression monitoring in *Saccharomyces cerevisiae*. *Nat. Biotechnol.* 15: 1359-1367.

Zhao, N. D., Hashida, H., Takahashi, N., Misumi, Y., Sakaki, Y. 1995. High-density cDNA filter analysis - A novel approach for large-scale quantitative analysis of gene expression. *Gene* 156:207-213.

Table :1. Details of genes used in the array blot.

| Abbreviations Used | GenBank Accession # | Gene Name | Abbreviations Used | GenBank Accession # | Gene Name |
|--------------------|---------------------|---|--------------------|---------------------|--|
| ANF | M27498 | Atrial natriuretic factor | NOS(I) | U03699 | Inducible nitric oxide synthase |
| β -Act. | V01217 | β -actin | pc2.1 | NA* | TA cloning vector pCR2.1 (Invitrogen, Carlsbad, CA). |
| cFn-EIIIA | X15906 | Cellular fibronectin | PDGF-A | S57864 | Platelet-derived growth factor A-chain |
| E-sel | L25527 | E-selectin (ELAM-1) | p53 | X13058 | Nuclear oncoprotein p53 |
| HO | J05405 | Heme oxygenase-2 | SAPK | L27112 | Stress activated protein kinase |
| hsp70 | Z27118 | Heat shock protein 70 | SK-5 | U31321 | EST : U31321 from C3H10T1/2 cells |
| ICAM-1 | D00913 | Intercellular adhesion molecule-1 | SK-15 | NA* | Male specific Cytochrome P-450 IIA2 partial cDNA |
| IFN- γ | AF010466 | Interferon gamma | SP-A | X13177 | Surfactant protein A |
| IL-1 β | M98820 | Interleukin-1 β | SP-D | M81231 | Surfactant protein D |
| IL-6 | M26744 | Interleukin-6 | TGF- β 1 | X52498 | Transforming growth factor -beta 1 |
| MAP- α 1 | Y02299 | Major acute phase alpha-1 protein | TIMP-1 | U06179 | Metalloproteinase inhibitor (TIMP-1) |
| MIP-1 α | U06435 | Macrophage inflammatory protein-1 alpha | TIMP-2 | U14526 | Tissue inhibitor of metalloproteinase type 2 |
| MnSOD | Y00497 | Manganese-containing superoxide dismutase | Thrombo | AF022743 | Thrombomodulin |
| NF- κ B | L26267 | Nuclear factor kappa B p105 subunit | VCAM-1 | X63722 | Vascular cell adhesion molecule-1 |
| NOS | D12520 | Nitric oxide synthase | VEGF-D | AF014827 | Vascular endothelial growth factor D |

* NA : not in GenBank.

Table 2. Densitometric evaluation of array blots depicting ROFA, Ni or V-induced increases in gene expression.

| Genes | Control IDV* Units | | ROFA IDV Units | | Nickel IDV Units | | Vanadium IDV Units | |
|----------------|-----------------------|--------|-------------------|--------|---------------------|--------|-----------------------|--------|
| | 3 h | 24 h | 3 h | 24 h | 3 h | 24 h | 3 h | 24 h |
| IL-1 β | 7,158 | 8,146 | 18,734 | 12,789 | 10,243 | 9,875 | 19,376 | 13,765 |
| cFn-EIII A | 4,903 | 8,697 | 15,276 | 11,212 | 9,035 | 12,371 | 16,348 | 10,652 |
| PDGF-A | 5,683 | 7,248 | 14,859 | 10,136 | 10,357 | 9,254 | 15,568 | 9,865 |
| VCAM-1 | 7,513 | 8,124 | 15,652 | 10,474 | 11,654 | 10,137 | 12,108 | 9,843 |
| MIP-1 α | 6,271 | 4,258 | 17,693 | 5,268 | 7,347 | 5,073 | 8,572 | 4,784 |
| ICAM-1 | 8,424 | 7,876 | 16,848 | 8,638 | 8,956 | 8,132 | 9,037 | 8,875 |
| SP-A | 14,001 | 9,846 | 18,471 | 10,120 | 18,746 | 10,860 | 19,012 | 9,321 |
| SP-D | 9,436 | 5,932 | 12,269 | 6,873 | 11,861 | 6,547 | 8,827 | 6,138 |
| TIMP-1 | 4,656 | 2587 | 7,876 | 1850 | 1875 | 4266 | 3654 | 2076 |
| β -actin | 25,547 | 18,746 | 30,725 | 23,125 | 28,749 | 21,486 | 29,027 | 20,764 |
| TGF- β | 5,341 | 1987 | 8,327 | 1543 | 3276 | 1306 | 6,874 | 1673 |

*IDV, integrated density volume automatically corrected for background. Values are given for those gene markers, which were found to be altered 3 or 24 h following exposure to either ROFA or metals. Each value is an average of two spots.

Table 3. Densitometric evaluation of pulmonary northern blots obtained from control, ROFA, Ni or V-exposed rats..

| | *IDV for 3 h time point | | | | *IDV for 24 h time point | | | |
|---------|-------------------------|---------|---------|---------|--------------------------|---------|---------|---------|
| | Control | ROFA | Ni | V | Control | ROFA | Ni | V |
| VCAM-1 | 89,396 | 147,264 | 140,074 | 137,290 | 128,430 | 112,145 | 75,793 | 78,296 |
| SP-A | 104,336 | 122,093 | 165,455 | 127,020 | 115,032 | 142,882 | 125,049 | 131,942 |
| 28S RNA | 109,438 | 114,461 | 113,515 | 111,092 | 110,254 | 114,876 | 113,210 | 110,897 |

*IDV, integrated density volume automatically corrected for background. Values are given for those gene markers, evaluated by northern analysis for the purpose of confirmation of array blot results. Density scanning of 28S RNA is also provided to confirm equal loading in each lane. Each value is an average of two bands.

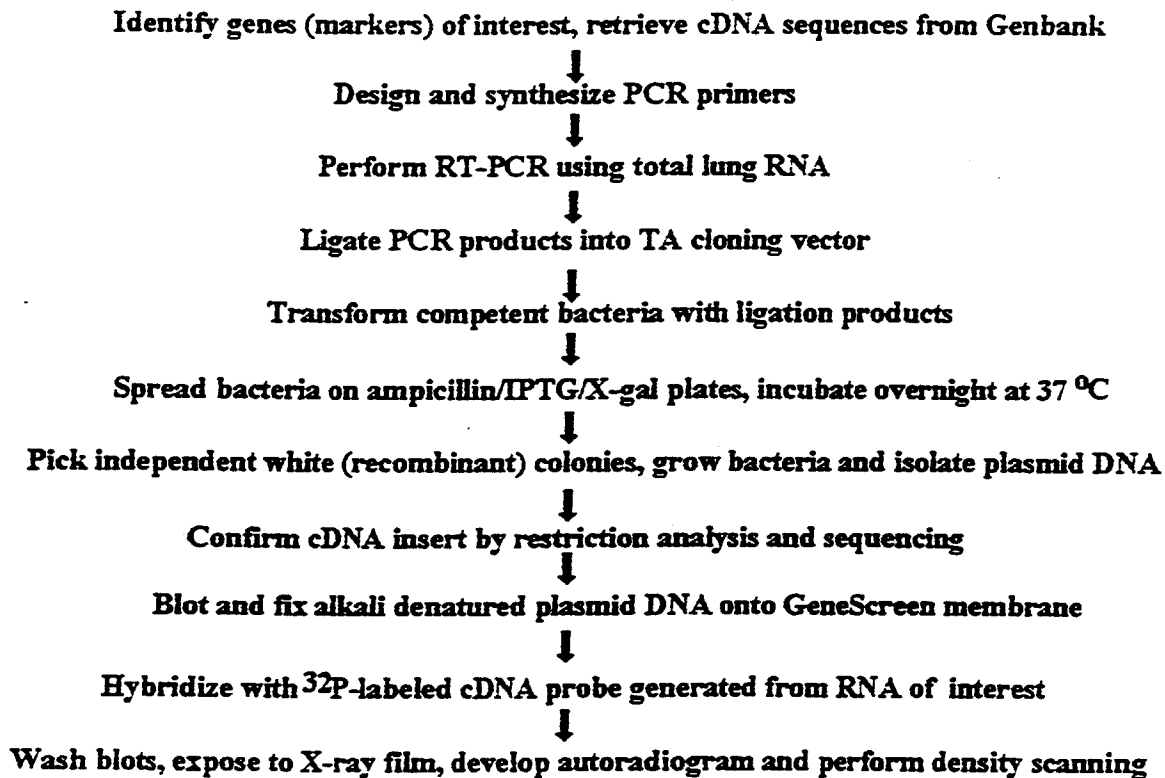


Fig. 1. Protocol for the PCR cloning and development of a cardiopulmonary rat gene array.

Array Blot

| | A | B | C | D |
|---|----------------|------------------|----------------|----------------|
| 1 | IL-1 β | cF β -E11A | PDGF-A | SAPK |
| 2 | IL-6 | VCAM-1 | IFN- γ | HO-2 |
| 3 | MIP-1 α | ICAM-1 | TGF- β | hsp70 |
| 4 | | SP-A | VEGF-D | MnSOD |
| 5 | TIMP-1 | SP-D | ANF | MAP-1 α |
| 6 | TIMP-2 | E-Selectin | NF- κ B | NOS |
| 7 | SK-5 | Thromb | p53 | NOS(1) |
| 8 | β -Act | Pc2.1 | SK15 | |

Fig. 2. Array blot template indicating spot locations for cDNAs blotted onto GeneScreen membrane. Full explanations of abbreviations used for gene names are given in table 1.

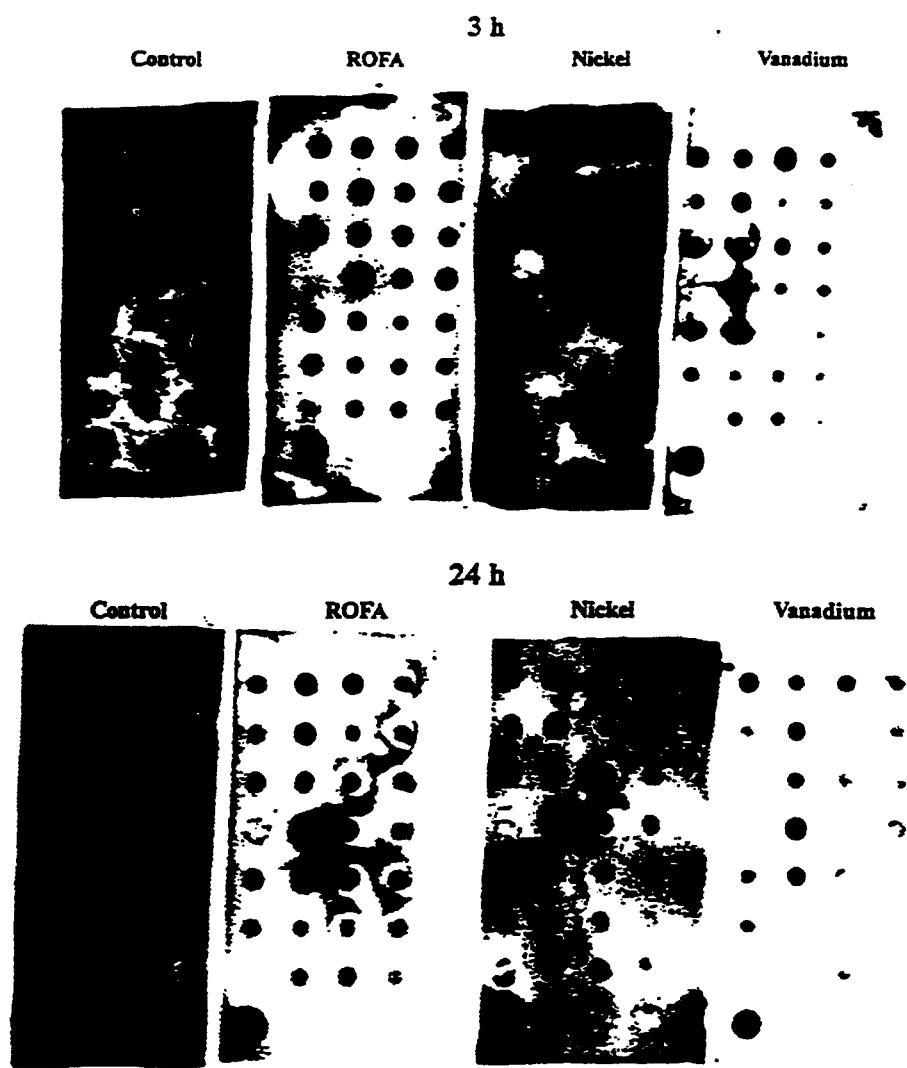


Fig. 3. Hybridization analysis of array blot with ^{32}P -labeled cDNA derived from rat lungs treated with residual oil fly ash (ROFA), nickel (Ni) or vanadium (V). 20 mg of total RNA derived from rat lung tissue was converted to cDNA in a reverse transcription reaction and hybridized to array filters for 15 h at 42°C .

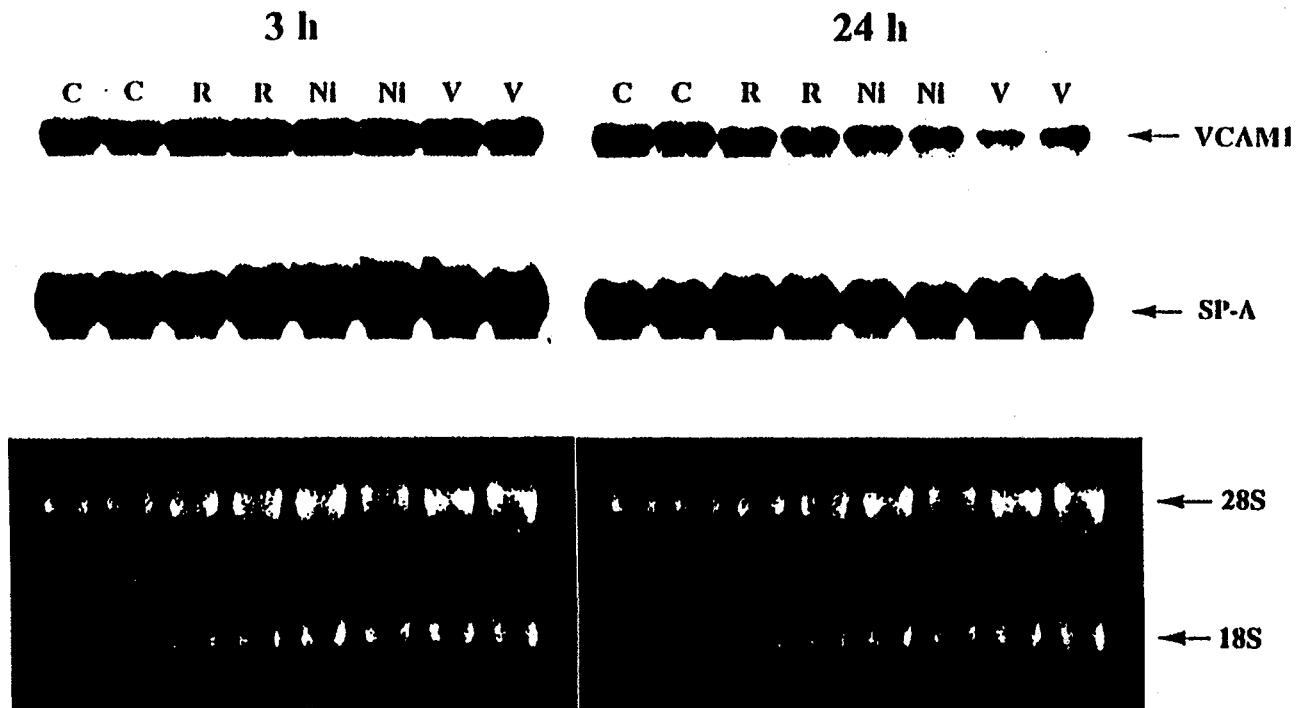


Fig. 4. Northern blot analysis of VCAM-1 expression using RNA derived from ROFA, Ni, or V exposed rat lung. 15 mg of total RNA derived from rat lung lobes were run on formaldehyde agarose gels and RNA was transferred to GeneScreen plus membrane. The blots were hybridized with ^{32}P -labeled cDNA inserts of VCAM-1 and SP-A. A picture of the RNA gel (stained with ethidium bromide) of same samples is shown in the bottom panel indicating equal loading in all lanes. © = control; R = ROFA; Ni = nickel; V = vanadium). Two RNA samples of the same treatment groups were pulled and the blotting procedure was repeated twice.

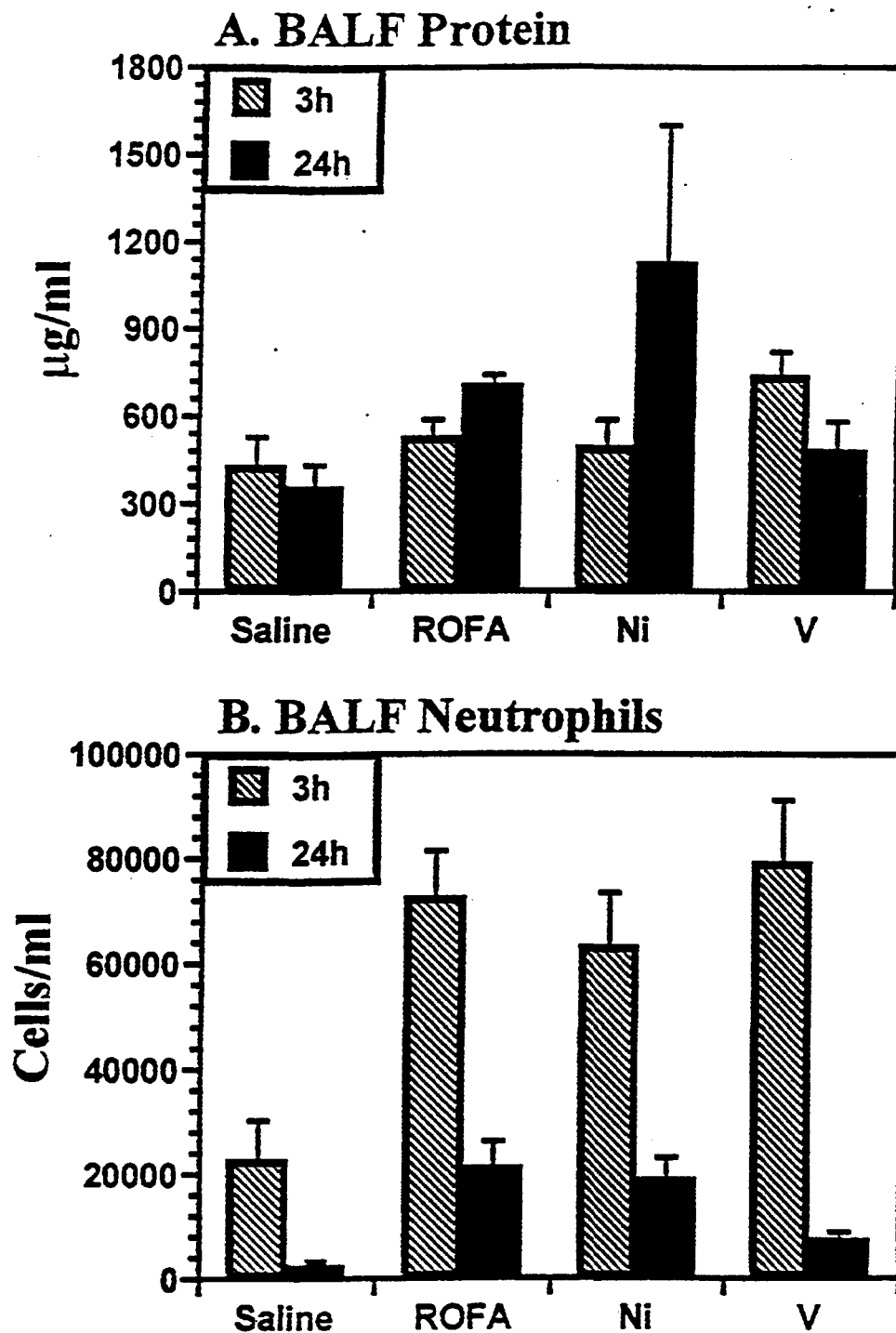


Fig. 5. Increases in BALF protein and neutrophils following ROFA or metal exposure. Each value represent mean \pm SE of 4 animals. BALF LDH activity was increased following ROFA or metal exposure but changes in alveolar macrophage numbers were less dramatic.

Effect Of Acute Exposure To Acid Aerosol On Heart Rate

Christine Nadziejko, Kaijie Fang, Lung Chi Chen, Richard Schlesinger, Terry Gordon, Department of Environmental Medicine, New York University School of Medicine, Tuxedo, New York

A number of studies have shown that exposure to elevated levels of particulate air pollution (PM) is associated with a small but significant increase in heart rate. The physio-chemical properties of PM that cause this increase are not known. The purpose of this project was to determine whether inhalation of sulfuric acid aerosol, a component of PM, affects heart rate. Male F344 rats (8 mo old) with implanted EKG transmitters were exposed to air (n=10) or acid aerosol (n=11) for 6 hours. The target concentration of the acid was 100 $\mu\text{g}/\text{m}^3$ and the particle size was < 0.3 μm . Heart rate and body temperature were monitored every 5 min for 24 hr before exposure and for 18 hrs after exposure. The acid-exposed rats had a small but statistically significant increase in heart rate after exposure that persisted for 14 hours. These results suggest that inhalation of acid aerosol causes a slight increase in heart rate.

There is increasing evidence that the adverse effect of PM on the cardiovascular system is a significant public health issue. Studies of mortality data from recent decades show that PM-associated deaths from cardiovascular disease equal or exceed deaths from respiratory causes (Schwartz, 1994; Pope et al., 1992). Particulate air pollution has also been shown to be associated with increased cardiovascular morbidity. Approximately 1 in 50 heart attacks in the London area were found to be due to air pollution (Poloniecki et al., 1997). An air pollution episode in Germany in 1985 was shown to be associated with a 19% increase in hospital admissions for cardiovascular causes as compared to a 7% increase in respiratory-related admissions (Peters et al., 1997).

Although the epidemiological evidence linking increases in PM to cardiac morbidity and mortality is consistent and reproducible, the physical and/or chemical properties of PM responsible for these serious health effects are currently unknown. Recent studies indicate that PM causes a small but consistent increase in heart rate in animals and humans. We have reported that a single 3 hr exposure of normal and compromised rats to concentrated ambient New York City PM 2.5 (with removal of gaseous pollutants) at concentrations ranging from 100-350 $\mu\text{g}/\text{m}^3$ resulted in a small (7-11%) increase in heart rate that persisted for 2-6 hrs after exposure (Nadziejko et al., 1997). Similar PM-associated increases in heart rate (as well as decreased heart rate variability, increased blood viscosity and increased blood pressure) have recently been reported in several human panel studies in the US and in a retrospective analysis of data from the MONICA study in Europe (Gold et al., 1998; Pope et al., 1999; Shy et al., 1998, Peters et al., 1998).

Reproducible markers of the effects of PM on the cardiovascular system, such as increased heart rate and decreased heart rate variability, are very valuable endpoints that can be used to identify the physical/chemical properties of PM that are responsible for cardiovascular health effects. In contrast, sudden death, myocardial infarction, and arrhythmia are physiologically complex, multifactorial events and are thus are very cumbersome tools for probing the components of PM

for cardiac health effects. Also a case can be made that the small PM-induced changes in heart rate and heart rate variability represent an adverse health effect due to the large population that experiences these small changes in cardiovascular homeostasis.

Acid is one of the chemical constituents of PM that has been implicated in some of the health effects of particulate air pollution (Thurston et al., 1994). Inhalation of acid aerosols could potentially cause cardiovascular effects by stimulating irritant receptors in the airway epithelium (Zhang et al., 1997). Although the effects of inhalation of acidic aerosols on respiratory function and lung morphology have been studied extensively in humans and animals, little information exists on the acute cardiovascular effects of environmentally realistic concentrations of acid aerosol. The purpose of this study was to determine whether inhalation of sulfuric acid aerosol has any acute effects on heart rate or EKG.

Methods

Animals

The animals used in this study were 8 month old, specific pathogen free, male Fisher 344 rats (Charles River Laboratories, Raleigh NC). The rats were housed in polycarbonate cages with corncob bit bedding within an HEPA-filtered laminar flow animal isolator. All rats were provided with food (Purina Rodent Chow, Purina Mills Inc., St. Louis, MO) and water *ad libitum* except during the exposure period. The animals were kept on a 12-hour on/off light cycle.

Experimental Design

Rats were exposed nose-only to sulfuric acid aerosol (target concentration $100 \mu\text{g}/\text{m}^3$) or filtered air for 6 hours with physiological monitoring before and after exposure. Two exposures were done a month apart using a cross-over design as shown below:

| | |
|---------------|--------------|
| Experiment I | |
| Group I | Air (n = 5) |
| Group II | Acid (n = 6) |
| Experiment II | |
| Group I | Acid (n = 5) |
| Group II | Air (n = 5) |

Transmitter failure occurred in one rat after Experiment I and that animal was sacrificed. Heart rate, EKG and temperature were monitored for 24 hours before exposure and for 18 hours after exposure. These physiological parameters were also monitored during exposure in Experiment I. However, since there were no significant changes during acid exposure in Experiment I, monitoring was not done during exposure in Experiment II.

Sulfuric Acid Aerosol Generation

The sulfuric acid generation system has been previously described (Chen et al. 1992): briefly, 0.1N sulfuric acid (Fisher Scientific, Fadem, NJ) was nebulized with a Collision nebulizer using compressed air at a pressure of 30 psi. The size distribution of the sulfuric acid aerosols was measured using a piezo-electric cascade impactor (QCM, California Measurements, Inc). Sulfuric acid concentration was monitored by collecting samples on Teflon filters (Millipore Corp., Bedford, MA) followed by measurement of the sulfate concentration using ion chromatography. The particle size of the sulfuric acid aerosol was $< 0.3 \mu\text{m}$ and the average concentration was $98 \mu\text{g}/\text{m}^3$.

Physiological Monitoring

Heart rate, temperature, and EKG were monitored by telemetry using hardware and software from Data Sciences International (St. Paul, MN). The EKG/temperature transmitters (Model TA11-CTA-F40) were inserted in the peritoneal cavity of rodents under aseptic conditions and Brevital (25-mg/kg) anesthesia. To establish a lead II EKG configuration, the negative lead of the transmitter was placed in the area of the right clavicle region and the positive lead was placed in the left groin region. EKG transmitters were surgically implanted more than 6 months prior to acid exposure.

Two days prior to exposure, the animals were brought to the exposure room and housed individually in cages that were placed on Data Sciences' receivers (Model #JA1020). The telemetry data were transmitted to a computer located in the exposure room for 24 hrs immediately prior to exposure. Heart rate and temperature were measured every 5 minutes. Each individual heart rate and temperature measurement was the average of a 10-second recording. EKG was recorded every 30 minutes. EKG waveforms were sampled at an acquisition rate of 1000 Hz for 10 seconds and stored digitally.

EKG Waveform Analysis

Several characteristic indices of the EKG waveform were measured in each animal as shown in Table I. These parameters were calculated from the 10-second waveform recordings collected every 30 minutes after exposure. In general, only the first EKG sample recorded each hour was analyzed. However, if there was excessive electrical noise or other artifacts then the second EKG sample was used for analysis. The mean of each parameter (intervals, segments, or duration) within each 10-second ensembled waveform was determined using software developed by Dr. W. Penn Watkinson and Sean Dodd at the U.S. EPA (Watkinson et al., 1985). This software superimposes all the waveforms in a 10 second recording to create a single ensembled EKG complex. The waveform parameters were then automatically measured on the ensembled EKG complex. A pilot study was done to confirm that the measurements made with this method agreed with manual measurements of EKG complexes selected at random within a 10-second recording.

Data Analysis

Heart rate and temperature measurements made before, during and after exposure were expressed as hourly averages. Baseline values of heart rate and temperature were collected for 24 hours the day before exposure. The post-exposure hourly averages for heart rate and temperature were normalized for circadian rhythm effects by subtracting the baseline pre-exposure hourly averages (of the identical time on the preceding day) from the post-exposure value for each animal. These normalized values are presented as the change in heart rate (beats per minute) or temperature (C°) at each post-exposure time period. The normalized values were then used in the statistical comparison of the effect of air or acid on heart rate. Data from Experiments I and II were pooled prior to analysis. Statistical significance of differences in group means for heart rate and temperature was tested by analysis of variance with repeated measures using Statview software (Abacus Concepts, Berkeley, CA). EKG waveform durations and intervals for the first 6 hours after exposure were averaged for each animal. Statistical significance of differences in the exposure group means was tested by the two-tailed Student's t test.

Results

Exposure of rats to sulfuric acid aerosol at a concentration of 98 $\mu\text{g}/\text{m}^3$ for 6 hours had no significant effect on body temperature (data not shown). There was a small but statistically significant ($P < 0.005$) increase in heart rate in acid-exposed rats as compared to air-exposed (Figure 1). The increase in heart rate averaged 9.3 beats per minute (bpm) and persisted for 14 hours after exposure. Heart rate one hour after exposure was approximately 70 bpm greater than baseline values in both exposure groups. This increase was due to the grooming activity of the rats when they were returned to their cages after nose only-exposure.

Table 1 shows the average values for a number of EKG waveform intervals and durations measured after exposure to air or acid aerosol. There were no statistically significant differences in any of the waveform parameters between the two groups. We have previously examined the effect of heart rate on EKG waveform intervals and durations (data not shown) and have determined that none of the parameters shown in Table I are affected by heart rate.

Discussion

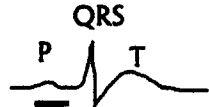
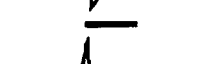
This study indicates that inhalation of 100 $\mu\text{g}/\text{m}^3$ sulfuric acid aerosol by rats for 6 hours results in a small but persistent increase in heart rate as compared to rats exposed to filtered air. Surprisingly, there was no significant effect on heart rate during exposure' as would be expected if the change in heart rate were mediated by stimulation of irritant receptors. It is possible that the effect of acid aerosol on heart rate during exposure was masked by the response of the rats to the nose-only exposure system, which caused heart rate to increase by an average of 60 bpm in air and acid-exposed rats. The mechanism by which inhalation of acid aerosol could cause a persistent increase in heart rate lasting more than 12 hours after exposure is not known. We have previously shown that inhalation of 300 $\mu\text{g}/\text{m}^3$ sulfuric acid aerosol by rats for 4 hrs had no morphological effects on the lung (Kimmel et al., 1997). Thus, acid exposure in the current study would not be expected to cause any lung injury or inflammation. Additional studies with lower acid concentrations and with more realistic particles (such as acid-coated carbon) are needed to confirm this initial result.

References

- Chen, L.C., Fine, J.M., Qu, Q.-S., Amdur, M.O., and Gordon, T. 1992. Effects of fine and ultrafine sulfuric acid aerosols in guinea pigs: alterations in alveolar macrophage function and intracellular pH. *Toxicol. Appl. Pharmacol.* 113:109-117.
- Gold, D.R., Litonjua, A., Schwartz, J., Verrier, M., Milstein, R., Larson, A., Lovett, E., and Verrier, R. 1998. Cardiovascular vulnerability to particulate air pollution. *Am. J. Respir. Crit. Care Med.* 157:A261.
- Kimmel, T.A., Chen, L.C., Bosland, M.C., and Nadziejko, C. 1997. Influence of acid aerosol droplet size on structural changes in the rat lung caused by acute exposure to sulfuric acid and ozone. *Tox. Appl. Pharm.* 144:348-355, 1997.
- Nadziejko, C., Chen, L.C., Zelikoff, J.T., and Gordon, T. 1997. Hematological and cardiovascular effects of acute exposure to ambient particulate matter. *Am. J. Respir. Crit. Care Med.* 155:A247.
- Peters, A., Doring, A., Wichmann, H.E., and Koenig, W. 1997. Increased plasma viscosity during an air pollution episode: a link to mortality? *Lancet* 349:1582-87.
- Peters, A., Perz, S., Doring, A., Stieber, J., Koenig, W., and Wichmann, H.E. 1998. Increased heart rate during an air pollution episode. *Fourteenth HEI Annual Conference, April 5-7, 1998, Boston MA.*
- Poloniecki, J.D., Atkinson, R.W., Ponce de Leon, A., and Anderson, H.R. 1997. Daily time series for cardiovascular hospital admissions and previous day's air pollution in London, UK. *Occ. Envir. Med.* 54:535-540.
- Pope, C.A., Dockery, D.W., Kanner, R.E., Villegas, G.M., and Schwartz, J. 1999. Oxygen saturation, pulse rate, and particulate air pollution: A daily time-series panel study. *Amer J Respir Crit Care Med.* 159:365-72 1999.
- Pope, C.A., Schwartz, J., and Ransom, M.R. 1992. Daily mortality and PM10 pollution in Utah Valley. *Arch. Envir. Health* 47:211-220.
- Schwartz, J. 1994. What are people dying of on high air pollution days? *Environ. Res.* 64:26-35.
- Shy, C., Creason, J., Williams, R., Liao, D., Zweidinger, R., Watts, R., Devlin, R., Hazucha, M., and Nestor, J. 1998. Physiological responses of elderly persons to particulate air pollution. *Fourteenth Health Effects Institute Annual Conference, April 5-7, 1998, Boston MA.*
- Thurston, G.D., Ito, K., Hayes, C.G., Bates, D.V., Lippmann, M. 1994. Respiratory hospital admissions and summertime air pollution in Toronto, Ontario: consideration of the role of acid aerosols. *Environ. Res.* 65:271-290.

Zhang, T., Huang, C., and Johns, E. 1997. Neural regulation of kidney function by the somatosensory system in normotensive and hypertensive rats. *Am. J. Physiol.* 273:R1749-R1757.

Table 1. Effect of acid aerosol exposure on EKG waveform intervals and durations

| Parameter | | Air | Acid | P value |
|-------------------|---|-------------|-------------|---------|
| P wave duration |  | 13.5 ± 0.5 | 12.3 ± 0.7 | 0.18 |
| QRS duration |  | 12.8 ± 0.3 | 12.3 ± 0.3 | 0.36 |
| T wave duration |  | 60.9 ± 2.7 | 59.5 ± 2.7 | 0.72 |
| PR interval |  | 39.0 ± 0.6 | 37.4 ± 0.8 | 0.14 |
| PR segment |  | 25.6 ± 0.5 | 25.1 ± 0.5 | 0.58 |
| PT interval |  | 112.1 ± 4.7 | 110.6 ± 3.4 | 0.79 |
| RT interval |  | 74.2 ± 3.8 | 72.2 ± 3.1 | 0.68 |
| R apex-T interval |  | 33.9 ± 0.8 | 33.9 ± 0.6 | 0.98 |
| ST interval |  | 61.5 ± 3.9 | 59.9 ± 3.0 | 0.76 |

Note. Data are mean ± SEM for each group. All data are in milliseconds.

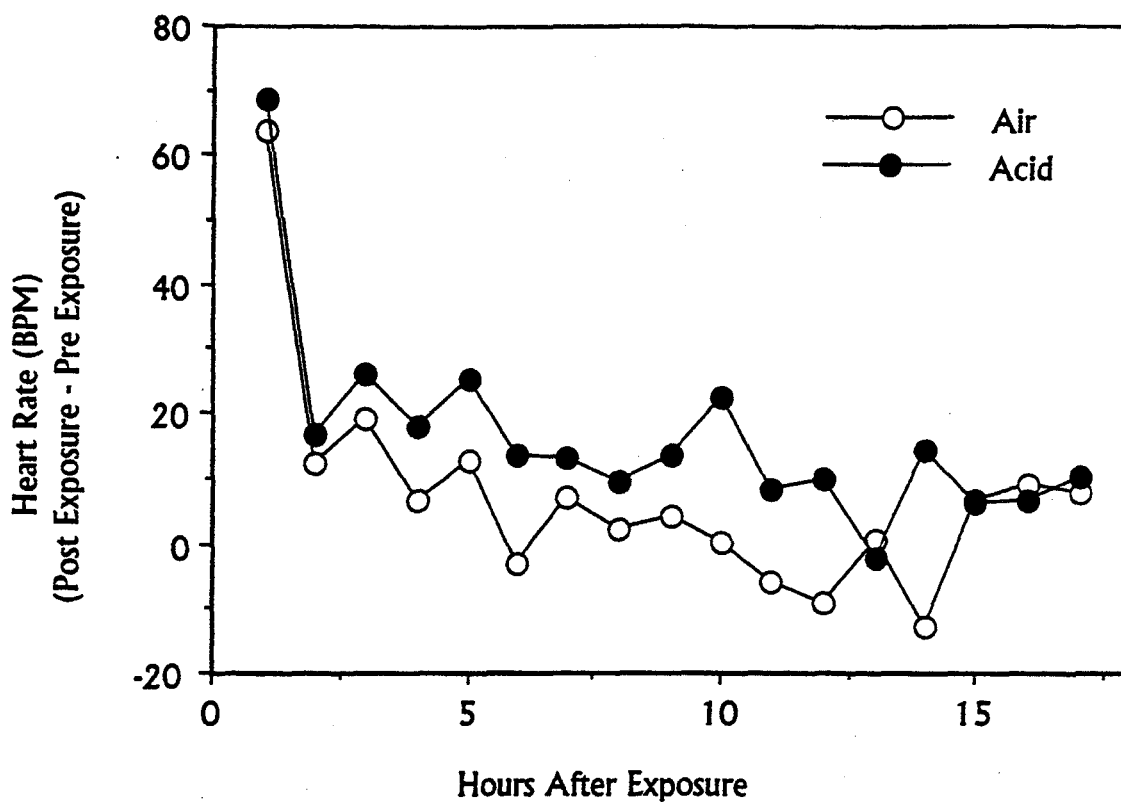


Figure 1. Effect of exposure to sulfuric acid aerosol on heart rate. Rats were exposed nose only to 100- $\mu\text{g}/\text{m}^3$ sulfuric acid aerosol ($< 0.3 \mu\text{m}$) or filtered air for 6 hrs. Results shown are the mean differences in heart rate from pre-exposure values for both exposure groups. The acid-exposed rats had a significantly greater heart rate than air-exposed rats ($P < 0.005$, analysis of variance with repeated measures).

A NEUROGENIC EXPLANATION FOR PARTICULATE MATTER INFLAMMATION IN THE AIRWAYS

Marga Oortgiesen¹, Sidney A. Simon¹ and Bellina Veronesi²

¹Departments of Neurobiology and Anesthesiology, Duke University Medical Center, Durham, N.C. and ²Neurotoxicology Division, National Health and Environmental Effects Research Laboratory, U. S. Environmental Protection Agency, Research Triangle Park, N.C.

PM toxicity:

Exposure to airborne PM pollutants is epidemiologically associated with increased morbidity and mortality in the human population. PM is thought to initiate and/or exacerbate respiratory disorders, such as asthma and airway hyperresponsiveness. Human susceptibility to airborne pollutants is highly variable, with increased sensitivity in the young and old and in individuals with compromised cardiopulmonary systems. Airborne PM pollutants are generated from diverse sources (e.g. industrial, urban, naturally occurring), however, they share common features as they consist of complex aggregates of elemental and organic carbons, metals, sulfates and microbial contaminants. This heterogeneous composition has complicated identifying the culpable components or characteristics of PM and has given rise to multiple hypotheses underlying the observed symptoms. Explanations for causes of PM toxicity have mainly focussed on transition metal contents (Carter et al., 1997; Dreher et al., 1998), biologicals (Hatch et al., 1985; Becker et al., 1996), and acidity (Brauer et al., 1995; Dockery et al., 1992; Kimmel et al., 1997; Lippmann and Thurston, 1996). Our studies support this latter mechanism and suggest that activation of sensory irritant receptors by acidic components of PM initiates the early, inflammatory events associated with PM exposure.

Neurogenic Inflammation:

An extensive body of clinical and experimental literature links the sensory nervous system to pulmonary inflammation through the pathophysiology of *neurogenic inflammation* (Baluk, 1997; Barnes, 1991; Maggi, 1993; Lundberg, 1995). In this process, neuropeptides such as substance P (SP), calcitonin gene related protein (CGRP), vasointestinal protein and neurokinin A initiate and modulate expressions of airway inflammation (e.g., vasodilatation, bronchoconstriction, mucous secretion, and cytokine release). Neuropeptides can directly influence immune cells (e.g., eosinophils, neutrophils, lymphocytes, mast cells, monocytes, macrophages) to stimulate or intensify inflammatory events in the airways. They also act on non-

Address correspondence to Dr. Bellina Veronesi, Neurotoxicology Division MD74B, National Health and Environmental Effects Research Laboratory, U. S. Environmental Protection Agency, Research Triangle Park, N.C. 27711. E-mail: Veronesi.Bellina@epamail.epa.gov

Disclaimer: This manuscript has been reviewed by the National Health Effects Environmental Research Laboratory, U.S. Environmental Protection Agency and approved for publication. Approval does not signify that the contents necessarily reflect the view and policies of the Agency, endorsement or recommendation for use.

immune targets (e.g., epithelial, endothelial, smooth muscle) to modulate inflammation and hyperresponsiveness. Neuropeptides are released from sensory nerves in response to activation of irritant receptors, which are located on their terminals and cell bodies (i.e., from dorsal root ganglia (DRG), nodose and trigeminal ganglia). Physiological and pharmacological studies indicate that these sensory irritant receptors (e.g., capsaicin, acid sensitive, mechanoreceptors) respond to a wide variety of noxious or tissue damaging stimuli such as chemical irritants (Wood and Docherty, 1997), heat, cold, and pressure (Cesare and McNaughton, 1997). The C-fibers, which express these irritant receptors and release the neuropeptides, innervate the upper, lower airway and nasal passages and extend throughout the epithelial layer lining the lumen. Here, they form a morphological and functional complex with non-neuronal target cells.

Various types of respiratory epithelial cells (e.g., neuroendocrine cells, Clara cells, and Type II alveolar cells) contain neuropeptide granules, neuropeptide receptors and respond to neuropeptide exposure with cytokine release (Mullol et al., 1997; Stevens et al., 1997). Serous epithelial cells have been shown to contain granules of CGRP, which are released upon exposure to capsaicin, the principle pungent ingredient in hot peppers (Baluk et al., 1993). Although respiratory epithelial cells are the first cells to encounter chemical irritants, their interactions with neuropeptides and other inflammatory mediators are poorly understood. Recently, we showed that a human bronchial epithelial cell line (i.e., BEAS-2B) was activated by capsaicin as well as by physiological concentrations of SP, CGRP, and acidic pH with increases in intracellular calcium ($[Ca^{2+}]_i$), synthesis of inflammatory cytokine transcripts, and the release of IL-6, IL-8 and TNF α (Veronesi et al., 1999a). Moreover, this release occurred in a receptor-mediated fashion, since cytokine levels were reduced by pharmacological receptor antagonists. Numerous studies have implicated capsaicin and neuropeptide receptors with airway disorders that are associated with environmental pollutants, such as ozone (Yeadon et al., 1992; Joad et al., 1996), sulfuric acid (el-Fawal et al., 1995), hydrogen sulfide (Prior et al., 1990), acrolein (Springall et al., 1990), and toluene diisocyanate (Gagnaire et al., 1997). In addition, studies show that pollutant induced airway inflammation and hyperresponsiveness are markedly reduced in animals whose C-fibers have been destroyed or inactivated (Nielsen, 1991; Prior et al., 1990; Satoh et al., 1993; Scheerens et al., 1996; Yeadon et al., 1992). In view of this literature, and the observation that BEAS-2B cells are activated by both neuropeptides and capsaicin, experiments were performed which examined the relevance of neuropeptide and irritant receptors to PM airway inflammation.

Irritant (e.g., capsaicin and acid sensitive) receptors are activated by ROFA:

Residual oil fly ash (ROFA), an industrial emission source air pollutant generated from the burning of low sulfur residual oil, is composed of highly soluble transition metals, sulfates bound to a carbon core (Pritchard et al., 1996; Dreher et al., 1997). Although ROFA does not resemble most urban or ambient PM, it does contain components (i.e., metals, sulfates, acids) that appear to be relevant to mechanisms underlying ambient PM toxicity. In rats and mice tracheal instillation of ROFA produces airway hyperresponsiveness and acute lung injury, consisting of epithelial damage, pulmonary edema, hemorrhage, and influx of neutrophils, macrophages and eosinophils (Su et al., 1995; Kodavanti et al., 1997; Dye et al., 1997). In cultured rodent alveolar macrophages, ROFA causes the release of inflammatory cytokines and apoptosis, whereas, it produces an oxidative burst and apoptosis in human alveolar macrophages (Becker et al., 1996; Holian et al., 1998; Rahman et al., 1997). We suggested that neurogenic factors could initiate ROFA (and other PM) inflammation by activation of capsaicin and/or acid sensitive

irritant receptors located on C-fibers that innervate the epithelial interstitium and on epithelial cells themselves (Veronesi et al., 1999b). Activation of these receptors would initiate the events of neurogenic inflammation (i.e., immediate increases in $[Ca^{2+}]_i$, release of neuropeptides from sensory terminals and proinflammatory cytokines from the airway epithelial cells, subsequent interaction of airway target cells). This was first demonstrated using the BEAS-2B cell line, which has been featured in numerous studies on ozone and PM inflammation. BEAS-2B cells were first exposed to field ROFA, synthetic mixtures of the major transition metals found in ROFA, and vanadate oxide, its predominant transition metal. For each compound, BEAS-2B cells responded with an immediate increase in $[Ca^{2+}]_i$ and a concentration-dependent release of IL-6 (Veronesi et al., 1999b). To test the relevance of neuropeptide or capsaicin receptors to these changes, BEAS-2B cells were pretreated (15 min) with receptor antagonists selective for SP (CP96,345) and CGRP (CGRP 8-37) neuropeptide receptors, or with capsazepine (CPZ), an antagonist for capsaicin (i.e., vanilloid) receptors (Bevan et al., 1992). Although the neuropeptide antagonists reduced ROFA-stimulated IL-6 cytokine production by ~25-50% (data not shown), pretreatment of cells with CPZ inhibited the increases in $[Ca^{2+}]_i$, diminished transcript (i.e., IL-6, IL-8, TNF α) levels and reduced IL-6 cytokine release to control levels (Figure 1). In addition, we showed that these changes were dependent on extracellular calcium sources.

ROFA, urban air particles (UAP), and other PM produce a variable release of inflammatory cytokines, oxidative burst and apoptosis in human alveolar macrophages (HAM). For example, silica and ROFA do not induce cytokines in HAM but stimulate the oxidative burst (as measured by chemiluminescence) and subsequently induce apoptosis. Recent studies (Mudpalli et al., 1999) pre-exposed HAM to CPZ (15 min), before ROFA exposure and prevented this oxidative burst in a concentration-dependent manner. Subsequent studies indicate that apoptosis itself could be blocked in ROFA-exposed HAM and macrophages from the murine RAW 167 cell line by pretreatment with CPZ (S. Becker, B. Veronesi, M. Oortgiesen unpublished data). The relevance of capsaicin receptors to ROFA inflammation was also examined in animal models of

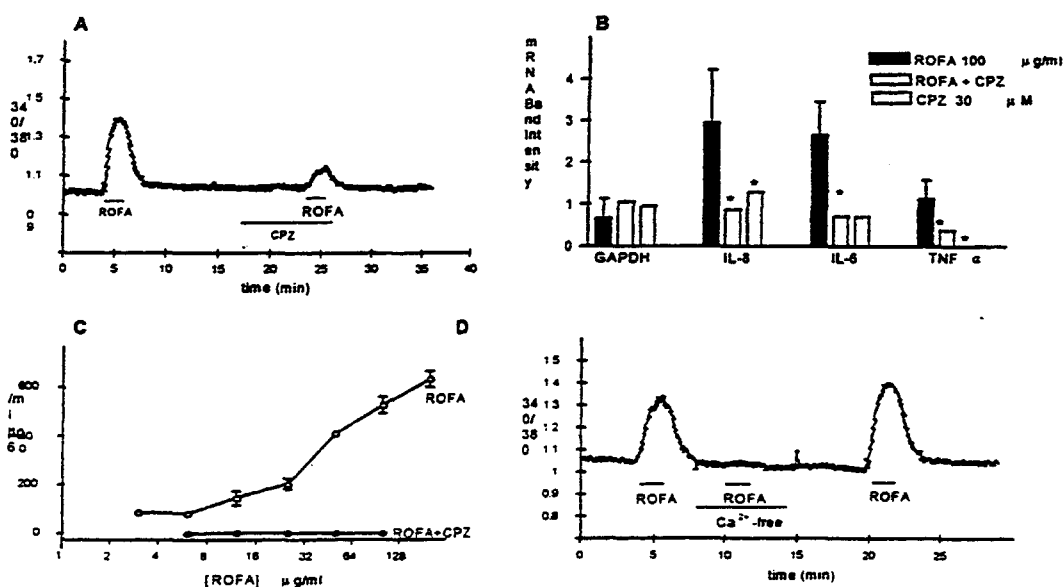


Figure 1: (A) Capsazepine (CPZ) inhibited the ROFA-induced increase in $[Ca^{2+}]_i$, (B) IL-8, IL-6 and TNF α transcript and (C) IL-6 release in BEAS-2B cells. (D) The ROFA response was abolished in the absence of extracellular calcium. Adapted after (Veronesi et al., 1999b).

airway hyperresponsiveness (Gavett et al., 1998). BALB/c mice were denervated of polymodal sensory C fibers by neonatal capsaicin treatment. As adults, ROFA was administered by tracheal instillation. Such animals showed a significant reduction in airway hyperresponsiveness, inflammatory cell (neutrophils) influx and LDH release compared to normal ROFA exposure. Taken collectively, these data indicated that the capsaicin irritant receptor played an initiating role in ROFA inflammation in two critical human airway target cells (i.e., bronchial epithelial cell, alveolar macrophage) and in whole animals.

Recent reports show that sensory irritant receptors are not confined to neuronal cells, since mast cells (Biro et al., 1998a), glial cells (Biro et al., 1998b) and BEAS-2B cells (Veronesi et al., 1999c) also expressed capsaicin and acid sensitive receptors (Figure 2). Based on these findings, we hypothesize that ROFA and other PM, activate capsaicin and/or acid sensitive receptors found on sensory neurons, alveolar macrophages and airway epithelial cells and initiate airway inflammation through the pathophysiology of neurogenic inflammation. An extension of this hypothesis suggests that factors, which modify receptor sensitivity, could modify an individual's inflammatory response to PM.

Effects of ROFA and SPM analogues:

To determine relevant physicochemical properties of ROFA, the size of ROFA particles were measured by microscopic (40X objective) inspection and their electrophoretic mobility by microelectrophoresis (Oortgiesen et al., 1999a). The zeta potential of ROFA particles was calculated from their electrophoretic mobility in an electric field, using the Helmholtz-Smoluchowski formula (Sennet and Olivier, 1965). The zeta potential of ROFA particles, 1-10 μm diameter, measured -28 ± 1.3 mV. Based on this, synthetic polymer microspheres (i.e., poly(methacrylic acid-co-methyl-enebisacrylamide), SPM) of 2 and 6 μm diameter were synthesized (Eichenbaum et al., 1998) with zeta potentials of -29 ± 0.9 mV. Thus these SPM acted as ROFA surrogates with respect to their size and zeta potential, but were devoid of the other inflammatory components of ROFA such as metals or biological contaminants. The effects of SPM on $[\text{Ca}^{2+}]_i$ increases and cytokine release were examined in epithelial BEAS-2B cells and DRG neurons. Cultured DRG respond to prototype irritants with an ion influx, and release neuropeptides and pro-inflammatory cytokines (i.e., IL-6) from their somata (Palma et al., 1997; Marz et al., 1998), making them an established experimental model of sensory irritant receptors.

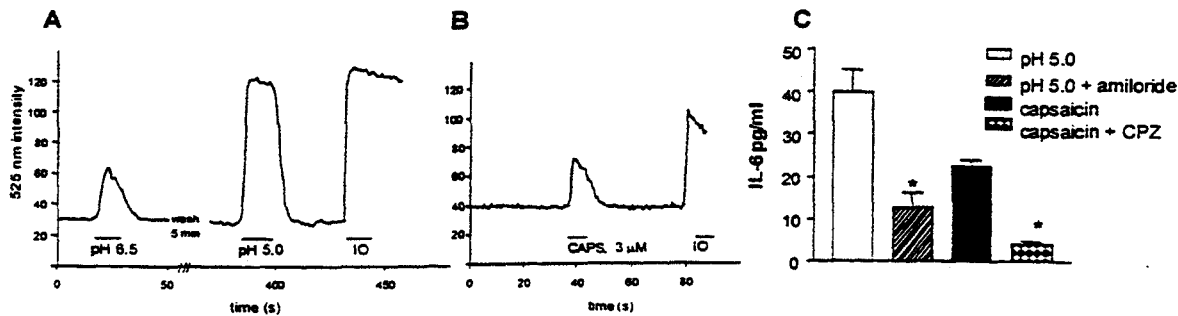


Figure 2: Responses to changes in external pH and capsaicin in BEAS-2B cells (A) Exposure to pH 6.5 and pH 5.0 increased $[\text{Ca}^{2+}]_i$ to near-maximal values as compared to ionomycin (IO). (B) Capsaicin (CAPS, 3 μM) also caused a transient increase in $[\text{Ca}^{2+}]_i$. (C) BEAS-2B cells exposed to pH 5.0 for 15 min, released low levels of IL-6, when measured in the culture medium after 4 hr. This release was insensitive to CPZ and partially blocked by amiloride. Capsaicin (10 μM) induced IL-6 release that was blocked by CPZ. Adapted from (Oortgiesen et al., 1999a).

Exposure of either BEAS-2B cells or DRG to ROFA (50 $\mu\text{g/ml}$) or SPM (2 $\times 10^4$ particles/ml) elicited increases in $[\text{Ca}^{2+}]_i$ with variable amplitudes and time courses. SPM also induced the release of IL-6 in BEAS-2B cells and DRG (Figure 3). DRG exposed to neutral SPM (i.e., zeta potential of 0 mV) released minimal amounts of IL-6 suggesting that the charge carried by the SPM was responsible for the cytokine release. CPZ, and an acid-sensitive receptor antagonist, amiloride, differentially inhibited the $[\text{Ca}^{2+}]_i$ increase and IL-6 release in BEAS-2B, suggesting that capsaicin and/or acid sensitive receptors were involved in the cellular activation by ROFA and SPM. This was further corroborated by experiments showing that the SPM sensitivity appeared localized in the nociceptive population of DRG (i.e., neurons sensitive to chemical irritants, capsaicin and/or acid pH) (Oortgiesen et al., 1999a). Based on these data, we hypothesized that the acidic microenvironment associated with negatively charged colloids like ROFA and SPM is responsible for the activation of capsaicin and/or acid sensitive receptors located on the cell surface of airway target cells.

Physicochemical analysis of PM:

PM, collected from many sources, share several features as they consist of acids, soluble metals, sulfates, biologics, and a carbon core. We are currently evaluating the contribution of separate physicochemical characteristics of a range of urban, industrial and naturally occurring PM with their inflammatory effects in both respiratory epithelial and sensory neurons. In pilot studies (Oortgiesen et al., 1999b), we have shown that exposure of BEAS-2B cells to various PM (50 $\mu\text{g/ml}$) produced immediate increases in $[\text{Ca}^{2+}]_i$ in the majority (80-90%) of cells. However, the magnitude and the time course of these increases varied according to the PM. For instance, PM from St. Louis caused maximal and immediate increases in $[\text{Ca}^{2+}]_i$, that returned to control levels during wash. In contrast, Mt. St. Helen's dust caused fluctuating increases in $[\text{Ca}^{2+}]_i$ that continued even after several minutes of wash. Exposure to Coal Fly Ash induced responses that consisted of a combination of the immediate $[\text{Ca}^{2+}]_i$ increase and continued $[\text{Ca}^{2+}]_i$ fluctuations. BEAS-2B cells, exposed to these PM (100 $\mu\text{g/ml}$) for 4 hr released IL-6 which was differentially reduced by pretreatment with CPZ or amiloride (Figure 4).

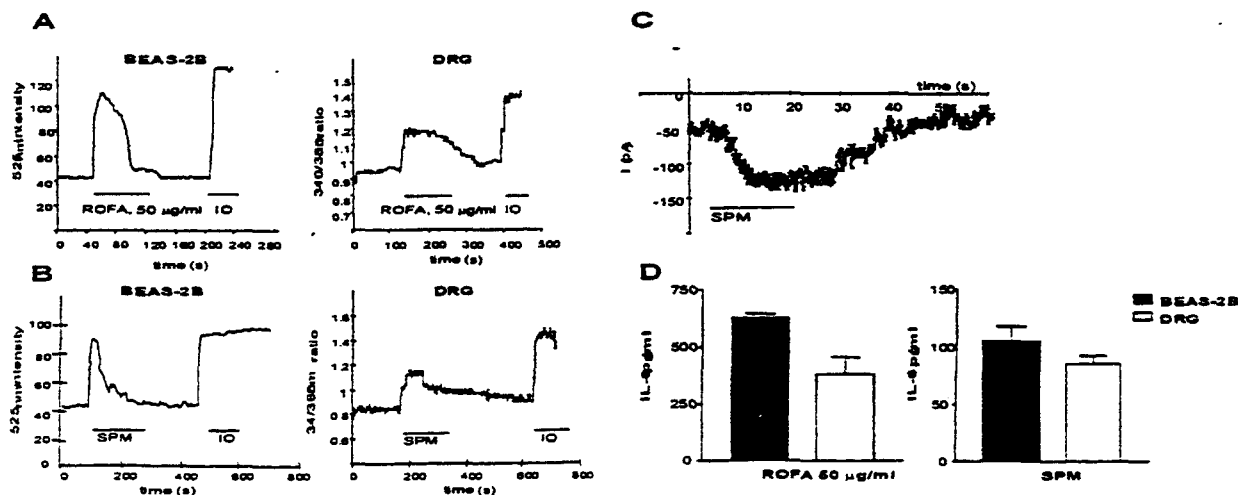


Figure 3: DRG and BEAS-2B cells respond to exposure to (A) ROFA (50 $\mu\text{g/ml}$) or (B) SPM (2 $\times 10^4$ particles/ml) with similar increases in $[\text{Ca}^{2+}]_i$ and the release of IL-6 (D). (C) In addition, voltage-clamped DRG respond to SPM exposure with a reversible inward ion current. Maximal increases in $[\text{Ca}^{2+}]_i$ were induced by exposure to 2 μM Ionomycin (IO). Adapted from (Oortgiesen et al., 1999a).

When compared to the PM induced cytokine release and their differential sensitivity to receptor antagonists, we interpreted the recorded differences in the profiles of calcium recordings as relating to different pathways by which PM might induce inflammation (e.g., irritant receptor activation, metal induced oxidative stress).

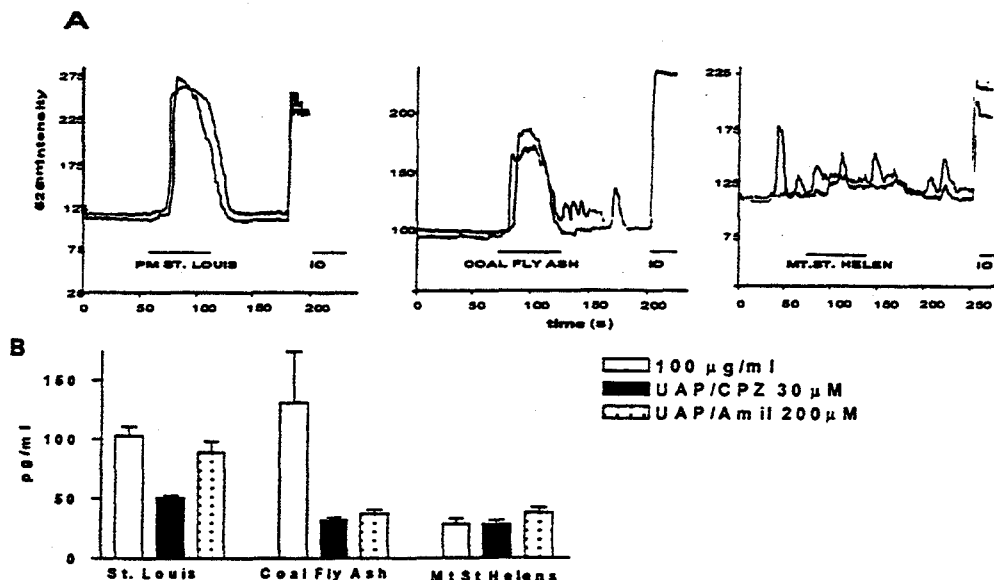


Figure 4: (A) Exposure of BEAS-2B cells to 50 µg/ml PM from St. Louis, Coal Fly Ash and Mt. St. Helen's dust caused a differential increase of $[Ca^{2+}]_i$. Depicted are representative examples of two individual cells for each PM exposure. (B) These PM also caused the release of IL-6 in BEAS-2B cells which was differentially inhibited by capsaizepine (CPZ, 30 µM) and amiloride (Amil, 200 µM).

Irritant receptors subserve strain-specific PM inflammation:

Airway pollutants are characterized by marked species and strain differences in their toxic response. We have recently shown a role for the irritant receptor in mouse-strain differences in response to industrial PM (Veronesi et al., 1999d). Using the mouse model of airway hyperresponsiveness, we first found that, in contrast to BALB/c mice, CD57Bl/6 (i.e., B6) mice were virtually non-responsive to equivalent concentrations of ROFA in terms of airway hyperresponsiveness and inflammatory cell influx obtained from bronchial lavage (Gavett et al., 1998). In keeping with our hypothesis that irritant receptors subserve PM inflammation, we proposed that there would be strain-specific differences in these receptors (i.e., quantitative, qualitative). To show this, we dissociated DRG from fetal BALB/c and B6 mice, cultured them at identical cell densities and exposed them to various irritants (e.g., capsaicin, acid pH) and a range of PM. These data showed that the mouse strain differences in response to PM noted *in vivo* were retained in culture (Figure 5).

Single cell recordings of increases in $[Ca^{2+}]_i$ were taken of cultured neonatal BALB/c and B6 mice in response to acid pH or capsaicin. These data showed that B6 mice had a significantly lower percentage of responding cells to the prototype irritants relative to the BALB/c neurons (data not shown). Collectively, these data not only underscored the role of sensory irritant receptors in PM airway inflammation but they also showed that the phenomenon of strain-specific sensitivity to PM described *in vivo* could be reproduced in cell culture.

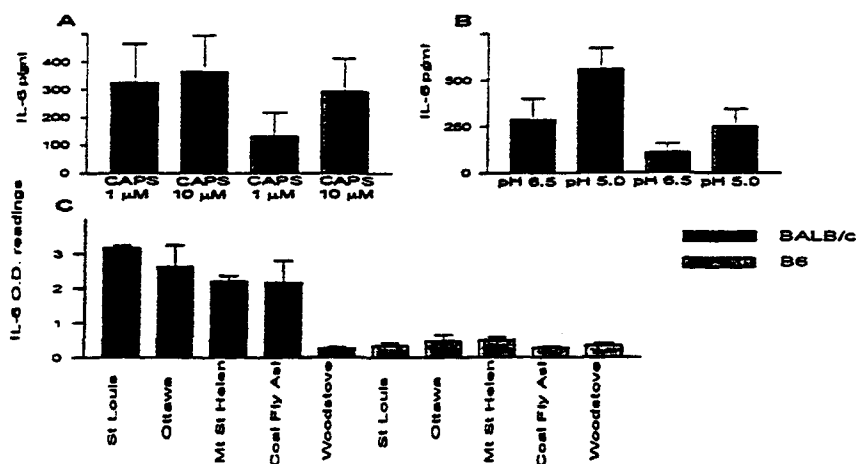


Figure 5: Release of IL-6 by BALB/c and B6 mouse DRG cultures after exposure to (A) capsaicin, (B) acid pH, and (C) various PM (50 μg/ml). DRG were cultured at identical cell densities, and exposed under identical conditions

Summary

This summary of our experiments to date, suggests a neuroimmunological explanation for PM toxicity. Data obtain from a variety of models indicate that acidic components associated with PM activate irritant sensitive receptors and pathways located on sensory nerve fibers and airway target cells (e.g., epithelium, alveolar macrophages). This activation initiates a cascade of inflammatory events associated with PM through the pathophysiology of neurogenic inflammation. We are currently collecting data to examine causal relationships between key physicochemical features of PM, activation of irritant receptors and release of proinflammatory cytokines. Additionally, we are pursuing the pivotal role of irritant receptors in the varying degrees of PM inflammation noted in different species and strains and examining factors that influence and modulate the sensitivity of these receptors to PM. Such data may offer insight into how predisposing or inherent conditions contribute to PM's susceptible subpopulations. In future studies, we will extend these observations and examine how PM's activation of irritant receptors located along sensory pathways and in higher neural centers influences cardiovascular function.

References

- Baluk P. 1997. Neurogenic inflammation in skin and airways. *J Investig Dermatol Symp Proc* 2:76-81.
- Baluk P, Nadel JA, McDonald DM. 1993. Calcitonin gene-related peptide in secretory granules of serous cells in the rat tracheal epithelium. *Am J Respir Cell Mol Biol* 8:446-453.
- Barnes PJ. 1991. Neurogenic inflammation in airways. *Int Arch Allergy Appl Immunol* 94:303-309.
- Becker S, Soukup JM, Gilmour MI, Devlin RB. 1996. Stimulation of human and rat alveolar macrophages by urban air particulates: effects on oxidant radical generation and cytokine production. *Toxicol Appl Pharmacol* 141:637-648.
- Bevan S, Hothi S, Hughes G, James IF, Rang HP, Shah K, Walpole CS, Yeats JC. 1992. Capsazepine: a competitive antagonist of the sensory neurone excitant capsaicin. *Br J Pharmacol* 107:544-552.
- Biro T, Brodie C, Modarres S, Lewin NE, Acs P, Blumberg PM. 1998b. Specific vanilloid responses in C6 rat glioma cells [In Process Citation]. *Brain Res Mol Brain Res* 56:89-98.
- Biro T, Maurer M, Modarres S, Lewin NE, Brodie C, Acs G, Acs P, Paus R, Blumberg PM. 1998a. Characterization of functional vanilloid receptors expressed by mast cells. *Blood* 91:1332-1340.
- Brauer M, Dumyahn TS, Spengler JD, Gutschmidt K, Heinrich J, Wichmann HE. 1995. Measurement of acidic aerosol species in eastern Europe: implications for air pollution epidemiology. *Environ Health Perspect* 103:482-488.

- Carter JD, Ghio AJ, Samet JM, Devlin RB. 1997. Cytokine production by human airway epithelial cells after exposure to an air pollution particle is metal-dependent. *Toxicol Appl Pharmacol* 146:180-188.
- Cesare P and McNaughton P. 1997. Peripheral pain mechanisms. *Curr Opin Neurobiol* 7:493-499.
- Dockery DW, Schwartz J, Spengler JD. 1992. Air pollution and daily mortality: associations with particulates and acid aerosols. *Environ Res* 59:362-373.
- Dreher KL, Jaskot RH, Kodavanti U., Lehmann JR, Winsett DW, Costa DL. Soluble transition metals mediate the acute pulmonary injury and airway hyperreactivity induced by residual oil fly ash particles. *Chest* 109, 33S. 1998.
- Dreher KL, Jaskot RH, Lehmann JR, Richards JH, McGee JK, Ghio AJ, Costa DL. 1997. Soluble transition metals mediate residual oil fly ash induced acute lung injury. *J Toxicol Environ Health* 50:285-305.
- Dye JA, Adler KB, Richards JH, Dreher KL. 1997. Epithelial injury by exposure to residual oil fly-ash particles - role of reactive oxygen species. *Am J Respir Cell Mol Biol* 17:625-633.
- Eichenbaum GM, Kiser PF, Simon SA, Needham D. 1998. pH and ion triggered volume response of anionic hydrogel microspheres. *Macromolecules* 31:5084-5093.
- el-Fawal HA, McGovern T, and Schlesinger RB. 1995. Nonspecific bronchial responsiveness assessed in vitro following acute inhalation exposure to ozone and ozone/sulfuric acid mixtures. *Exp Lung Res* 21:129-139.
- Gagnaire F, Ban M, Cour C, Micillino JC, Bonnet P, Hettich D. 1997. Role of tachykinins and neutral endopeptidase in toluene diisocyanate- induced bronchial hyperresponsiveness in guinea pigs. *Toxicology* 116:17-26.
- Gavett SH, Madison SL, Veronesi B. 1998. Capsaicin receptor antagonist and C-fiber depletion reduce pulmonary responses to particulate matter in BALB/c mice. *The Toxicologists* 18.
- Hatch GE, Boykin E, Graham JA, Lewtas J, Pott F, Loud K, Mumford JL. 1985. Inhalable particles and pulmonary host defense: in vivo and in vitro effects of ambient air and combustion particles. *Environ Res* 36:67-80.
- Holian A, Hamilton RFJ, Morandi MT, Brown SD, Li L. 1998. Urban Particle-induced Apoptosis and Phenotype Shifts in Human Alveolar Macrophages. *Environ Health Perspect* 106:127-132.
- Joad JP, Kott KS, Bric JM. 1996. The local C-fiber contribution to ozone-induced effects on the isolated guinea pig lung. *Toxicology & Applied Pharmacology* 141:561-567.
- Kimmel TA, Chen LC, Bosland MC, Nadziejko C. 1997. Influence of acid aerosol droplet size on structural changes in the rat lung caused by acute exposure to sulfuric acid and ozone. *Toxicol Appl Pharmacol* 144:348-355.
- Kodavanti UP, Jaskot RH, Costa DL, Dreher KL. 1997. Pulmonary proinflammatory gene induction following acute exposure to residual oil fly ash - roles of particle-associated metals. *Inhal Tox* 9:679-701.
- Lippmann M Thurston GD. 1996. Sulfate concentrations as an indicator of ambient particulate matter air pollution for health risk evaluations. *J Expo Anal Environ Epidemiol* 6:123-146.
- Lundberg JM. 1995. Tachykinins, sensory nerves, and asthma—an overview. *Can J Physiol Pharmacol* 73:908-914.
- Maggi CA. 1993. Tachykinin receptors and airway pathophysiology. *Eur Respir J* 6:735-742.
- Marz P, Cheng JG, Gadiant RA, Patterson PH, Stoyan T, Otten U, and Rose-John S. 1998. Sympathetic neurons can produce and respond to interleukin 6. *Proc Natl Acad Sci U S A* 95:3251-3256.
- Mudpalli A, Veronesi B, Becker S. Involvement of calcium and calcium channels in residual fly ash and silica-induced stimulation of human alveolar macrophages. *Third Colloquium on Particulate Matter and Human Health*. Durham NC. 1999.
- Mullol J, Baraniuk JN, Pitale M, Benfield T, Logun C, Picado C, Shelhamer JH. 1997. Vasoactive intestinal peptide (VIP) induces IL-6 and IL-8, but not G-CSF and GM-CSF release from a human bronchial epithelial cell line. *Neuropeptides* 31:119-124.
- Nielsen GD. 1991. Mechanisms of activation of the sensory irritant receptor by airborne chemicals. *Crit Rev Toxicol* 21:183-208.

- Oortgiesen M, Simon SA, Veronesi B. Physicochemical components of particulate matter contribute differentially to inflammatory responses in sensory neurons. *The Toxicologist*, 310. 1999b.
- Oortgiesen M, Veronesi B, Eichenbaum GM, Simon SA. 1999a. Residual oil fly ash (ROFA) and negatively charged synthetic polymers activate bronchial epithelial cells and nociceptive sensory neurons. *Am J Physiol* (submitted).
- Palma C, Minghetti L, Astolfi M, Ambrosini E, Silberstein FC, Manzini S, Levi G, Aloisi F. 1997. Functional characterization of substance P receptors on cultured human spinal cord astrocytes: synergism of substance P with cytokines in inducing interleukin-6 and prostaglandin E2 production. *Glia* 21:183-193.
- Prior M, Green F, Lopez A, Balu A, De Sanctis GT, Fick G. 1990. Capsaicin pretreatment modifies hydrogen sulphide-induced pulmonary injury in rats. *Toxicol Pathol* 18:279-288.
- Pritchard R, Ghio AJ, Lehmann JR, Winsett DW, Tepper JS, Park P, Girolomoni G, Dreher KL, Costa DL. 1996. Oxidant generation and lung injury after particulate air pollution exposure increase with the concentration of associated metals. *Inhal Tox* 8:457-477.
- Rahman Q, Norwood J, Hatch G. 1997. Evidence that exposure of particulate air pollutants to human and rat alveolar macrophages leads to differential oxidative response. *Biochem Biophys Res Commun* 240:669-672.
- Satoh H, Lou YP, Lundberg JM. 1993. Inhibitory effects of capsazepine and SR 48968 on citric acid-induced bronchoconstriction in guinea-pigs. *Eur J Pharmacol* 236:367-372.
- Scheerens H, Buckley TL, Muis T, Van Loveren H, Nijkamp FP. 1996. The involvement of sensory neuropeptides in toluene diisocyanate-induced tracheal hyperreactivity in the mouse airways. *Br J Pharmacol* 119:1665-1671.
- Sennet P, Olivier JP. 1965. Colloidal dispersions, electrokinetic effects and the concept of zeta potential. In: Ross S, editor. *Chemistry and physics of interfaces*. Washington, DC: American Chemical Society.
- Springall DR, Edginton JA, Price PN, Swanston DW, Noel C, Bloom SR, Polak JM. 1990. Acrolein depletes the neuropeptides CGRP and substance P in sensory nerves in rat respiratory tract. *Environ Health Perspect* 85:151-157.
- Stevens TP, McBride JT, Peake JL, Pinkerton KE, Stripp BR. 1997. Cell proliferation contributes to PNEC hyperplasia after acute airway injury. *Am J Physiol* 272:L486-L493.
- Su WY, Kodavanti UP, Jaskot RH, Costa DL, Dreher KL. 1995. Temporal expression and cellular distribution of pulmonary fibronectin gene induction following exposure to an emission source particle. *J Environ Pathol Toxicol Oncol* 14:215-225.
- Veronesi B, Carter J, Devlin RD, Simon SA, Oortgiesen M. 1999a. Neuropeptide, capsaicin and acidic pH stimulate the release of inflammatory cytokines in a human bronchial epithelial cell line. *Neuropeptides* (in press).
- Veronesi B, Carter JD, Devlin RD, Simon SA, Oortgiesen M. 1999c. Neuropeptides, capsaicin, and acidic pH stimulate the release of pro-inflammatory cytokines in a human bronchial epithelial cell line. *Am J Respir Cell Mol Biol*.
- Veronesi B, Oortgiesen M, Carter JD, Devlin RB. 1999b. Particulate matter (PM) initiates inflammatory cytokine release by activation of capsaicin receptors in a human bronchial epithelial cell line. *Toxicol Appl Pharmacol* 154:106-115.
- Veronesi B, Oortgiesen M, Simon SA, Madison S, Gavett S. 1999d. Vanilloid (capsaicin) and acid sensitive irritant receptors underlie mouse strain-sensitivity to particulate matter (PM). *The Toxicologist* 309.
- Wood JN, Docherty R. 1997. Chemical activators of sensory neurons. *Annu Rev Physiol* 59:457-482.
- Yeadon M, Wilkinson D, Darley-Usmar V, O'Leary VJ, Payne AN. 1992. Mechanisms contributing to ozone-induced bronchial hyperreactivity in guinea-pigs. *Pulm Pharmacol* 5:39-50.

**PARTICULATE MATTER INDUCTION OF PULMONARY GELATINASE A, GELATINASE B, AND
TISSUE INHIBITOR OF METALLOPROTEINASE EXPRESSION**

Wei-Yi Su,

Duke University Medical Center

Integrated Toxicology Program

Durham, NC 27710

Rick H. Jaskot and Kevin L. Dreher

U.S. Environmental Protection Agency

National Health and Environmental Effects Research Laboratory

Environmental Toxicology Division

Pulmonary Toxicology Branch, Mail Drop-82

Research Triangle Park, NC 27711

Running title: Metalloproteinase induction by particles

Corresponding to

Kevin L. Dreher, Ph.D.

U.S. EPA, NHEERL

ETD, PTB, Mail Drop-82

Research Triangle Park, NC 27711

Phone: (919)541-3691

Fax: (919)541-0026

E-mail: DREHER.KEVIN@epamail.epa.gov

This report has been reviewed by the National Health and Environmental Effects Research Laboratory, U.S. Environmental Protection Agency, and approved for publication. Approval does not signify that the contents reflect the views and policies of the Agency, nor does mention of trade names or commercial products constitute endorsement or recommendation for use.

ABSTRACT

Gelatinase A and B are capable of degrading type IV collagen and other major components of basement membrane. They are also involved in modulation of inflammation and tissue remodeling. We have reported that exposure to combustion particulate matter (PM) caused a significant induction of the fibronectin gene expression indicating an alteration of extracellular matrix (ECM). In addition, we have observed that matrilysin, one member of the metalloproteinase (MMP) family, was induced and activated early in rat lung after exposure to either combustion or ambient PM. The current study examines whether gelatinase A, B or tissue inhibitor of metalloproteinase (TIMP) are affected following exposure to PM. Sprague-Dawley rats were exposed to a combustion PM (residual oil fly ash, ROFA, 2.5 mg/rat) or saline by intratracheal-instillation and examined from 6 to 72 hr post-exposure. Induction of gelatinase A, gelatinase B, TIMP-1, and -2 was determined using reverse transcription-PCR. While gelatinase A and TIMP-1 are expressed constitutively in control animals, ROFA exposure increased their level of gene expression. However, gelatinase B was not expressed in control animals, but was significantly induced from 6 to 24 hr following ROFA exposure. TIMP-2 gene expression was suppressed by ROFA from 24 to 72 hr postexposure. Western blot analysis confirmed the presence of gelatinase A and B protein in lung tissue following ROFA exposure. Immunocytochemical analysis revealed that alveolar epithelial cells and inflammatory cells were major cellular sources for the pulmonary gelatinase A and B expression. To compare the effects of ambient PM with that of combustion PM and to further examine effects of ambient PM size on MMP induction, animals were treated with the same dose of the size-fractionated ambient PM ($PM_{<1.7}$, $PM_{1.7-3.7}$, $PM_{3.7-20}$ μm). Gelatinase A, B, and TIMP gene expression and cellular distribution were assessed using RT-PCR and immunocytochemistry, respectively. Interestingly, gelatinase B was induced significantly to the same extent by all three size-fractionated ambient PM. Gelatinase A and TIMP-1 expression were not changed while TIMP-2 expression was slightly decreased by $PM_{<1.7}$ and $PM_{1.7-3.7}$. Immunocytochemically, gelatinase A, B and TIMP-2 were localized mainly to the terminal bronchiole region and associated with inflammatory cells in ambient PM exposed animals. Thus, we have provided further evidence that MMP and TIMP expression were altered following exposure to either combustion or ambient PM supporting the hypothesis that MMP may be involved in pathogenesis of PM induced lung injury.

Key words: gelatinase, lung injury, particulate matter.

INTRODUCTION

Alteration of airway permeability and the induction of inflammation and fibrotic lesions are common pathological findings in animal models of combustion as well as ambient particulate matter (PM) caused lung injury (Dreher et al. 1997; Su et al. 1998; Su et al. 1995). Extracellular matrix degradation and reconstruction play a significant role during various stages of the complex processes. We hypothesized that induction and activation of matrix metalloproteinase (MMP) may play an important role in PM-induced lung injury. Previous studies have shown that exposure to combustion PM induced a significant fibronectin gene and protein expression (Kodavanti et al. 1997; Su et al. 1995). Recently, we have observed that matrilysin, one of the members of MMP, was induced and activated early in the rat lung after exposure to either combustion or ambient PM (Su et al. 1998). Altered MMP expression has been implicated in a variety of pulmonary disease conditions such as idiopathic pulmonary fibrosis (IPF) (Lemjabbar et al. 1999), pulmonary emphysema (Finlay et al. 1997), adult respiratory distress syndrome (ARDS) (Delclaux et al. 1997), and asthma (Hoshino et al. 1998). A direct role of MMP in animal models of lung injury has been established in immune complex-induced alveolitis (Gibbs et al. 1999), mineral fiber and cigarette smoke-caused lung injury (Morimoto et al. 1997), transgenic mice that overexpress collagenase and have a condition that resembles pulmonary emphysema in humans (D'Armiento et al. 1992), and hyperoxia caused lung injury (Pardo et al. 1998). We have examined the effects of PM exposure on induction of gelatinase A, B and tissue inhibitor of metalloproteinase (TIMP) to further characterize the role of MMP in PM-induced lung injury.

Gelatinase A (MMP-2) and B (MMP-9) are collagenases with the preferred substrates of type IV collagen, entactin, fibronectin, and laminin (D'Armiento et al. 1992), which are major components of basement membrane. Normally, gelatinase A is expressed basally in a variety of cells including epithelial cells, fibroblasts, macrophages, and neutrophils (Kumagai et al. 1999). Gelatinase B has a even lower level of basal expression, but can be induced in inflammatory cells and epithelial cells (Yao et al. 1996). Gelatinase A and B activity is tightly regulated, secreted in proenzyme and then activated in the extracellular environment. A distinctive post-translational regulation of gelatinase A and B is accomplished by their intrinsic inhibitors, TIMP, which bond with proenzymes as well as the active form of the enzyme. TIMP-1 and TIMP-2 are two major inhibitors, the structure and function of which have been well-characterized (Gomez et al. 1997).

Major goals of the present study were to examine whether gelatinase A, B and TIMP gene expression were altered following PM exposure; to identify the cellular distribution of gelatinase A, B and TIMP in the rat lung; and to determine differences between their induction following exposure to combustion and ambient PM.

MATERIALS AND METHODS

Animal and PM treatment

Sprague-Dawley male rats weighing 250 gm were purchased from Charles River Laboratory (Raleigh, NC) and were housed in an American Association for Accreditation of Laboratory Animal Care approved animal facility (72±2 °F, 50±5% relative humidity, 12 h light and dark cycle) during quarantine and after intratracheal (IT) instillation. All animals received a standard rat chow and water *ad libitum* before and during the experiments.

Combustion PM (residual oil fly ash, ROFA) was collected by Southern Research Institute, Birmingham, AL, using a Teflon-coated fiberglass filter downstream from the cyclone of a power plant in Florida which was burning a low sulfur #6 residual oil. The collection temperature was 204 °C. Physical and chemical properties of the combustion PM have been characterized previously (Dreher et al. 1997; Hatch et al. 1985). This combustion PM is characterized by high concentration of Ni, V and Fe sulfate, highly water soluble, and is acidic (pH~2.5) in the suspension used herein. A massive air volume sampler (MAVS) was used to collect gram quantities of size-fractionated ambient air PM (PM_{<1.7}, PM_{1.7-3.7}, PM_{3.7-20} µm). The MAVS was operated at a flow of 18.5 m³/min on the campus of Howard University in Washington, D.C. from the middle of May, 1995 to the middle of June, 1995. Animals were exposed to PM by intratracheal (IT) instillation using 0.3 ml of PM suspension at a dose of 2.5 mg/rat. IT instillation were performed as previously described (Costa et al. 1986). Control animals were IT-instilled with pyrogen-free saline.

Tissue preparation

At 3 to 72 h after IT-instillation, animals were anesthetized by i.p. pentobarbital injection (50-100 mg/kg of body weight), and exsanguinated by cutting the descending aorta. The right lung lobes were excised and quick frozen in liquid nitrogen for total RNA isolation using RNazol (Kodavanti et al. 1996). For immunocytochemistry, lung tissues were fixed *in situ* with 4% paraformaldehyde in PBS following cannulation of the trachea. The trachea was ligated and the intact lung was then removed and placed in 4% paraformaldehyde for overnight fixation at 4 °C. Lung tissues were subsequently processed for paraffin embedding. Four micron serial sections were mounted on Superfrost plus slides (Su et al. 1995).

Reverse transcription and PCR

Primer sequences for PCR were derived from published sequences in NCBI/Gene Bank using the software package Oligo 5TM (National Bioscience Inc., Plymouth, MN). These were gelatinase A: 5'-cgagaccgctatgccactgt-3' (Upper primer) and 5'-tcactgtccgccaataaacc-3' (Lower primer) (Marti et al. 1993); gelatinase B: 5'-gccaccaccgccaactatgac-3' (Upper primer) and 5'-tgggaggtgcagtggaacaca-3' (Lower primer) (Xia et al. 1996),

TIMP-1: 5'-gatatccgggttcgcctaca-3' (Upper primer) and 5'-ccccacagccagcact-3' (Lower primer) (Okada et al. 1994), and TIMP-2: 5'-gcaaccccatcaagaggat-3' (Upper primer) and 5'-cgcgcaagaacctact-3' (Lower primer) (Cook et al. 1994), and β -actin as house-keeping gene. The reverse transcription and PCR (RT-PCR) was carried out using total lung RNA and RNA-PCR Core Kit (Perkin Elmer Co., Norwalk, CT) according to manufacturer's specification. Briefly, total lung RNA (1.0 μ g) was reverse transcribed using MuLV reverse transcriptase and random hexamers in a total volume of 100 μ l for 45 min. PCR amplifications of gelatinase A, B, TIMP-1, TIMP-2, and β -actin were performed using each of a 10 μ l aliquot of cDNA from the same reverse transcription reaction to ensure minimum variability using a Perkin-Elmer thermal cycler (Model 480, Perkin Elmer Co., Norwalk, CT). PCR conditions were optimized to ensure that the amplifications were within linear range. The authenticity of each PCR product was verified by restriction enzyme site cleavage using specific six base pair recognition enzymes. The amplified DNA products were separated on 2% agarose gel, visualized by epifluorescent illumination, and recorded on a polaroid film (Polaroid Corp, Cambridge, MA).

Western blot analysis

Antibodies for gelatinase A and B were anti-peptide antibodies kindly provided by Dr. Stetler-Stevenson of NCI, NIH (Wacher et al. 1990). Rat lung tissue proteins were separated using 4-20% SDS-PAGE gradient gel (BioRad Laboratories, Hercules, CA) and transblotted to Immobilon-P membrane (Millipore, Bedford, MA). After blocking with 5 % dry milk in PBS, antibodies to gelatinase A (0.6 μ g/ml) and B (0.3 μ g/ml) in PBS containing 1% BSA were applied to the membrane for 1 hr. The membrane was washed and the goat anti-rabbit antibody conjugated with peroxidase (Cappel, Organon Teknika Corp., West Chester, PA) was applied (1:2,000 in PBS with 1% BSA) for 1 hr. The targeted protein bands were visualized and recorded on X-ray film using a ECL Western blot kit according to manufacturer's specification (Amersham Life Science, Arlington Heights, IL).

Immunocytochemistry of MMP and TIMP in lung tissue

Rat lung tissue sections were deparaffinized in xylene and rehydrated in graded ethanol. To block nonspecific binding of antibody, sections were incubated for 1 hour at room temperature with the 10% pre-immune serum in PBS. Antibodies to gelatinase A, B or TIMP-2 (Triple Point Biologics, Forest Grove, OR) were applied on tissue sections for 1 hour, followed by goat anti-rabbit IgG-biotin linker, for 20 min; and streptavidin-alkaline phosphatase, for 20 min. Tissue sections were rinsed 3 times in PBS, 5 min each during the intervals of antibody incubation. Detection of the antibody-target complex on tissue sections was accomplished using nitroblue tetrazolium and 5-bromo-4 chloro-3-indolyl phosphate toluidinium as the substrate for alkaline phosphatase as described previously (Su et al. 1995). The reaction product was a purple-brown color. Sections were counter

stained with methyl green, a light-green nuclear stain.

Data acquisition and analysis

DNA bands were digitized using a U-Max 1220 scanner with transparency adapter and quantified using the gel software UN-SCAN-IT™ (Silk Scientific, Inc. Orem, Utah). Gelatinase A, B, and TIMP expression were standardized with density values from their corresponding β -actin level observed in parallel RT-PCR reaction. The standardized gene expression was expressed as the relative mRNA level and presented in bar graphs as the mean (\pm standard error) of each group of treatments. For statistical analysis of data, either one-way ANOVA followed by Newman-Keuls multiple comparison test or t-test was applied. Statistical significance level was set at $p < 0.05$.

RESULTS

Gelatinase A, B and TIMP-2 gene expression induced by PM exposure

The gene expression of gelatinase A, B and TIMP was assessed from 6 to 72 hr following ROFA exposure (Figure 1A and 1B). There was a basal level of gelatinase A gene expression in the saline controls. Gelatinase A gene expression was increased as early as 6 hr after ROFA exposure and remain elevated for the observed period of time. In comparison, there was minimum basal level of gene expression of gelatinase B in saline-treated animals, but ROFA exposure induced a significant increase in gelatinase B gene expression that peaked at 6 hrs postexposure and returned to near control levels by 72 hr postexposure. To assess the expression of MMP inhibitors, TIMP-1 and TIMP-2 gene expression were examined. TIMP-1 gene expression paralleled the pattern of gelatinase A with a basal expression in control and an increased gene expression in ROFA treated groups. In contrast to TIMP-1, TIMP-2 gene expression was suppressed significantly from 24 to 72 hr following ROFA exposure.

Animals were exposed to the size-fractionated ambient air PM at the same dose as combustion PM to compare combustion PM with ambient air PM and to further examine the effect of ambient PM size on its capability to induce gelatinase and TIMP gene expression (Figure 2A and 2B). At three hours after PM exposure, gelatinase B gene expression was increased over control following exposure to all three ambient PM size fractions. However, there was no significant difference among three treatment groups. Gelatinase A and TIMP-1 expression were not significantly altered. Interestingly, TIMP-2 gene expression was slightly decreased in the two groups exposed to $PM_{<1.7}$ and $PM_{1.7-3.7}$.

Detection of gelatinase A and B by Western blot analysis

To examine translational regulation of gelatinase A and B, we assessed protein expression in lung tissue using Western blot analysis (Figure 3). Antibody to gelatinase A detected a major band of size 72 kD in saline control, which was compatible to the basal expression of gelatinase A proenzyme. The band density increased over time from 6 to 48 hr in ROFA treated groups. Gelatinase B protein expression was also detected in saline control and in ROFA treated animals in the size range of 92 kD which was compatible with gelatinase B proenzyme. Similarly, ROFA exposure appeared to increase gelatinase B protein level.

Cellular distribution of gelatinase A, B and TIMP-2

To further confirm in situ expression of gelatinase A, B, and TIMP-2 in rat lung and to identify their cellular distribution, we performed immunocytochemistry analysis of MMP (Figure 4). In saline control animals, there was a basal expression of gelatinase A, B or TIMP-2 which were focal, sporadic, and mainly in alveolar

epithelial cells (Fig 4, A, E, I). Twenty-four hour following exposure to ROFA, there was an increase in staining of gelatinase A both intracellularly and extracellularly. Under close examination, alveolar epithelial cells and inflammatory cells (mainly monocyte and macrophages) were responsible for gelatinase A expression (Fig.4, B). ROFA exposure also increased staining intensity of gelatinase B (Fig.4, F) and TIMP-2 (Fig.4, J) in the lung 24 hr postexposure. When compared to gelatinase A in the pattern of distribution, gelatinase B and TIMP-2 were more intracellularly distributed with less diffuse extracellular staining. Again, multiple cells including alveolar epithelial cells and monocyte/macrophages were stained positive for gelatinase B and TIMP-2. At 72 hr after ROFA exposure, there was still prominent staining of gelatinase A and B that was more concentrated in the proliferating alveolar epithelial cells (Fig.4, C, G). TIMP-2 staining was mainly in alveolar epithelial cells and cells in the thickened interstitium discernable as probable fibroblasts.

Following ambient PM exposure, there was an increased intensity of staining for gelatinase A, B as well as TIMP-2 (Fig.4, D, H, L). Interestingly, prominent protein staining of gelatinase A, B and TIMP-2 was located around terminal bronchioles where aggregates of ambient PM particles were present (Fig.4, D and H). Furthermore, gelatinase A, B and TIMP-2 were more induced in inflammatory cells when compared to epithelial cells as was observed in combustion PM treated lung.

DISCUSSION

We have demonstrated in the present study that both combustion and ambient air PM were capable of inducing and/or altering expression of gelatinase A, B as well as TIMPs in the rat lung. This study provided additional evidence supporting previous studies demonstrating that combustion PM exposure altered extracellular matrix gene (Su et al. 1995) and matrilysin (MMP-7) expression (Su et al. 1998). This and previous studies provided additional evidence supporting our hypothesis that induction/activation of metalloproteinases and the alteration of ECM of the lung may play an important role in combustion and ambient PM induced lung injury.

There appeared to be PM-related differences in the pattern of gelatinase A and B induction and their relative cellular distribution. Combustion PM exposure increased gelatinase A and B expression in a variety of lung cells (epithelial cells, inflammatory cells, interstitial cells) located throughout the lung regions while a similar dose of ambient air PM appeared to induce gelatinase A and B mainly in the inflammatory cells and around the terminal bronchioles where aggregates of PM were present. Given the good reproducibility of the intratracheal instillation technique (Costa et al. 1986) and the similar dosage, it seems unlikely that the observed differences were due to the initial PM distribution in the lung. More likely, differences in PM composition, solubility, physical and chemical properties underlie the distinctive observations. The combustion PM used in this study has a high content of transition metal elements including Fe, Ni, V and high water solubility, 94 % water soluble (Dreher et al. 1997). In contrast, the ambient PM has a greater than 90% of insoluble component and less metal. The water solubility of ROFA may have facilitated dispersion of PM to the peripheral region of the lung and explained the more extensive pulmonary response to combustion PM.

Ambient PM are complex aggregates of inorganic, organic and proteinaceous material. The coarse fraction ($PM > 2.5 \mu m$) is dominated by natural sources, while the fine fraction ($PM < 2.5 \mu m$) is dominated by anthropogenic emissions (Monn and Becker 1999). PM size has been a much debated issue in dosimetry, toxicity research and in the regulatory field. The conventional wisdom is that size of PM determines sites of PM deposition if inhaled and their composition, therefore influences PM toxicity. This study examined, in a simplified approach, whether ambient air PM from the same source but different size would vary in their respective abilities to induce gelatinase A, B or TIMP gene expression. While we did not find a significant difference in gelatinase A, B or TIMP-1 gene induction by the three size-fractionated ambient PM, we did observe a slight but statistically significant inhibition of TIMP-2 gene expression by the two smaller-sized ambient PM fractions ($PM_{<1.7}$ and $PM_{1.7-3.7}$). Our findings suggest that there may be somewhat greater potency of the smaller PM to alter TIMP-2 gene expression perhaps related to composition differences among size-fractionated ambient PM.

The induction of gelatinase A and B in the lung has been associated with pulmonary disease conditions in human and with experimental lung injury in animals. Delclaux et al. (1997) reported that gelatinase A and B activities were present in epithelial lining fluid of patients with ARDS and suggested that gelatinase might be involved in an increased alveolar-capillary permeability. In another study, Ohnishi et al. (1998) examined MMP localization in patients with pulmonary emphysema and found that gelatinase A and B levels were significantly higher in emphysema than in control subjects. Similarly, an increased expression of gelatinase A and B was also demonstrated in various interstitial lung diseases (Fukuda et al. 1998; Lemjabbar et al. 1999), and in asthma (Lemjabbar et al. 1999; Ohno et al. 1997). In addition, an increased expression and activity of gelatinase A and/or B were observed in several animal models of lung injury such as immune complex-induced alveolitis in rat (Gibbs et al. 1999), LPS-induced lung injury in guinea pigs (D'Ortho et al. 1994), and in hyperoxia induced pulmonary toxicity in rat (Pardoet al. 1998). Conversely, when TIMP-2 and secreted leukoprotease inhibitor (SLPI) were inhibited by antibodies conditions worsened in the model of immune complex-induced alveolitis (Gipson et al. 1999). In 1992, D'Armiento et al. (1992) demonstrated that transgenic mice overexpressing collagenase in their lungs developed morphologic changes strikingly similar to those associated with human pulmonary emphysema. These studies collectively indicate the importance of MMP in the pathogenesis of acute lung injury and its involvement in human pulmonary diseases.

The pathophysiological consequence of MMP induction and activation has been demonstrated by many studies. Gelatinase A and B can degrade most of ECM components in the basement membrane and interstitium of the lung including type IV collagen, entactin, laminin and elastin (Ohnishi et al. 1998). MMP can participate in activation of serine protease and other metalloproteinases, for example, stromelysin can activate serine protease and matrilysin can activate latent form of collagenase to their active form (Sang et al. 1996). The result is a cascade of reactions that increases the total pool of proteolytic activity in the lung. Gelatinase A, B and other MMP facilitate the release of the matrix-bound cytokines and growth factors such as $TNF\alpha$ and $TGF\beta$ (Goetzi et al. 1996; Imai et al. 1997). These cytokines and growth factors will have profound effects on the inflammatory response, epithelial and interstitial cell proliferation, and fibrosis which were all observed in our animal model of combustion PM-caused lung injury (Su et al. 1995). Moreover, MMP can also inactivate some intrinsic protease inhibitors such as $\alpha 1$ -protease inhibitor (α -PI) (Sires et al. 1994). Taken together, MMP activation can contribute to an increased proteolytic activity directly or indirectly by synergistic interaction with other proteases and by inactivation of intrinsic protease inhibitors resulting in an imbalance between protease and antiprotease, thus leading to tissue damage.

MMP, especially matrilysin, can activate a variety of biological mediators such as endothelin-1 which is a potent vasoactive peptide and has been implicated in the pathogenesis of cardiovascular dysfunction (Matsuura et al. 1992; Takahashi et al. 1993). Recently, Bouthillier et al. reported that exposure to ambient PM increased the plasma levels of endothelin-1 in rat (Bouthillier et al. 1998). These findings suggest that pathophysiological significance of pulmonary MMP induction may not be limited to the respiratory system but rather have a systemic consequence. Furthermore, the potential cardiopulmonary dysfunction that could be initiated by MMP via vasoactive factors including endothelin-1 may have a mechanistic implication in the PM exposure-related mortality observed in epidemiological studies (Dockery et al. 1993).

Our study provide evidence that gene expression of gelatinase A, B and TIMP were altered in both combustion and ambient PM-caused lung injury. The kinetics of induction and extensive cellular distribution of MMP suggested strongly the involvement of MMP in pathogenesis of PM induced lung injury.

ACKNOWLEDGMENTS

We would like to thank Dr. William Stetler-Stevenson of National Cancer Institute, National Institute of Health for kindly providing antibodies to gelatinase A and gelatinase B. We thank Mr. James Lehmann for his skillful intratracheal instillation, Dr. Urmila Kodavanti for RNA isolation from PM-treated rat lungs, and Dr. Dan L. Costa, Dr. Linda Birnbaum of NHEERL, US EPA and Dr. Guo-Bin Sun of University of North Carolina for their insightfull discussion and for critically reviewing of the manuscript. This work was partially supported by Duke-EPA Co-op #CT826514 (WY Su).

REFERENCES

- Bouthillier L, Vincent R, Goegan P, et al. 1998. Acute effects of inhaled urban particles and ozone: lung morphology, macrophage activity, and plasma endothelin-1. *Am J Pathol.* 153:1873-84.
- Cook TF, Burke JS, Bergman KD, Quinn CO, Jeffrey JJ, Partridge NC. 1994. Cloning and regulation of rat tissue inhibitor of metalloproteinases-2 in osteoblastic cells. *Arch Biochem Biophys.* 311:313-20.
- Costa DL, Lehmann JR, Harold WM, Drew RT. 1986. Transoral tracheal intubation of rodents using a fiberoptic laryngoscope. *Lab Anim Sci.* 36:256-61.
- D'Armiento J, Dalal SS, Okada Y, Berg RA, Chada K. 1992. Collagenase expression in the lungs of transgenic mice causes pulmonary emphysema. *Cell.* 71:955-61.
- Delclaux C, d'Ortho MP, Delacourt C, et al. 1997. Gelatinases in epithelial lining fluid of patients with adult respiratory distress syndrome. *Am J Physiol.* 272:L442-51.
- Dockery DW, Pope ACd, Xu X, et al. 1993. An association between air pollution and mortality in six U.S. cities. *N Engl J Med.* 329:1753-9.
- D'Ortho MP, Jarreau PH, Delacourt C, et al. 1994. Matrix metalloproteinase and elastase activities in LPS-induced acute lung injury in guinea pigs. *Am J Physiol.* 266:L209-16.
- Dreher KL, Jaskot RH, Lehmann JR, et al. 1997. Soluble transition metals mediate residual oil fly ash induced acute lung injury. *J Toxicol Environ Health.* 50:285-305.
- Finlay GA, O'Driscoll LR, Russell KJ, et al. 1997. Matrix metalloproteinase expression and production by alveolar macrophages in emphysema. *Am J Respir Crit Care Med.* 156:240-7.
- Fukuda Y, Ishizaki M, Kudoh S, Kitaichi M, Yamanaka N. 1998. Localization of matrix metalloproteinases-1, -2, and -9 and tissue inhibitor of metalloproteinase-2 in interstitial lung diseases. *Lab Invest.* 78:687-98.
- Gibbs DF, Warner RL, Weiss SJ, Johnson KJ, Varani J. 1999. Characterization of matrix metalloproteinases produced by rat alveolar macrophages. *Am J Respir Cell Mol Biol.* 20:1136-44.
- Gipson TS, Bless NM, Shanley TP, et al. 1999. Regulatory effects of endogenous protease inhibitors in acute lung inflammatory injury. *J Immunol.* 162:3653-62.
- Goetzl EJ, Banda MJ, Leppert D. 1996. Matrix metalloproteinases in immunity. *J Immunol.* 156:1-4.
- Gomez DE, Alonso DF, Yoshiji H, Thorgeirsson UP. 1997. Tissue inhibitors of metalloproteinases: structure, regulation and biological functions. *Eur J Cell Biol.* 74:111-22.
- Hatch GE, Boykin E, Graham JA, et al. 1985. Inhalable particles and pulmonary host defense: in vivo and in vitro effects of ambient air and combustion particles. *Environ Res.* 36:67-80.

- Hoshino M, Nakamura Y, Sim J, Shimojo J, Isogai S. 1998. Bronchial subepithelial fibrosis and expression of matrix metalloproteinase-9 in asthmatic airway inflammation. *J Allergy Clin Immunol.* 102:783-8.
- Imai K, Hiramatsu A, Fukushima D, Pierschbacher MD, Okada Y. 1997. Degradation of decorin by matrix metalloproteinases: identification of the cleavage sites, kinetic analyses and transforming growth factor-beta1 release. *Biochem J.* 322:809-14.
- Kodavanti UP, Jaskot RH, Bonner J, Badgett A, Dreher KL. 1996. Eosinophilic lung inflammation in particulate-induced lung injury: technical consideration in isolating RNA for gene expression studies. *Exp Lung Res.* 22:541-54.
- Kodavanti UP, Jaskot RH, Su WY, Costa DL, Ghio AJ, Dreher KL. 1997. Genetic variability in combustion particle-induced chronic lung injury. *Am J Physiol.* 272:L521-32.
- Kumagai K, Ohno I, Okada S, et al. 1999. Inhibition of matrix metalloproteinases prevents allergen-induced airway inflammation in a murine model of asthma. *J Immunol.* 162:4212-9.
- Lemjabbar H, Gosset P, Lechapt-Zalcman E, et al. 1999. Overexpression of alveolar macrophage gelatinase B (MMP-9) in patients with idiopathic pulmonary fibrosis: effects of steroid and immunosuppressive treatment. *Am J Respir Cell Mol Biol.* 20:903-13.
- Marti HP, McNeil L, Davies M, Martin J, Lovett DH. 1993. Homology cloning of rat 72 kDa type IV collagenase: cytokine and second-messenger inducibility in glomerular mesangial cells. *Biochem J.* 291:441-6.
- Matsuura A, Okumura H, Ashizawa N, Kobayashi F. 1992. Big endothelin-1-induced sudden death is inhibited by phosphoramidon in mice. *Life Sci.* 50:1631-8.
- Monn C, Becker S. 1999. Cytotoxicity and induction of proinflammatory cytokines from human monocytes exposed to fine (PM_{2.5}) and coarse particles (PM_{10-2.5}) in outdoor and indoor air. *Toxicol Appl Pharmacol.* 155:245-52.
- Morimoto Y, Tsuda T, Nakamura H, et al. 1997. Expression of Matrix Metalloproteinases, Tissue Inhibitors of Metalloproteinases, and Extracellular Matrix mRNA Following Exposure to Mineral Fibers and Cigarette Smoke in Vivo. *Environ Health Perspect.* 105S:1247-51.
- Ohnishi K, Takagi M, Kurokawa Y, Satomi S, Kontinen YT. 1998. Matrix metalloproteinase-mediated extracellular matrix protein degradation in human pulmonary emphysema. *Lab Invest.* 78:1077-87.
- Ohno I, Ohtani H, Nitta Y, et al. 1997. Eosinophils as a source of matrix metalloproteinase-9 in asthmatic airway inflammation. *Am J Respir Cell Mol Biol.* 16:212-9.

- Okada A, Garnier JM, Vicaire S, Basset P. 1994. Cloning of the cDNA encoding rat tissue inhibitor of metalloproteinase 1 (TIMP-1), amino acid comparison with other TIMPs, and gene expression in rat tissues. *Gene*. 147:301-2.
- Pardo A, Barrios R, Maldonado V, et al. 1998. Gelatinases A and B are up-regulated in rat lungs by subacute hyperoxia: pathogenetic implications. *Am J Pathol*. 153:833-44.
- Sang QA, Bodden MK, Windsor LJ. 1996. Activation of human progelatinase A by collagenase and matrilysin: activation of procollagenase by matrilysin. *J Protein Chem*. 15:243-53.
- Sires UL, Murphy G, Baragi VM, Fliszar CJ, Welgus HG, Senior RM. 1994. Matrilysin is much more efficient than other matrix metalloproteinases in the proteolytic inactivation of alpha 1-antitrypsin. *Biochem Biophys Res Commun*. 204:613-20.
- Su WY, Jaskot RH, Kodavanti UP, Costa DL, Dreher KL. 1998. Early induction of matrix metalloproteinase and TIMP gene expression by ambient air particles. *Am. J. Respir. Critical Care Med*. 157:A152 (Abs).
- Su WY, Kodavanti UP, Jaskot RH, Costa DL, Dreher KL. 1995. Temporal expression and cellular distribution of pulmonary fibronectin gene induction following exposure to an emission source particle. *J Environ Pathol Toxicol Oncol*. 14:215-25.
- Takahashi M, Matsushita Y, Iijima Y, Tanzawa K. 1993. Purification and characterization of endothelin-converting enzyme from rat lung. *J Biol Chem*. 268:21394-8.
- Wacher MP, Krutzsch HC, Liotta LA, Stetler-Stevenson WG. 1990. Development of a novel substrate capture immunoassay for the detection of a neutral metalloproteinase capable of degrading basement membrane (type IV) collagen. *J Immunol Methods*. 126:239-45.
- Xia Y, Garcia G, Chen S, Wilson CB, Feng L. 1996. Cloning of rat 92-kDa type IV collagenase and expression of an active recombinant catalytic domain. *FEBS Lett*. 382:285-8.
- Yao PM, Buhler JM, d'Ortho MP, et al. 1996. Expression of matrix metalloproteinase gelatinases A and B by cultured epithelial cells from human bronchial explants. *J Biol Chem*. 271:15580-9.

FIGURE LEGENDS

Figure 1. Combustion PM effects on gene expression for gelatinase A, B, TIMP-1 and -2 in combustion PM treated animals. A. Representative gel of RT-PCR products. Total RNA from lung tissues was analyzed for gene expression of gelatinase A, B, TIMP-1, TIMP-2, and β -actin using RT-PCR kit. B. The average of relative mRNA level following exposure to combustion PM. Each group represented an average of three animals for ROFA and two for saline-treatment. (*, significantly different from control, $p < 0.05$)

Figure 2. Ambient PM effects on gene expression for gelatinase A, B, TIMP-1 and -2 three hour postexposure to the size-fractionated ambient PM. A. Representative gel of RT-PCR products. Total RNA from lung tissues was analyzed for gene expression of gelatinase A, B, TIMP-1, TIMP-2, and β -actin using RT-PCR kit. B. The relative mRNA level induced following exposure to ambient PM. Each group represented an average of three animals for ambient PM and four for saline-treatment. (*, significantly different from control, $p < 0.05$)

Figure 3. Combustion PM induction of pulmonary gelatinase A and B protein. An equal amount of lung tissue protein was separated on 4-20% SDS-PAGE gel and transblotted to PVDF membrane. Anti-bodies to gelatinase A or B were used to identify gelatinase A (72 kD) and gelatinase B (92 kD) with ECL kit following manufacturer's specifications.

Figure 4. Cellular origin of PM-induced MMP and TIMP expression. Immunocytochemical analysis of gelatinase A, B, and TIMP-2 in rat lung tissue sections 24 and 72 hr following exposure to combustion or ambient PM. Paraffin lung sections were processed for immunocytochemical staining as detailed in Materials and Methods. A purple-brown colored deposit indicates a positive staining. Cellular distribution of gelatinase A, B and TIMP-2 in saline controls (A, E, I); combustion PM-treated rats at 24 hr (B, F, J); combustion PM-treated rats at 72 hr (C, G, K); and ambient PM-treated rats at 24 hr (D, H, L).

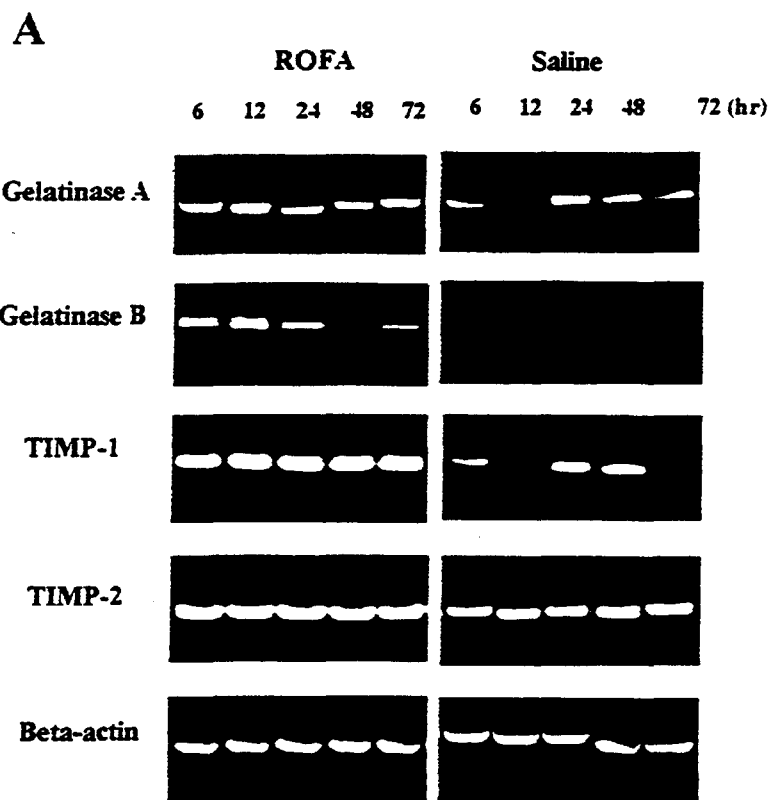


Figure 1-A

B

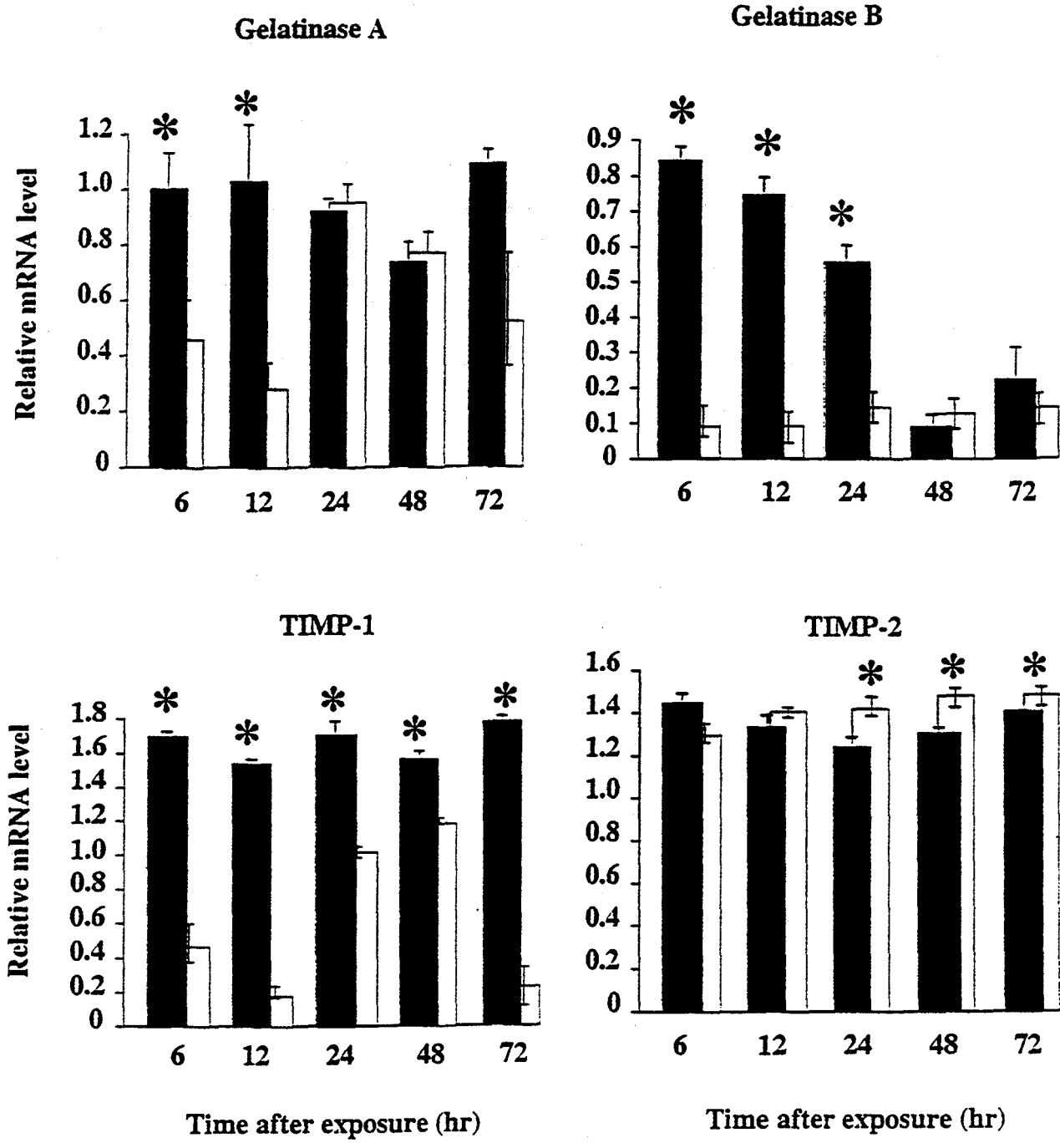


Figure 1-B

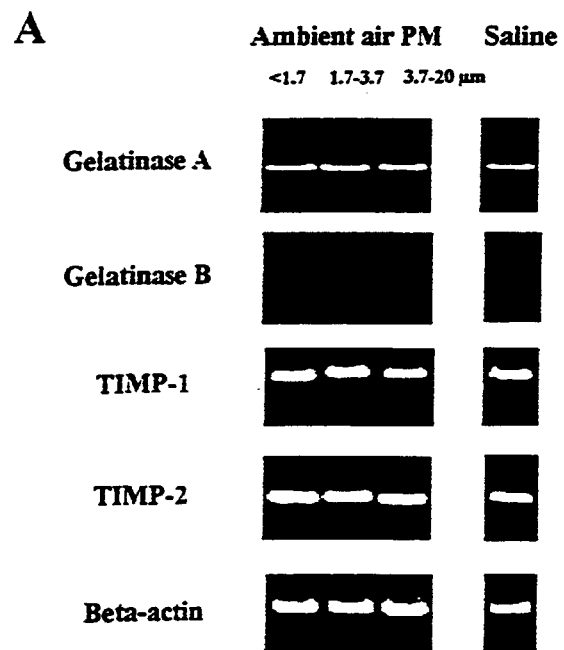


Figure 2-A

B

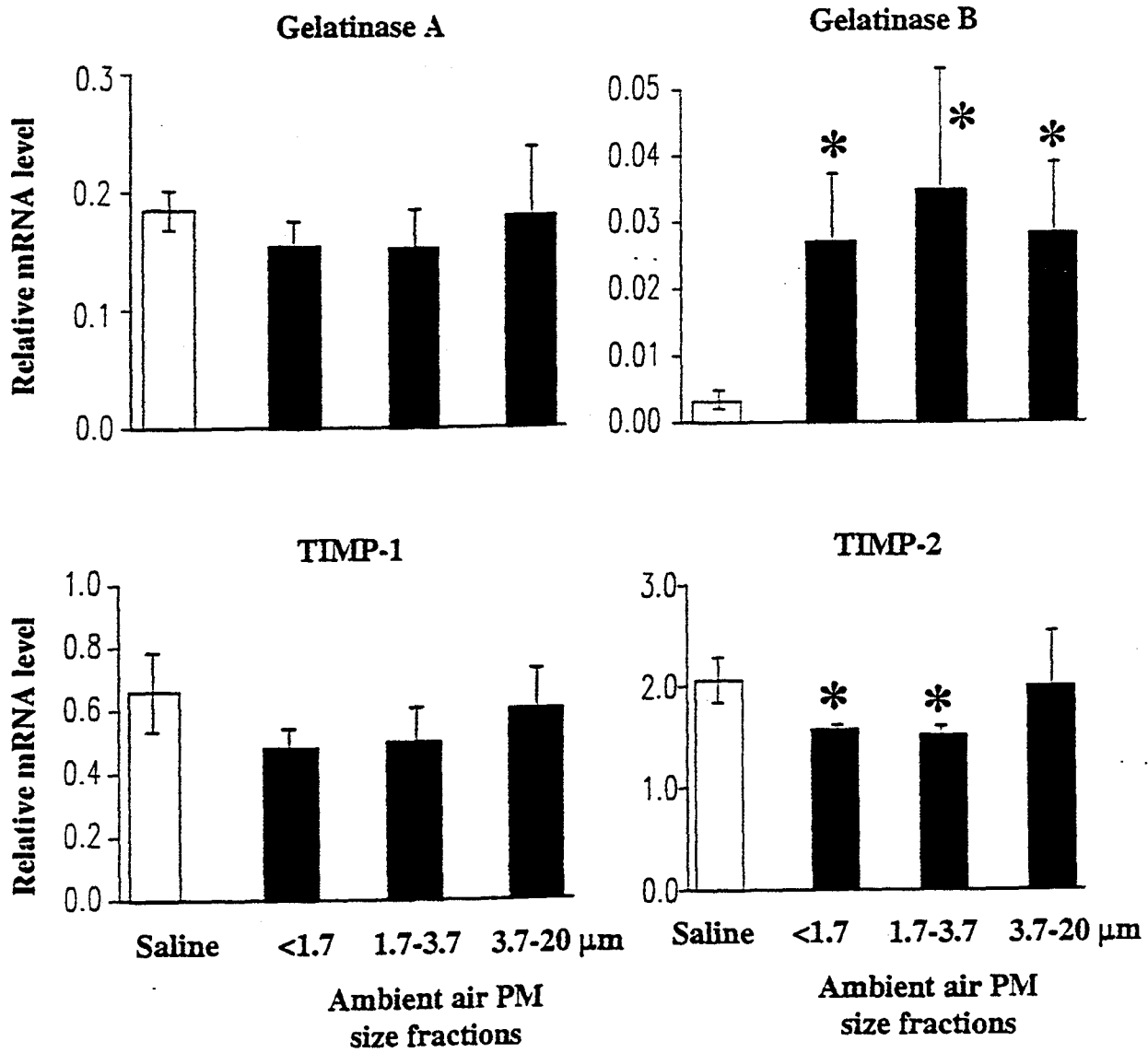


Figure 2-B

Gelatinase protein expression

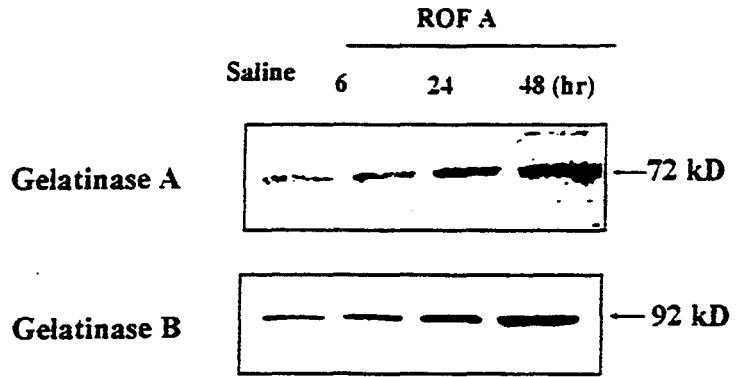


Figure 3

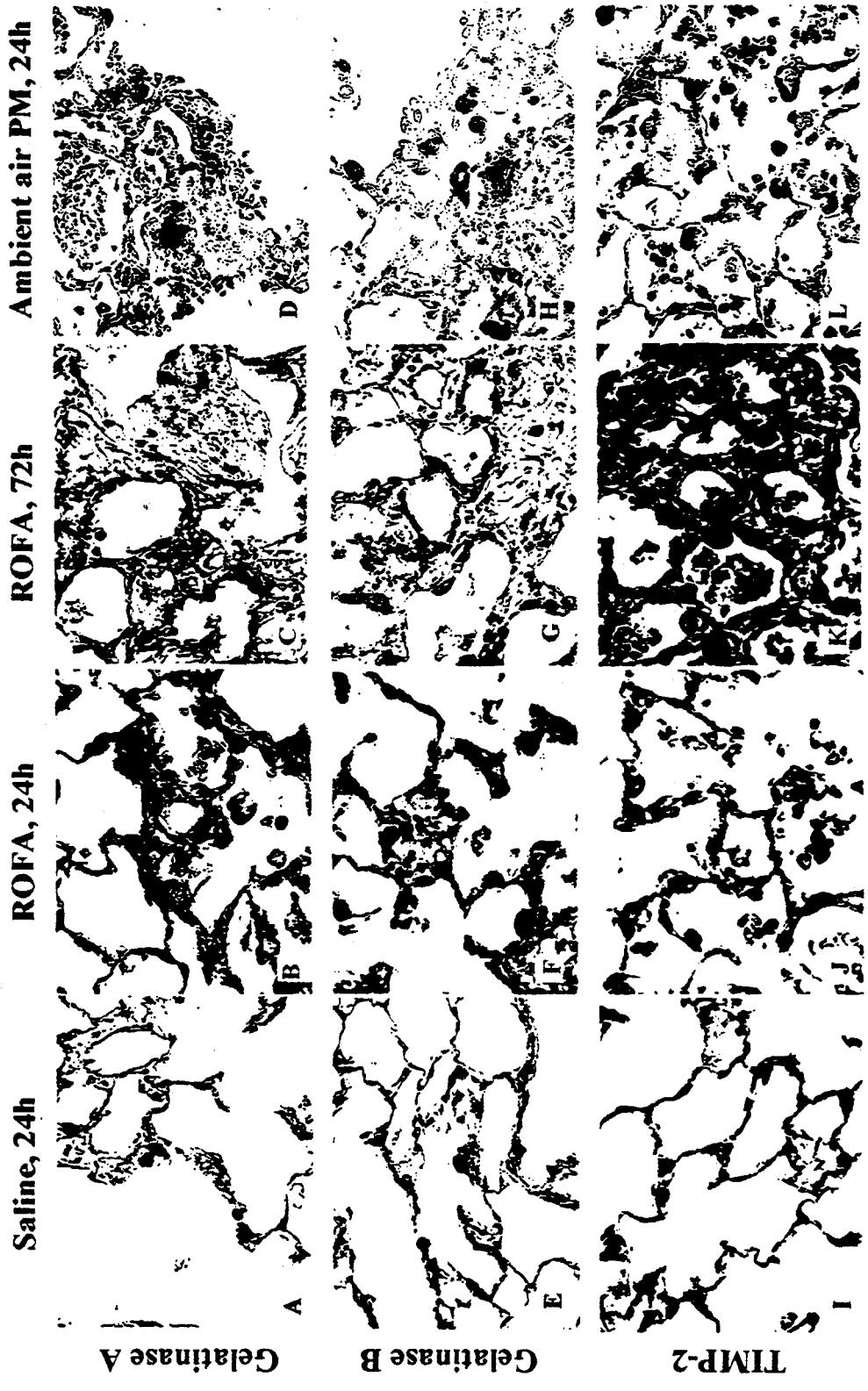


Figure 4
6-96

BRADYCARDIA, HYPOTHERMIA, AND IMMINENT DEATH IN AKR/J INBRED MICE

**Clarke Tankersley, Susan Flanders, Richard Rabold, Rafael Irizarry,
Ronald Berger, and Robert Frank**

**The Johns Hopkins Schools of Public Health and Medicine
Departments of Environmental Health Sciences, Biostatistics, and Cardiology**

ABSTRACT

Many recent epidemiological studies demonstrate a positive association between daily mortality rates and sudden increases in concentration of particulate matter (PM) in urban ambient air. This association is most prominent among the very elderly and in the presence of chronic cardiorespiratory disease states. We hypothesize that disease- and age-dependent loss of homeostasis, characterized in the present study by the loss of cardiac and thermal stability, signals imminent death in susceptible individuals, and therefore, may prove important in this epidemiological association. To test this hypothesis, we assessed cardiac and thermal homeostasis by describing the circadian pattern in heart rate (HR) and deep-body temperature (T_{db}) in AKR/J (AK) mice, an inbred strain predisposed to accelerated senescence. Radiotelemeters were surgically implanted in male AK mice ($n = 9$) at ~200 d of age to repeatedly measure HR and T_{db} . Measurements were acquired by a dedicated computer at 30 min intervals during 48 h periods 14 d following surgery and 3 d prior to natural death while each animal was maintained on a 12/12 light/dark cycle. Following surgery, the daily average HR at 14 d was 612 ± 7 bpm and the T_{db} was $36.7 \pm 0.1^\circ\text{C}$. Bradycardia and hypothermia were evident 3 d prior to death as the daily average HR and T_{db} was reduced to 460 ± 38 bpm and $32.5 \pm 0.9^\circ\text{C}$, respectively. In addition, there was a significant decay in the circadian pattern of each parameter 3 d prior to death. Thus, declines in daily average HR and T_{db} of 25% and 12%, and the decay in circadian pattern represented indicators of homeostatic incompetence, and signaled imminent death in AK mice. In conclusion, these findings suggest that bradycardic and hypothermic mechanisms predict an increased risk of mortality associated with senescence. Future studies will explore the role that environmental stressors such as PM exposure pose to exacerbate susceptibility to premature death.

The authors would like to acknowledge the constructive oversight provided by Drs. Ronald Wyzga and Tina Bahadori of the Electric Power Research Institute (WO8203-01). The authors would also like to recognize the resources provided by the NIEHS Center at the Johns Hopkins School of Public Health (ES03819).

INTRODUCTION

A positive association between daily mortality and airborne particulate has been found in many cities across the U.S. (e.g. Dockery et al., 1993; Pope et al., 1992) and in other industrialized nations (Borja-Aburto et al., 1997). The increase in mortality rate emerges during and immediately following sudden exacerbations in air quality. Efforts to identify specific constituents (e.g. air pollutant species or climatic conditions) of the environment which hasten death have not pointed to a plausible mechanism or culpable characteristic (Bates, 1995). Natural aging and preexisting cardiopulmonary disease appear to be important risk factors (Dockery and Pope, 1994; Utell and Samet, 1996). Therefore, our hypothesis focuses on individual susceptibility by suggesting that mortality provoked by reduced air quality is a characteristic operationally defined by an inability to maintain homeostasis during or closely following exposure to environmental stressors like airborne particulate.

We are developing an empiric model of homeostasis to test our hypothesis that impairment of key regulatory systems within the individual underlies a causal association between daily fluctuations in airborne particulate matter and mortality rate (Frank, 1997). Our objective in the present study is to identify individuals at risk of succumbing to modest levels of environmental stress. This preliminary report describes two homeostatic parameters, heart rate (HR) and deep-body temperature (T_{db}), and the age-dependent changes that occur in these parameters. The AKR/J inbred mouse strain has been routinely used as a model of aging owing to its unique shortened life-span (Takeda et al., 1981, Teramoto et al., 1992). Parameters of homeostasis such as HR and T_{db} can be measured repeatedly without eliciting an acute stress response. We initiated our studies by exploring the circadian oscillations in HR and T_{db} to operationally define homeostasis. The aims of the present study also included characterizing the decay in homeostasis by describing the age-dependent loss in circadian regulation of these parameters.

METHODS

Animals. Male, retired breeders of the AKR/J (AK) inbred strain were procured from Jackson Laboratories (Bar Harbor, ME) at ~200 days of age, and were housed in three different facilities; a microisolation facility, post-surgical facility, and another routine housing facility at the Johns Hopkins Medical Institutions. The ambient temperature and relative humidity of each housing facility was 22-23°C and 70-75%, respectively. We selected AK mice to control for genetic variability among individuals, and because this strain demonstrates accelerated senescence. All procedures used in the present study were reviewed and approved by the Animal Care and Use Committee at the Johns Hopkins School of Public Health.

Surgical procedures. Heart rate, T_{db} , and electrocardiographic (ECG) recordings were measured simultaneously using a transmitter implant and a radiotelemetry system (Data Sciences, International, St. Paul, MN). The dimensions of the transmitter (model TA10ETA-F20) were 2 cm long, 1 cm wide, and 0.7 cm deep, and its weight was ~3.5 g. The implant surgery was initiated by anesthetizing each animal with a mixture of

acepromazine (0.5 ml @ 10 mg/ml) and ketamine (5 ml @ 100 mg/ml) at a dose of $\sim 2 \mu\text{l/g}$ after obtaining the animal's pre-surgical weight. The hair covering the abdomen and chest wall was clipped, and further removed using a depilatory. Surgery was performed with the animal on a heating pad, betadine was applied to the exposed region of skin, and a sterile field was established surrounding the animal. A midline incision was made to open the intraperitoneal cavity, and the transmitter was inserted and sutured to the abdominal muscle. The negative ECG lead was guided through the muscle, and directed subcutaneously to the right shoulder. The positive ECG lead, also guided through the muscle, was directed laterally (left side), and positioned ~ 1 cm below the rib cage. Both leads were sutured to secure a lead placement resembling Lead II in traditional human ECGs. Surgery was completed within 30 min, and recovery from anesthesia generally occurred within 60-90 min. Following surgery, each animal was placed in a holding cage set upon a heating pad for the first 24 hr following surgery. Additional details concerning the instrumentation have been described elsewhere (Kramer et al., 1993).

Experimental Design. After 14 d of surgical recovery, control measurements for HR (verified by an ECG recording) and T_{db} were sampled for a 15 sec duration, and the average was reported at 30 min intervals. Time-dependent observations were used to evaluate the circadian pattern of HR and T_{db} as indices of cardiac and thermal stability. Activity counts represent an indication of the animal's physical movement within a 10-min interval. A majority of the sampling was collected during weekend periods beginning at 1700 hr on Friday and continuing to 0900 hr on Monday. The light/dark cycle of the housing facility was set on a 12/12 hr cycle with lights-off occurring at 1800 hr. Longitudinal data were summarized by computing a daily mean and range (i.e. minimum and maximum) for HR and T_{db} over two consecutive days.

Parameters of cardiac and thermal stability were recorded intermittently until each animal's death. The time of death for each animal was verified by a flat ECG, and data were retrospectively analyzed for a 48 h period 3 d prior to death.

Statistical Analyses. The data were summarized by computing the daily average HR and T_{db} , which represented the average of two consecutive 24 h periods for each phase of senescence. However, we are precluded from reporting p-values since our estimate of the daily average and the standard error of the mean (SEM) must be viewed with circumspection. For a given animal, within-day measurements are not independent, but instead, appear to follow a circadian pattern. Future work will include statistical models that account for circadian pattern, and generate confidence intervals for our estimate of SEM. Correlation coefficients were computed to evaluate the relationship between HR and T_{db} .

RESULTS

As shown in Figure 1, there were no detectable differences in life-span due to variation among housing facilities. In addition, the average (mean \pm SEM) life-span of the surgically-implanted animals (339 ± 15 d; $n = 17$) was not different from untreated controls (317 ± 17 d; $n = 25$). Inadvertent surgical deaths were not included in the determination of life-span among the surgically-implanted group. Experimental limitations that resulted

in incomplete data sets included faulty transmitters (e.g. dead battery) and an inadequate data sample to meet the 48 h interval 3 d prior to death. For the present study ($n = 9$), results for two time periods (i.e. 14 d after surgery and 3 d prior to death) were analyzed at an average age of 219 ± 3 d and 304 ± 9 d.

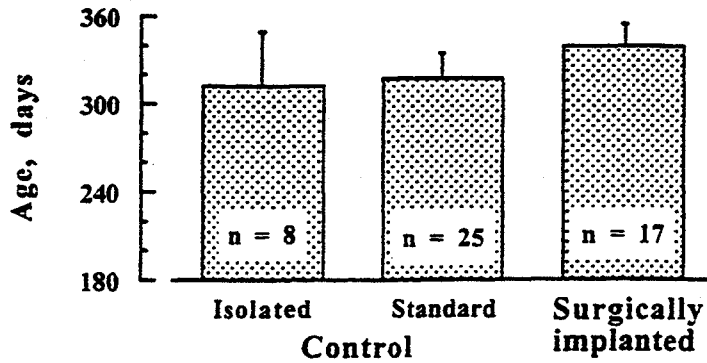


Figure 1. The average life-spans (\pm SEM) of control (no surgery) mice housed in a microisolation facility (i.e. isolated) or in a routine housing facility (i.e. standard) were not significantly different ($p < 0.05$) from surgically-implanted AKR/J mice. This strain demonstrated characteristics of accelerated senescence as defined by a substantially shortened life span.

In Figure 2, the average (i.e. over all individuals at each time point) circadian pattern in HR is illustrated. Following surgery, the circadian pattern in HR was tightly regulated between a minimum of 553 ± 13 and a maximum of 681 ± 15 bpm. Prior to death, HR was significantly ($P < 0.01$) depressed ranging between 399 ± 46 and 517 ± 43 bpm. The two time periods also differed with respect to the variance in HR among individuals within the group. At 14 days, there was a homogenous HR response among individuals as suggested by a relatively small group variance. With imminent death, there was a heterogenous HR response among individuals characterized by a relatively large group variance.

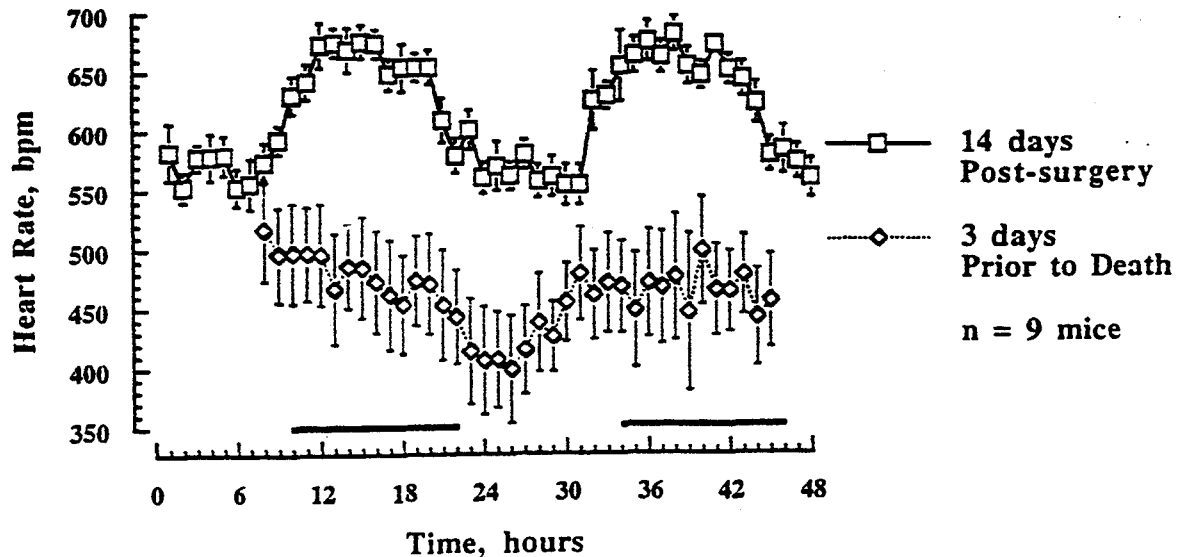


Figure 2. The average circadian pattern in heart rate (HR) for inbred AKR/J mice is illustrated for two periods: 14 d following surgery and 3 d prior to death. The circadian pattern in HR 14 d after surgery suggested that cardiac homeostasis is tightly regulated. However, a decline in cardiac homeostasis 3 d prior to death is indicated by a significant ($P < 0.01$) bradycardia. The group variance is significantly greater 3 d prior to death as compared to 14 d following surgery. The dark phase is represented by the black bars shown along the ordinate. Values are expressed as a means \pm SEM.

In Figure 3, the average circadian pattern in T_{db} is shown. The T_{db} response 14 d after surgery indicated that thermal homeostasis was tightly regulated between a minimum of $35.8 \pm 0.1^\circ\text{C}$ to a maximum of $37.7 \pm 0.1^\circ\text{C}$. The decline in thermal stability 3 d before death was characterized by a significant ($P < 0.01$) hypothermia ranging between $31.7 \pm 1.0^\circ\text{C}$ and $33.1 \pm 0.9^\circ\text{C}$. A loss in circadian regulation of T_{db} was also evident, such that the diurnal cycle was no longer synchronized to changes in the light/dark phase. As with HR at 14 d following surgery, the small group variance in T_{db} indicated a homogenous response among individuals. In contrast, there was a heterogenous T_{db} response among individuals approaching death as suggested by a relatively large group variance.

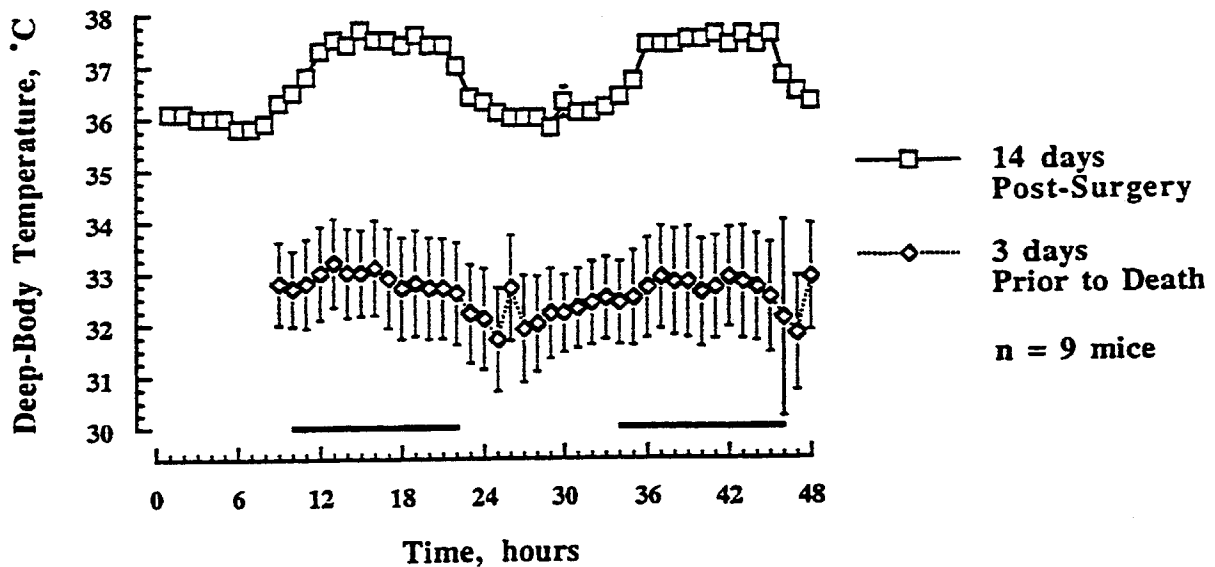


Figure 3. The average circadian pattern in deep-body temperature (T_{db}) is shown for inbred AKR/J mice. The T_{db} response 14 d after surgery suggested that thermal homeostasis was being tightly regulated. The decline in thermal stability 3 d before death was demonstrated by a significant ($P < 0.01$) hypothermia and loss of circadian pattern in T_{db} . The group variance in T_{db} was significantly increased with imminent death. The dark phase is represented by the black bars shown along the ordinate. Values are expressed as means \pm SEM.

The average circadian pattern in activity is illustrated in Figure 4. As expected the circadian pattern in activity 14 d following surgery was characterized by a peak which occurred at the latter stage of the dark phase. The activity approached zero during the light phase. The average activity was significantly ($P < 0.01$) diminished 3 d before death, and there was no observable change in the circadian oscillation of activity in response to the light/dark cycle. In contrast to HR and T_{db} , the group variance in activity 14 d following surgery was greater relative to the activity counts 3 d prior to death. These results suggest that inactivity is associated with imminent death; a response which is homogenous among individuals. Moreover, in this model, bradycardia and hypothermia cannot be attributed solely to reduced activity patterns.

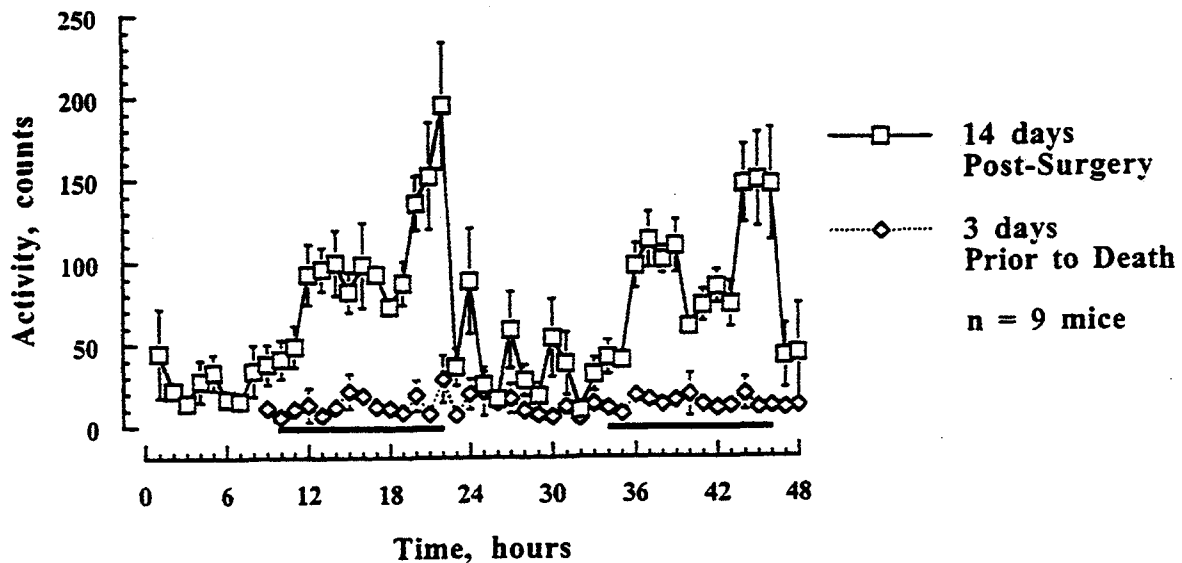


Figure 4. The average circadian pattern in activity is illustrated for AKR/J mice. The peak in activity occurred during the dark phase, and approached zero activity during the light phase. The average activity was significantly diminished 3 d before death, and there was no evident change in activity in response to the light/dark cycle. The dark phase is represented by the black bars shown along the ordinate. Values are expressed as means \pm SEM.

In Figure 5, the age-dependent change in the relationship between HR and T_{db} is shown. At 14 d following surgery, the correlation coefficient (r) suggest that HR and T_{db} were highly associated. The relationship between HR and T_{db} was similarly associated 3 d prior to death. Furthermore, the slopes for this relationship were comparable between different stages of the animal's life. However, differences in intercepts between the two time periods indicated that a leftward-shift in the HR to T_{db} relationship occurred with imminent death. Therefore, the within-day change in HR remained constant relative to a change in T_{db} with imminent death; however, the absolute HR was significantly greater for a given absolute T_{db} .

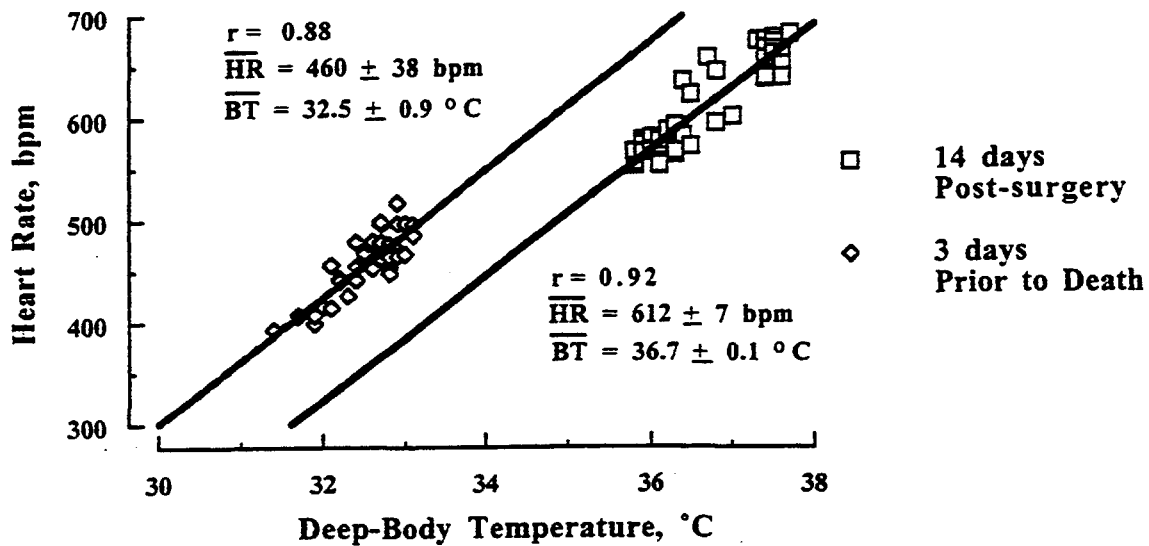


Figure 5. The relationship between HR and T_{db} is shown. The correlation coefficients (r) for both time periods suggest that HR and T_{db} were tightly interrelated. Although the absolute HR and T_{db} are lower with imminent death, the change in HR remained constant relative to a change in T_{db} . However, the HR at a given absolute T_{db} was elevated.

Discussion

The aim of the present study was to characterize the age-dependent changes in homeostasis in a laboratory animal model to mimic likely susceptibility factors that occur in humans facing chronic disease and natural aging processes. Homeostasis, an organism's capacity to maintain an optimal steady state or dynamic equilibrium, is eroded by disease and aging. As homeostatic loss progresses, the risk of dying increases (Doubal and Klemra, 1990). The accelerated aging observed in AK mice permits an experimental design where individuals can be tested repeatedly during relatively short periods of time when homeostasis is tightly regulated and later, during homeostatic decay. If a reasonably short-list of parameters can be used to define homeostasis operationally, it should be possible to identify increasing and severe instability in an organism. We found bradycardia and hypothermia were characteristics that signaled imminent death in AK mice.

Table 1 summarizes several criteria to evaluate altered cardiac and thermal stability. First, cardiac homeostasis can be defined by a daily average HR of 612 ± 7 bpm, and the HR is regulated with a circadian pattern (fig. 2). In contrast, a decay in cardiac homeostasis 3 d prior to death included bradycardia as suggested by a decline in the daily average HR of 460 ± 38 bpm, as well as a loss of circadian HR regulation. Secondly, the daily average T_{db} decreased from $36.7 \pm 0.1^\circ\text{C}$ at 14 d following surgery to $32.5 \pm 0.9^\circ\text{C}$ at 3 d prior to death indicating a substantial hypothermia. There was also a loss of circadian T_{db} regulation (fig. 3). Other characteristics of homeostatic decay in AK mice include a reduction in the average daily activity as well as a reduction in body weight with imminent death.

| | HR (bpm) | T_{db} (°C) | Activity (counts) | Body Weight (gms) |
|----------------------------------|--------------------|-------------------------------|-----------------------------|-----------------------------|
| 14 days Post-surgery | 612 ± 7 | 36.7 ± 0.1 | 67.3 ± 4.0 | 37.86 ± 1.0 |
| 3 days Prior to Death | 460 ± 38 | 32.5 ± 0.9 | 11.0 ± 3.1 | 32.04 ± 2.6 |

• Values are expressed as 48 hr averages (± SEM).

The regulation of circadian rhythms is considered essential to the maintenance of homeostasis. Circadian rhythm represents minute changes in a set-point, and these changes are associated with autonomic responses to environmental cues such as light and temperature variations. The result is a predictable, time-dependent oscillation in these set-points. The regulation of body temperature is an example. The regulation of HR is a key element in the maintenance of cardiovascular homeostasis. The decline in cardiac stability leading to persistent bradycardia may be due to a sympathetic-parasympathetic imbalance in the nervous control of HR or altered pacemaker cell function at the sinus node (Hardouin et al., 1998; Rodriguez and Schocken, 1990; Umetani et al., 1998). Age-dependent changes may include a reduction in cardiac β -adrenergic receptor responsiveness (Hardouin et al., 1998), which depresses the sympathetic or excitatory branch of HR regulation, as well as sick sinus syndrome (Rodriguez and Schocken, 1990). Both may contribute to age-dependent bradycardia.

Mature, healthy AK mice (219 ± 3 d of age) demonstrated circadian HR regulation that ranged between 550 and 675 bpm (fig. 2), a range similar to that reported in other mouse strains (Richards et al., 1953). The average excursion in circadian T_{db} ranged between 35.7° to 37.7°C (fig. 3) which may represent a strain-specific characteristic; that is, the maximum T_{db} appeared to be 0.4 - 1.1°C higher in AK mice relative to other mouse strains (Watkinson et al., 1996). Since HR and T_{db} are tightly synchronized to changes in the light/dark cycle, their regulation appears to be integrated.

A significant loss in the circadian regulation of both cardiac and thermal homeostasis was seen with imminent death. The associated fall in mean daily temperature may reflect impaired autonomic thermoregulation, which is mediated by the hypothalamus. The tendency toward a fall in body weight (table 1) may also indicate that hypothalamic

dysfunction is integral to the decay in homeostasis. The fall in HR and T_{db} cannot be solely attributable to a fall in activity, since at comparable levels of activity during the light phase both HR and T_{db} were consistently higher following surgery relative to periods prior to death. The age-dependent fall in activity and loss of circadian pattern observed in the present study has been demonstrated in other rodent species including another inbred mouse strain (Valentinuzzi et al., 1997).

To test whether or not the declines in HR and T_{db} are interdependent, we correlated the circadian change in HR and T_{db} at different phases of senescence. The correlation coefficients (fig. 5) approached 1 both in homeostasis and with imminent death. This result suggested that the within-day HR and T_{db} relationships were tightly coupled. Also, the change in HR remained constant relative to a change in T_{db} during both time periods. However, if the age-dependent fall in HR was simply a function of the decline in T_{db} , a lower HR would have been predicted (i.e. following the within-day linear trend established 14 d following surgery). The leftward-shift in the HR to T_{db} relationship that occurred with imminent death indicated the absolute HR was higher for a given absolute T_{db} . Collectively, these results suggest that the within-day HR to T_{db} relationship was similar between the two phases of senescence. However, the bradycardic response with imminent death was not solely dependent on the hypothermic response. Alternatively, there were likely independent factors that proportionally increased HR with imminent death.

In summary, the present study demonstrated that the imminence of death may be defined by the inability to maintain cardiac and thermal homeostasis. Specifically, bradycardia, hypothermia, and the loss of circadian HR and T_{db} regulation can be used to signal imminent death in AK mice. At this stage of advanced decline, HR and T_{db} remain interrelated; however, HR is shifted upward, possibly, to compensate for hypothermia. By operationally defining homeostasis using cardiac and thermal indices, we appear able to predict imminent death in inbred AK mice. Future studies will investigate the interaction between homeostatic loss and environmental stress including air pollutant exposure.

References

- Bates, D.V. Summary of the colloquium on particulate air pollution and human mortality and morbidity, Irvine, California, 24 and 25 January, 1994. Inhal. Toxicol. 7: ix-xiii, 1995.
- Borja-Aburto, V.H., D.P. Loomis, S.I. Bangdiwala, C.M. Shy, R.A. Rascon-Pacheco. Ozone, suspended particulates, and daily mortality in Mexico City. Am. J. Epidemiol. 145: 258-268, 1997.
- Dockery, D.W., A. Pope, X. Xu, J.D. Splengler, J.H. Ware, M.E. Fay, B.G. Ferris, and F.E. Speizer. An association between air pollution and mortality in six U.S. cities. N. Engl. J. Med. 329: 1753-1759, 1993.
- Dockery, D.W., and C.A. Pope. Acute effects of particulate air pollution. Ann. Rev. Pub. Health. 15:107-132, 1994.

- Doubal, S., and P. Klemra. Influence of aging rate change on mortality curves. Mech. Ageing Dev. 54: 75-85, 1990.
- Frank, R. The association between airborne particulate matter (PM) and daily mortality rate: an hypothesis.(Abstract). International Symposium on Health Effects of Particulate Matter in Ambient Air. p.29, 1997.
- Hardouin, S., F. Bourgeois, M. Toraasson, A. Oubenaissa, J.M. Elalouf, D. Fellmann, T. Dakhli, B. Swynghedauw, and J.M. Moalic. Beta-adrenergic and muscarinic receptor mRNA accumulation in the sinoatrial node area of adult and senescent rat hearts. Mech. Ageing Dev. 100: 277-297, 1998.
- Kramer, K., S.A. van Acker, H.-P. Voss, J.A. Grimbergen, W.J. van der Vijgh, and A. Bast. Use of telemetry to record electrocardiogram and heart rate in freely moving mice. J. Pharmacol. Toxicol. Meth. 30: 209-215, 1993.
- Pope, A., J. Schwartz, and M. Ransom. Daily mortality and PM10 pollution in Utah Valley. Arch. Environ. Health. 47: 211-217, 1992.
- Richards, A.G., E. Simonson, and M.B. Visscher. Electrocardiogram and phonogram of adult and newborn mice in normal conditions and under the effect of cooling, hypoxia and potassium. Am. J. Physiol. 174: 293-298, 1953.
- Rodriguez, R.D., and D.D. Schocken. Update on sick sinus syndrome, a cardiac disorder of aging. Geriatrics. 45: 26-36, 1990.
- Takeda, T., M. Hosokawa, S. Takeshita, M. Irino, K. Higuchi, T. Matsushita, Y. Tomita, K. Yasuhira, H. Hamamoto, K. Shimizu, M. Ishii, and T. Yamamuro. A new murine model of accelerated senescence. Mech. Ageing Dev. 17: 183-194, 1981.
- Teramoto, S., Y. Fukuchi, Y. Uejima, H. Ito, and H. Orimo. Age-related changes in GSH content of eyes in mice - a comparison of senescence-accelerated mouse (SAM) and C57BL/J mice. Comp. Biochem. Physiol. 102A: 693-696, 1992.
- Umetani, K., D.H. Singer, and R. McCarty, and M. Atkinson. Twenty-four hour time domain heart rate variability and heart rate: relations to age and gender over nine decades. J. Am. Coll. Cardiol. 31: 593-601, 1998.
- Utell, M and J. Samet. Airborne particle and respiratory disease: clinical and pathogenic considerations. In: Particles in Our Air: Concentrations and Health Effects. Eds: R. Wilson and J.D. Spengler. Harvard University Press. pp. 169-188, 1996.
- Valentinuzzi, V.S., K. Scarbrough, J.S. Takahashi, and F.W. Turek. Effects of aging on the circadian rhythm of wheel-running activity in C57BL/6 mice. Am. J. Physiol. 273: R1957-R1964, 1997.
- Watkinson, W.P., J.W. Highfill, R. Slade, and G.E. Hatch. Ozone toxicity in the mouse: comparing and modeling of responses in susceptible and resistant strains. J. Appl. Physiol. 80: 2134-2142. 1996.

VII. DOSIMETRY-RELATED PAPERS (SESSION 4)

Lungs from Residents of Mexico City Contain Large Quantities of Aggregated Ultrafine Particles

M. Brauer^{1,3}, B. Stevens², S. Vedal³, C Avila-Casado⁴, TI Fourtoul⁵, A. Churg². Occupational Hygiene Program¹, Depts of Pathology² and Medicine³, University of British Columbia, Vancouver, BC, Canada, Instituto Nacional de Cardiologia Ignacio Chavez, Mexico, DF, Mexico⁴, and UNAM, Mexico DF, Mexico⁵

Abstract

Epidemiological evidence has associated inhalable particulate (PM₁₀) air pollution with cardiopulmonary morbidity and mortality. The biological mechanisms underlying these associations are not clear nor is the relationship between ambient levels PM₁₀ and retained particles in the lung. To investigate this problem, we examined the mineral particle content in the parenchyma of 10 autopsy lungs from never smoking female residents of Mexico City, a region with high ambient PM₁₀ levels (3 year mean = 65 µg/m³), and 10 control residents of Vancouver, British Columbia, a region with relatively low PM₁₀ levels (3 year mean = 14 µg/m³). Autopsy lungs were dissolved in bleach and particles identified and counted by analytical electron microscopy. Lungs from both sites contained a variety of crustal type particles including silica, mica, talc, and particles of iron oxide and titanium dioxide. Total particle concentrations in the Mexico City lungs were significantly higher (geometric mean 2080, [GSD 4.2] vs 305 [1.9] x 10⁶ particles/gm dry lung). Lungs from Mexico City contained numerous chain-aggregated masses of ultrafine (geometric mean diameter 0.06µm) carbonaceous spheres, some of which contained sulfur; and aggregates of ultrafine (geometric mean diameter 0.06µm) aluminum silicate resembling kaolinite. These aggregates made up an average of 22% of the total particles (or the majority of particles if the individual particles in the aggregates were counted separately) in the lungs from Mexico City, but were never seen in lungs from Vancouver. These observations indicate for the first time that residence in a region with high levels of PM₁₀ results in pulmonary retention of large quantities of fine and ultrafine particle aggregates, some of which appear to be combustion products.

Introduction

Numerous epidemiological studies have indicated that current levels of particulate air pollution are associated with adverse health outcomes, including increased daily mortality (Utell and Samet, 1993; Dockery and Pope, 1994). Although much evidence points to a causal relationship, questions remain over biologic plausibility and the responsible agent(s) contained within particulate matter. Here we examine lungs from female, non-smoking, long-term residents of Mexico City, a region with high ambient particulate levels, and Vancouver, a region of much lower ambient particulate levels.

It is our hypothesis that exposure to high levels of PM₁₀ in Mexico City is reflected in increased interstitial particulate burdens. While this hypothesis may seem simplistic, there has been no direct demonstration that increased ambient particle exposure in fact results in higher particle retention (and, by implication, deposition) in the lung over a lifetime. Such a finding would provide pathological evidence to support the epidemiological data associating chronic particulate exposure to adverse health outcomes. This would provide additional evidence that the observed epidemiological associations are, in fact, biologically plausible. Failure to find significant

differences between the Vancouver and Mexico City populations, would lead to the conclusion that residence in an area of high ambient PM₁₀ is not associated with increased particle retention. This possibility would suggest either that the observed epidemiological associations may be driven by soluble particles (which would be cleared from the airways and parenchyma) or that the epidemiological findings are confounded and hence argue against their plausibility.

Recently, we used analytical electron microscopy to determine parenchymal particle burden in the lungs of 10 never-smoking long term residents of Vancouver, counting particles as small as 0.005 μm (Churg and Brauer, 1997). Our analysis of calculated aerodynamic diameters indicates that 96% of the retained particles are $<2.5 \mu\text{m}$ in aerodynamic diameter, therefore suggesting that epidemiological investigations should focus upon this size class of particles. Additionally we found that particles of $\leq 0.2 \mu\text{m}$ were almost entirely metallic (geometric mean diameter for iron, aluminum and titanium particles = 0.17 μm) whereas silica and silicate particles were larger (geometric mean diameter = 0.49 μm). Although, these size distributions do not match those found in ambient air for particles of combustion source (fine and ultrafine modes) and crustal (coarse mode) origin, the two distinct size fractions do suggest different origins of the different particulate species. In particular, these data argue that retained metallic particles originate in combustion processes. These observations therefore suggest that analysis of retained particles in lungs can be used to indicate the burden of both combustion-source and crustal particles.

It has recently been hypothesized that the ultrafine particle size fraction is responsible for the epidemiological observations. This hypothesis is partly based upon the fact that the majority of atmospheric particles, by number, are in the ultrafine mode. These particles, produced in combustion processes, are likely to contain condensates of toxic metals, as well as surface acidity. In animal models, ultrafine particles appear to induce an intense inflammatory reaction and are translocated to the pulmonary interstitium in large numbers (Ferein et al, 1992; Oberdorster et al, 1992). One postulated mechanism by which ultrafine particles may be responsible for morbidity and mortality associated with PM₁₀, involves alveolar inflammation which results in a release of mediators which increase blood coagulation (Seaton et al, 1995). Here we also test whether ultrafine particles are present in any greater numbers in lungs of subjects from a more highly polluted location.

Materials and Methods

Case Selection: Lungs for this study were obtained from a general autopsy service at a Cardiovascular referral hospital in Mexico City and compared to lungs obtained from a general hospital autopsy population in Vancouver. To avoid occupational dust exposures as much as possible, only lungs from women were examined. Occupational, smoking, and residential histories were obtained by interviews with relatives using a standardised questionnaire. All subjects were lifetime non-smokers, and none had had occupational dust exposure, including, for the Mexico City lungs, domestic wood smoke exposure. The lungs from Mexico were collected from women who had been lifetime residents of Mexico City while the lungs from Vancouver were from residents of Vancouver for 20 years or more. The mean ages were 80 ± 12 (SD) and 62 ± 9 years for Vancouver and Mexico City, respectively. None of the patients had died of lung disease, and the lungs were all morphologically normal except for the presence of minor degrees of pneumonia at autopsy.

Dissection Procedure: All tissues were handled with dust-free gloves. Dissections were performed on formalin inflated, well fixed, right lungs using a dissecting microscope. The Mexican lung samples consisted of central airways and parenchyma, and a sample of parenchyma weighing 1 to 2 grams was selected for analysis, along with an equivalent size sample that was dried to constant weight to allow expression of results as particles/gm dried tissue. A fairly central sample of upper lobe parenchyma was similarly selected from the control lungs,

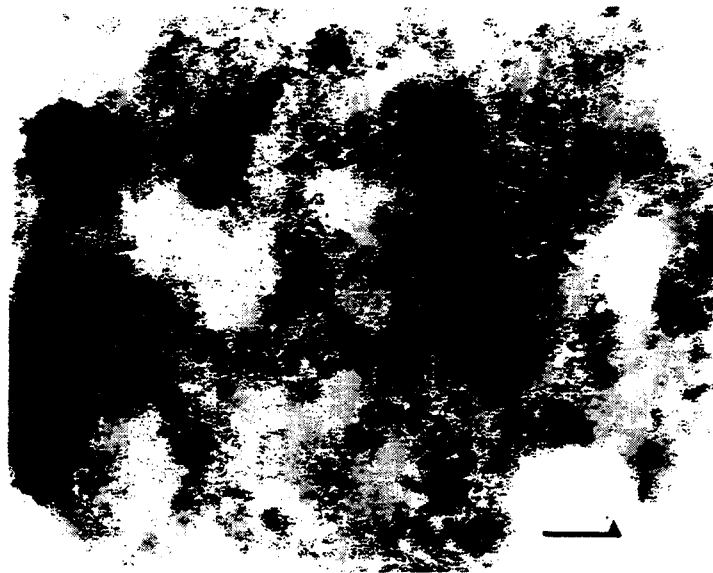
Tissue Dissolution and Particle Counting: Tissue samples were dissolved in bleach and centrifuged at 30,000 x g for 20 minutes; the sediment was washed once to remove the bleach and recentrifuged at 30,000 x g to ensure that very small particles were not lost during preparation. We have previously shown that 0.1 μm Millipore filters appear to give the best particle retention (Churg et al, 1990) and the initial preparation was resuspended and collected on 0.1 μm filters.

Particles were transferred from the Millipore filters to coated electron microscope grids. Particles larger than 0.010 μm were counted, sized, and identified using a Phillips 400T electron microscope equipped with Kevex energy dispersive x-ray spectrometer. Approximately 100 particles were counted per sample; particles were measured, and identified by a combination of morphology and chemistry as determined by x-ray spectroscopy. Numbers of particles/gm dry tissue were calculated using an algorithm relating weight of tissue utilized and numbers of squares of the electron microscope grid counted.

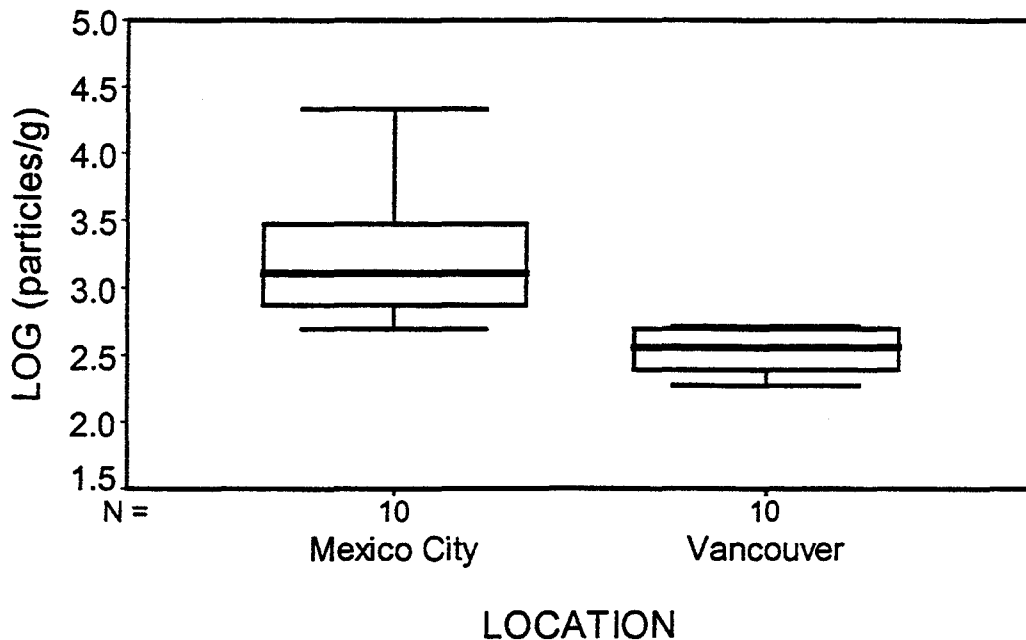
Results



Representative illustration of chained aggregated spherical particles giving no signal (i.e., carbonaceous particles) from a Mexico City lung. Bar = 0.15 μm



Representative illustration of aggregated aluminum silicate particles with a composition similar to that of kaolinite, from a Mexico City lung. Bar = 0.30 μ m



Concentration of particles/gram of dry tissue in Mexico City and Vancouver samples. Number below x-axis indicates the number of samples from each location. Top and bottom of box indicate the 25th and 75th percentiles, length of box is interquartile distance. Upper and lower box whiskers extend to the largest and smallest measured values that are 1 interquartile distance from 75th and 25th percentiles, respectively. Line inside box indicates the median value.

**Table 1: Particle Concentrations in Mexico City and Vancouver
(as Millions of Particles/Gm Dry Lung)***

| Case | Mexico City | Vancouver |
|-------------------------|-------------|-----------|
| 1 | 500 | 66 |
| 2 | 640 | 190 |
| 3 | 750 | 250 |
| 4 | 770 | 260 |
| 5 | 940 | 310 |
| 6 | 1800 | 430 |
| 7 | 2800 | 460 |
| 8 | 3000 | 500 |
| 9 | 22000 | 520 |
| 10 | 26000 | 530 |
| Geometric Mean (GSD) | 2080 (4.2) | 310 (1.9) |

*Particle aggregates in the Mexico City lungs were each counted as one particle for calculating concentrations

Table 2: Details of Aggregated Fine and Ultrafine Particles in Mexico City Lungs

| | Carbon aggregates 14.3% | Carbon aggregates with sulfur 3.5% | Kaolinite-like aggregates* 4.3% |
|--|-------------------------------|--|---------------------------------------|
| % of Total Particles | | | |
| Geometric mean particle diameter (μm) [GSD] | 0.057 [2.4] | | 0.055 [1.2] |
| Geometric mean aggregate diameter (μm) [GSD] | 0.39 [1.6] | | 0.59 [1.8] |

*Aluminum silicate particles with a composition and morphology similar to kaolinite

Conclusions

Total retained particulate burdens are significantly higher in lungs of individuals dwelling in Mexico City, but not in Vancouver.

Aggregates of ultrafine particles can be found in large numbers in the lungs of individuals dwelling in Mexico City, an area with high levels of PM₁₀, but not in Vancouver, an area of low PM₁₀.

Aggregated ultrafine particles make up the numerical majority of particles in the Mexico City lungs.

At least some of these particles appear to be combustion-derived as they are morphologically and chemically similar to particulates found in motor vehicle exhaust and industrial emissions. The origin of the kaolinite-like aggregates is not clear.

Acknowledgments

Supported by grants from the British Columbia Lung Association, the American Lung Association and the Medical Research Council of Canada

References

- Churg A, Wright JL, Stevens B. Exogenous mineral particles in the human bronchial mucosa and lung parenchyma, I: Nonsmokers in the general population. *Exp Lung Res* 1990; 16:169-173.
- Churg A, Brauer M. Human lung parenchyma retains PM_{2.5}. *Am J Resp Crit Care Med*, 1997; 155:2109-2111.
- Dockery DW and Pope CA. Acute respiratory effects of particulate air pollution. *Annu Rev Public Health* 1994; 15:107-132
- Ferin J, Oberdorster G, Penney DP. Pulmonary retention of ultrafine and fine particles in rats. *Am J Respir Cell Mol Biol*. 1992; 6(5):535-42.
- Utell MJ, Samet JM. Particulate air pollution and health. New evidence on an old problem. *Am Rev Respir Dis*. 1993; 147(6 Pt 1):1334-5.
- Oberdorster G, Ferin J, Gelein R, Soderholm SC, Finkelstein J. Role of the alveolar macrophage in lung injury: studies with ultrafine particles. *Environ Health Perspect*. 1992; 97:193-9.
- Seaton A, MacNee W, Donaldson K, Godden D. Particulate air pollution and acute health effects. *Lancet* 1995; 345:176-178.

Methodology for Delivery and Kinetics of Clearance of Insoluble Particles From Sublobar Lung Segments

WM Foster, K Macri, S McCulloch, T Myers and AN Freed

Department of Environmental Health Sciences, School of Hygiene and Public Health, The Johns Hopkins University, Baltimore, MD 21205

ABSTRACT

Anesthetized, mixed breed dogs were studied in a supine position, mechanically ventilated and imaged from the ventral aspect by γ -camera. Five dogs were evaluated; 4 of these were restudied to determine repeatability of the methods. A ventilation scan (^{133}Xe gas) was used to characterize the homogeneity of ventilation and to outline regions of analysis. An aqueous, insoluble radiolabeled aerosol ($^{99\text{m}}\text{Tc}$ -sulfur colloid) was generated by ultrasonic nebulization and delivered directly through a channel of a bronchoscope into sublobar bronchi. Lung retention of particles was measured continuously for ~1 hour, followed by recovery; and dogs were re-imaged at 6- and 24-hour time points post-deposition. After the initial hour of clearance, mean particle retention tended to be lower in left lung segments as compared to the right lung segments, i.e., 57.3% ($\pm 5.0\%$ SE) and 75.4% ($\pm 6.7\%$), respectively; however these differences were not significant. At 6-hour time post-deposition clearance was more comparable between lung segments, i.e., mean retention of 43.3% for the left versus 50.4% for the right lung segments. A small, additional amount of particle clearance occurred by the 24-hour endpoint; and the final mean retention levels were 34.8% and 47.1% for respective left and right lung segments. This technique assesses mucociliary clearance of aqueous aerosols delivered directly to the epithelial surfaces of sublobar bronchi.

INTRODUCTION

For particulate aerosols that deposit onto the epithelial surfaces of the respiratory tract, a complex defense system exists which is capable of dissolution and clearance of particles. The heterogeneous nature of the lung's structure and the mosaic pattern of the epithelial cell types that cover the airway surfaces can sometimes complicate interpretation of airway injury caused by inhalation of airborne particulate.

The fate of particles entered into the defense system depends upon the deposition site, solubility and the infectious, chemically reactive, or bland nature of the material, as well as physical characteristics of size and shape. Laboratory studies are difficult to design that investigate airway injury and decipher relationships between aerosol deposition and clearance (Foster and Freed, 1999). Our approach was to use bronchoscopic methods to deliver aerosol particles and thereby limit the deposition site(s) and by selecting to utilize insoluble particles, establish the kinetics of a single clearance route, i.e., airway mucociliary function. We modeled our approach after the method of Wolff and associates (1989). The objective of the research was two-fold. 1) Develop methodology for the delivery and assessment of clearance kinetics of insoluble particulate delivered by aerosol onto epithelial surfaces of sublobar lung segments. 2) Distinguish if regional differences in clearance occur during the initial hour after deposition and subsequently at reassessment, i.e., 6- and 24- hour time points post-deposition.

METHODS

Conditioned, mixed breed dogs ($n=7$, mean weight = 18.1 kg, 1-3 years of age) were lightly anesthetized with a thiopental sodium infusion ($4-6 \text{ mg}\cdot\text{kg}^{-1}\cdot\text{hr}^{-1}$) supplemented with fentanyl citrate ($25-50 \text{ }\mu\text{g}$ iv every 15-20 minutes) and intubated with a cuffed endotracheal tube. Dogs were ventilated with a mechanical volume respirator (tidal volume: $17 \text{ ml}\cdot\text{kg}^{-1}$ body weight). Alveolar ventilation was gauged by monitoring the end-tidal levels of respiratory gases. The dog was placed in a supine position and a γ -camera was aligned to image the chest from the ventral aspect. To properly position the camera a ^{133}Xe ventilation gas scan was acquired by ventilating the dogs from a gas mixture containing a fixed concentration of ^{133}Xe in room air. External markers were also demarcated on the chest to assist in re-positioning during subsequent imaging at 6 and 24 hr post inhalation of aerosol. Immediately following the ventilation scan a fiber-optic bronchoscope (5.5 mm OD; Olympus BF type PIO) was placed through the endotracheal tube and visually guided into a sublobar airway lumen (\sim diameter = 6.5 mm) of the left lower (LL) or right lower (RL) lobes of the lung. The tip of the bronchoscope was flexed towards an airway wall. An insoluble $^{99\text{m}}\text{Tc}$ technetium-labeled sulfur colloid aerosol was generated by an ultrasonic nebulizer (DeVilbiss, model 100) and added to a gas mixture of 5% CO_2 in air and at a flow rate of $200 \text{ ml}\cdot\text{min}^{-1}$. The aerosol-gas mixture was added to a channel of the bronchoscope and delivered to the sublobar airway lumen. During aerosol delivery (15 second) the respirator was stopped at end-expiration, followed by an additional 15 second of breath-hold time, before the respirator was turned back on. Immediately after aerosol delivery, the bronchoscope was unflexed and repositioned into the contralateral lower lobe bronchus. The bronchoscope tip was flexed as described above and aerosol was then delivered to the 2nd lobar airway lumen as done previously, i.e., 15 second of aerosol, followed by 15 second of breath hold. Aerosol delivered in this manner had a count mean diameter of $0.6 \text{ }\mu\text{m}$ and a $\sigma_g = 1.2$. The total time necessary to complete both aerosol deliveries was \sim 6-8 minutes.

Clearance of the ^{99m}Tc -sulfur colloid was monitored for approximately 60-70 minutes, after which the dogs were permitted to recover. At 6- and 24-hour time points post-delivery of aerosol, the dogs returned to the laboratory, were anesthetized as above (thiopental and fentanyl citrate), intubated and re-imaged for lobar retention of the labeled sulfur colloid.

RESULTS

Ventilation (^{133}Xe) scans demonstrated a uniform distribution of radioactivity. In contrast to the ventilation scan, the initial clearance image acquired immediately following deposition of the insoluble radio-labeled sulfur colloid aerosol, was not homogeneous and the radioactivity was focally distributed in sublobar regions. In Figure #1 representative plots of retention of the ^{99m}Tc -labeled colloid particles within sublobar bronchi (right lower and left lower) are presented. As shown in the figure, the rate of particle clearance from the lower left bronchus appeared to be more rapid for the initial 60 minute period after deposition of the particles, than for the lower right bronchus. This pattern held for the dogs evaluated with the protocol and although there was a trend for there to be right/left differences in retention at 1-, 6- and 24-hour time points post-deposition, differences in retention between right and left bronchi did not reach significance. This is shown in Figure #2 where the mean retention \pm SE of the particles within respective sublobar bronchi of 5 dogs (4 studied twice with the protocol and 1 evaluated once) at 1-, 6- and 24-hour time points post-deposition are indicated.

There was an association between the amount of radiolabeled material retained within sublobar bronchi at the 6- and 24-hour time points post-deposition and this is presented in Figure #3. A linear regression for the best fit to the relationship had a correlation coefficient equal to 0.848 ($P < 0.01$) and suggested the utility of the 6-hour retention level for predicting the final retention at 24 hours.

Four of the dogs were re-tested with the protocol and the mean retention data at 1-, 6- and 24-hour time points post-deposition are presented in figure #4 for the 2 retention studies in a given dog. These data demonstrate the reproducibility of the methods in the dog model.

DISCUSSION

The bronchoscopic aerosol delivery technique appears to be a reliable method in the anesthetized dog model for the administration of aqueous aerosol particles onto the epithelial surface of lower sublobar bronchi. Aerosols can be radiolabeled and clearance followed non-invasively by γ -camera for evaluation of airway mucociliary transport. The fractional retention of aerosol particles at the 24-hour time point post-deposition suggested that during the delivery of the aerosol there was some dispersal of the aerosol and particle deposition had occurred onto slowly clearing airway and alveolar epithelial surfaces.

Although the mean retention of particles within sublobar bronchi was not significantly different between lower right and left bronchi at the 1-, 6- and 24-hour time points post-deposition, there was a trend for mucociliary clearance to be faster from the lower left bronchus. However in part right to left differences in sublobar clearance may be related to penetration of the aerosol during delivery. Such that, aerosol particles that deposit less peripherally, have shorter path lengths to traverse to exit the segment and as suggested by prior *in vitro* studies (Asmundson and Kilburn, 1970) perhaps also clear at faster transport rates if deposited within larger airways. In support of this concept, the left sublobar segment (Figure #2) tended also to have a smaller fractional retention of particles at the 24 hour endpoint, i.e., during delivery of the aerosol, less penetrated and deposited within slowly clearing lung regions. In comparison to

other studies in the dog model, our retention data are comparable to the study reported by Wolff et al. These investigators also used a bronchoscopic technique to deliver labeled aerosol to sublobar airway surfaces of the right lower lobe. The major differences being that their aerosol was a mixture of 2 particles, monodisperse (diameters of 3 and 9 μm) in size and delivered as a dry dust, whereas our particles were polydisperse (mean diameter of 0.6 μm) in size and delivered as an aqueous aerosol. Wolff and associates found mean retention in the right lobe of 71 and 33% at the 6- and 24-hour measurement points, respectively. Even considering the differences between the aerosols, the retention results are comparable. For example, in the lower right segment we observed a mean retention of 75 and 47% at the 6- and 24-hour time points, respectively. The larger fractional retention at 24 hours in our study was likely attributable to greater peripheral penetration of the submicronic aerosol. Other techniques in the dog model have not used aerosols but rather liquid suspensions were sprayed onto airway surfaces with a bronchoscopic delivery (Lay et al., 1995; Snipes et al., 1996). However solutions sprayed onto epithelial airway surfaces estimate liquid clearance and epithelial transport that is separate of airway mucociliary function, and thus clearance kinetics are less informative for understanding kinetics and dosimetry of environmental particles that are inhaled as respirable aerosols and deposit onto tracheobronchial airway surfaces.

We suggest that the dog model and the bronchoscopic technique provide advantages to study mucociliary/particle clearance interactions by limiting the dose and localizing the delivery site of test aerosol particles. Although general anesthesia in the dog model has been noted to modify airway mucociliary clearance both *in vivo* (Forbes, 1979) and *in vitro* (King et al., 1979), in our study design the initial hour of clearance is subject to this complication. However the clearance that occurred between the 1st and 6th hour and 6th and 24th hour were not directly influenced by anesthetics. The utility of our methods is supported also by comparability to airway mucociliary clearance in the human. For example, similar to mucociliary clearance studies in human subjects (Svartengren et al., 1990), we found that particle retention levels at the 6-hour measurement point correlated to the final retention levels attained at 24-hour post-deposition. Lastly, although the sample size (n=4) was small, the reproducibility of the aerosol delivery methods and clearance within a given dog appeared to be good. An added advantage of our approach is that the resolution afforded by the γ -camera permits simultaneous assessment of mucociliary clearance within lung segments spatially separable by 2 dimensional imaging.

REFERENCES

- Asmundsson, T. and Kilburn, K.H. 1970. Mucociliary clearance rates at various levels in dog lungs. *Am. Rev. Resp. Dis.* 102:388-397.
- Forbes, A.R., and Gamsu, G. 1979. Mucociliary clearance in the canine lung during and after general anesthesia. *Anesthes.* 50:26-29.
- Foster, W.M., and Freed, A.N. 1999. Regional clearance of solute from peripheral airway epithelia: recovery after sublobar exposure to ozone. *J. Appl. Physiol.* 86:641-646.
- King, M., Engel, L.A., and Macklem, P.T. 1979. Effect of pentobarbital anesthesia on rheology and transport of canine tracheal mucus. *J. Appl. Physiol.* 46:504-509.
- Lay, J.C., Berry, C.R., Kim, C.S., and Bennett, W.D. 1995. Retention of insoluble particles after local intrabronchial deposition in dogs. *J. Appl. Physiol.* 79:1921-1929.
- Snipes, M.B., Spoo, J.W., Muggenburg, B.A., Nijkula, K.J., Hoover, M.D., Griffith, W.C., and Guilmette, R.A. 1996. Evaluation of the clearance of particles deposited on the conducting airways of beagle dogs. *J. Aer. Med.* 9:477-499.

- Svartengren, M., Anderson, M., Bylin, G., Philipson, K., and Camner, P. 1990. Regional deposition of 3.6 μm particles in subjects with mild to moderately severe asthma. *J. Aer. Med.* 3:197-207.
- Wolff, R.K., Tillquist, H., Muggenburg, B.A., Harkema, J.R., and Mauderly, J.L. 1989. Deposition and clearance of radiolabeled particles from small ciliated airways in beagle dogs. *J. Aer. Med.* 2:261-270.

ACKNOWLEDGEMENT

The research was supported by National Institute of Environmental Health Sciences, ES-03819 and by National Heart, Lung, and Blood Institute, HL-50579.

FIGURE LEGENDS

Figure #1. Representative Plot of Retention of ^{99m}Tc -particles in Sublobar Bronchi. The fractional retention versus time for sublobar bronchi (lower right and left as indicated) during the initial 60 min of mucociliary clearance post-deposition and at the subsequent time points, 6- and 24-hour post-deposition. Retention is expressed as a fraction of the amount initially deposited onto the epithelial surfaces at $T = 0$; retention data have been corrected for background and isotopic decay.

Figure #2. Particle Retention within Lower Right and Left Sublobar Bronchi. Mean retention \pm SE of particles within respective sublobar bronchi of 5 dogs (4 studied twice and 1 evaluated once) at 1-, 6- and 24-hour time points post-deposition.

Figure #3. Association between Particle Retention at 6 hr and 24 hr Time Points. Includes the retention data for both lower right (solid circle) and left (triangle) sublobar bronchi. Solid line, linear regression of best fit to the relationship, and correlation coefficient are indicated for respective relationship. The presented data are based upon 4 dogs studied twice and one dog evaluated once.

Figure #4. Repeatability of Clearance of ^{99m}Tc -aerosol from Lower Left and Right Sublobar Bronchi. Mean retention data ($n=4$ dogs) at the indicated time points are compared for study 1 vs. study 2 for lower left (upper panel) and lower right (lower panel) sublobar bronchi.

FIG. #1.

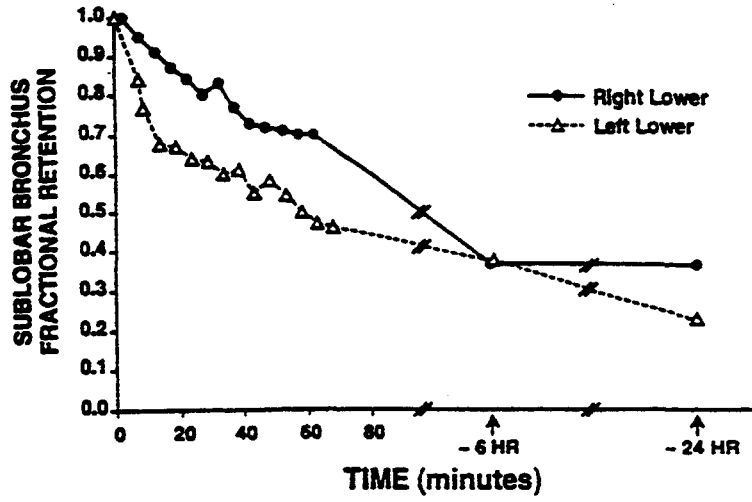


FIG. #2.

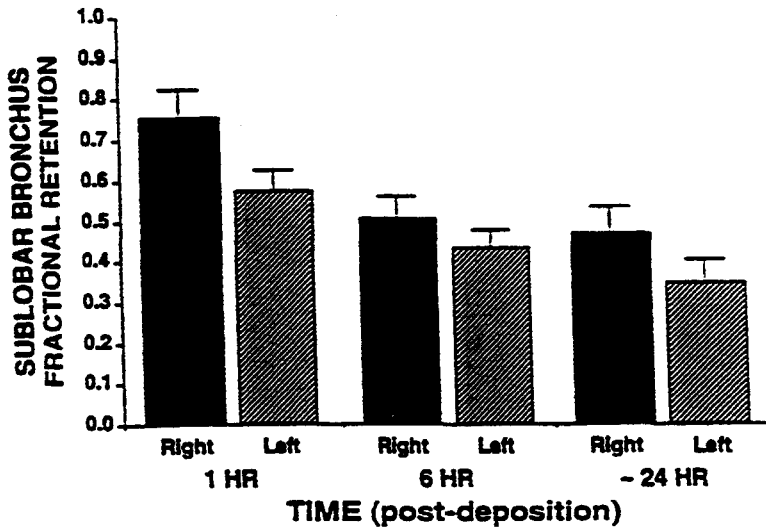


FIG. #3.

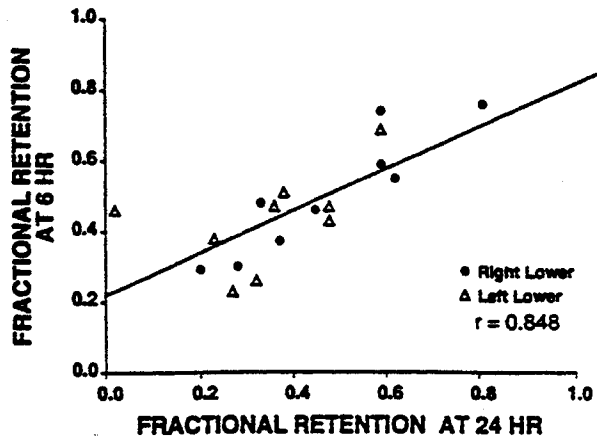
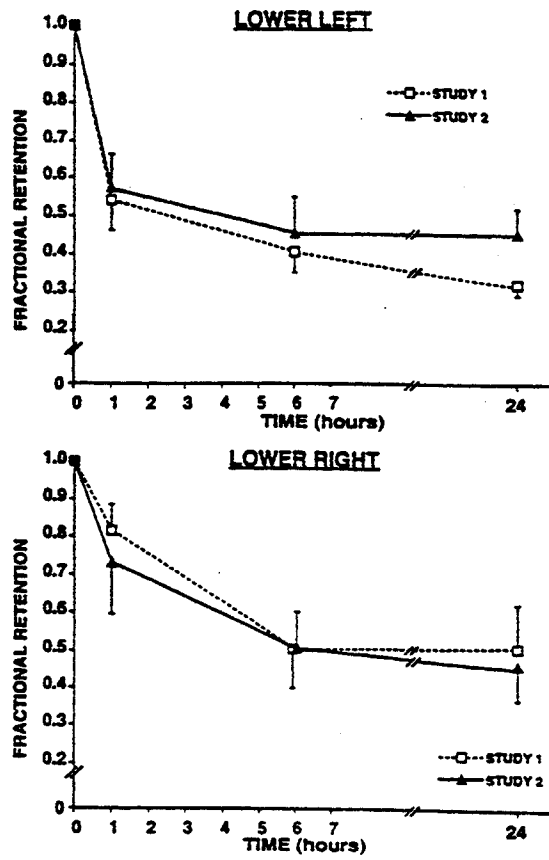


FIG. #4.



Predicted Deposition Patterns Of Ambient Particulate Air Pollutants In Children's Lungs Under Resting Conditions

C. J. Musante

University of North Carolina, Curriculum in Toxicology, Chapel Hill, North Carolina, USA

T. B. Martonen

U.S. Environmental Protection Agency, National Health and Environmental Effects Research Laboratory, Experimental Toxicology Division, Research Triangle Park, North Carolina, USA

We have developed an age-dependent theoretical model to predict particle dosimetry in children's lungs. Algorithms that define the morphologies of growing human lungs have been derived; that is, computer codes describe the dimensions of individual airways and the geometries of branching airway networks within lungs. Likewise, breathing parameters have been formulated as functions of human subject ages. The results of computations indicate that particle sizes, subject ages, and ventilatory conditions affect the deposition patterns of inhaled air pollutants. Herein, we compare particle deposition efficiencies for monodisperse aerosols ranging from 0.25-5 μm in the lungs of children and adults under resting conditions. As an example, for 1- μm particles inhaled at a sedentary activity level, total (i.e., lung) deposition is 21% in an adult but is 29% in a 48-month-old subject, a relative increase of 38%. Total deposition can also be broken down into its tracheobronchial (TB) and pulmonary (P) components. For toxicological reasons it is important to determine compartmental dose because the TB and P airways have different clearance processes (i.e., mucociliary transport and macrophage action, respectively). The results of such simulations may provide a basis for integrating children into regulatory standards for air pollutants.

Deposition patterns of inhaled particulate matter (PM) in children's lungs are not well known (National Research Council, 1998). The experimental dosimetry data available suggest that

DISCLAIMER: This manuscript has been reviewed in accordance with the policy of the National Health and Environmental Effects Research Laboratory, U.S. Environmental Protection Agency, and approved for publication. Approval does not signify that the contents necessarily reflect the views and policies of the agency, nor does mention of trade names or commercial products constitute endorsement or recommendation for use.

C. J. Musante's research was funded by the EPA/UNC Toxicology Research Program, Training Agreement CT902908, with the Curriculum in Toxicology, University of North Carolina at Chapel Hill.

Address correspondence to Cynthia J. Musante, Ph.D., c/o U.S. Environmental Protection Agency, National Health and Environmental Effects Research Laboratory, Experimental Toxicology Division, Mail Drop 74, 86 T. W. Alexander Drive, Research Triangle Park, NC 27711 USA. E-mail: musante.cynthia@epa.gov

children have greater deposition efficiencies than adults under resting conditions (Becquemin et al., 1986; Schiller-Scotland et al., 1994), and therefore may be more susceptible to adverse health effects from environmental pollutants. Epidemiological investigations lend further support to a relationship between outdoor air pollution and respiratory illnesses in children (Bates, 1995; Koren, 1995). As a result, the US Environmental Protection Agency has identified children as a sensitive subpopulation to be addressed in the determination of regulatory standards for air pollutants (Browner, 1996).

Therefore, an age-dependent mathematical model has been developed to aid in the risk assessment process. The model describes the behavior and fate of inhaled particles in the developing human lung, and therefore, may provide additional insight into health risks associated with exposure to airborne particulate matter (PM).

The results presented herein compare particle deposition efficiencies in adults (360 months) and children aged 7, 22, 48, and 98 months under resting conditions. Differences between deposition for sedentary and heavy physical activity levels among the age groups have also been studied (Musante and Martonen, 1999).

Methods

A physiologically realistic mathematical model describing inhaled particle deposition in the developing human lung has previously been reported (Martonen et al., 1989). The age-dependent lung morphologies, which assume a Weibel (1963) branching structure, are based on the descriptions of Hofmann (1982) for the tracheobronchial (TB) airways and Dunnill (1962) for the pulmonary (P) region. The number of TB airways are considered to be fixed at birth, but the number of P airways changes as the lung develops. Other age-dependent morphologies and particle deposition codes have been proposed (e.g., Phalen et al., 1985; Xu and Yu, 1986; Hofmann et al., 1989), and comparisons summarized elsewhere (Hofmann et al., 1989; Martonen et al., 1989).

Data in Table 1 were used to simulate sedentary conditions and corresponding variations in respiratory parameters as a function of age. The values are based on equations formulated by Hofmann (1982).

A variety of monodisperse aerosols were simulated, ranging from 0.25-5.0 μm . These particle diameters were chosen to reflect typical constituents of ambient PM.

Table 1. Definition of age-dependent breathing patterns for resting (sedentary) conditions.

| <i>Age (months)</i> | <i>Flow rate (ml/sec)</i> | <i>Tidal volume (ml)</i> |
|-------------------------|-------------------------------|------------------------------|
| 7 | 48.8 | 42 |
| 22 | 78.5 | 84 |
| 48 | 111.8 | 152 |
| 98 | 159.3 | 266 |
| 360 | 233.7 | 500 |

Results And Discussion

Total lung (total = TB + P), tracheobronchial (TB), and pulmonary (P) deposition fractions are shown in Figures 1-3, respectively, as a function of particle diameter and subject age for sedentary breathing conditions. Deposition efficiencies are mass-based (assuming unit densities and spherical particles), and are normalized to the amount entering the trachea. This normalization was performed because the experimental data used as comparison with the original dosimetry model for adults were presented in that format.

For sedentary breathing and each monodisperse aerosol considered, the predicted total deposition efficiency was highest for either the 22- and 48-month-old subjects, and lowest for the adult. Tracheobronchial deposition monotonically decreased with age, whereas pulmonary deposition was generally highest for the 48- and 98-month-olds.

Total lung deposition efficiencies for the smallest particle size (0.25- μm) ranged from 0.33-0.44, and approximately doubled for the largest (5- μm) particles, ranging from 0.68-0.80. The minimum total deposition for all age groups was observed for the 1- μm monodisperse aerosol (range 0.21-0.29).

A measure of uniformity of dose is the TB/P ratio. For values close to 1, an aerosol is considered evenly distributed within the TB and P regions; for values greater than (less than) one, the conducting (pulmonary) airways receive a greater percentage of the dose delivered. Knowledge of regional deposition is important in risk assessment due to the different clearance processes in the TB and P regions. Particles deposited along the bronchial airways will generally be cleared from the lung within 24 hours by mucociliary transport processes, whereas those deposited in the peripheral airways may remain there for weeks or months due to the slower clearance rate of pulmonary macrophages. Figure 4 shows a comparison of TB/P as a function of particle size and subject age. The model predicts that the youngest child (7 months) will receive a higher

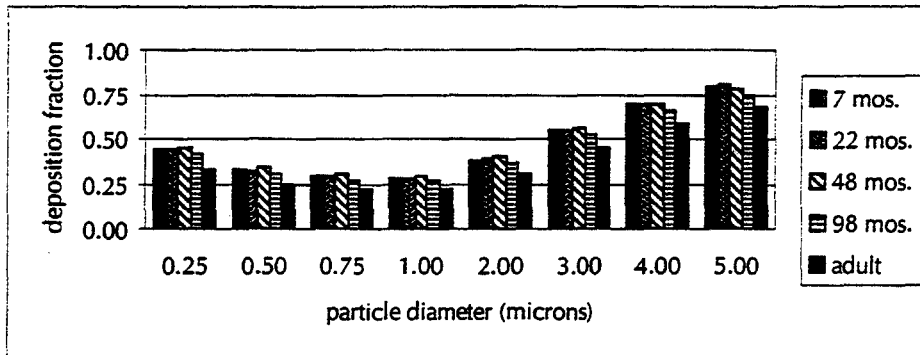


Figure 1. Total deposition in the developing human lung under sedentary conditions.

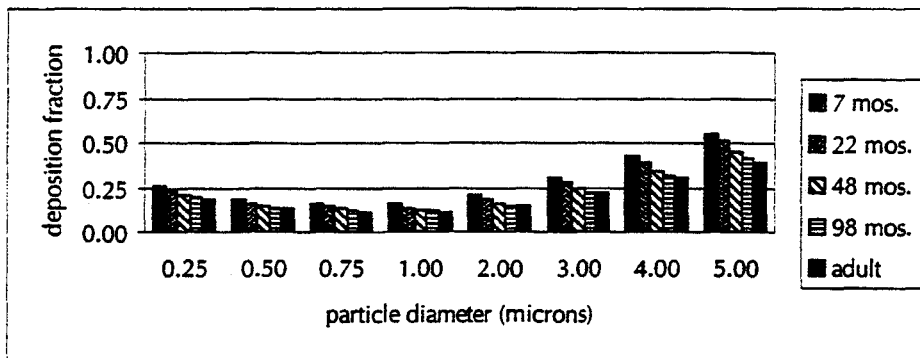


Figure 2. Tracheobronchial deposition in the developing human lung under sedentary conditions.

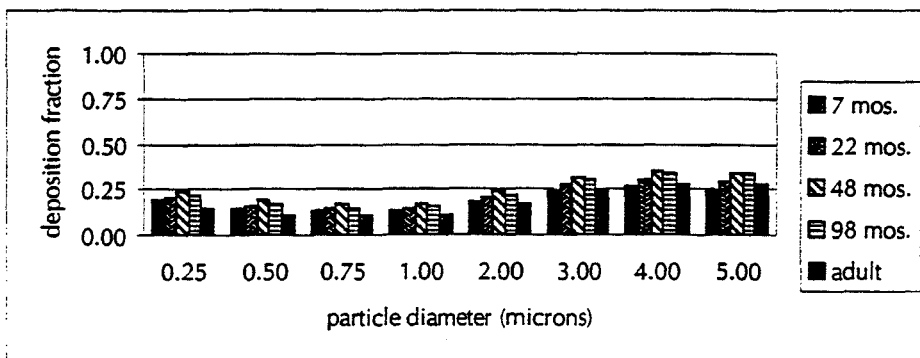


Figure 3. Pulmonary deposition in the developing human lung under sedentary conditions.

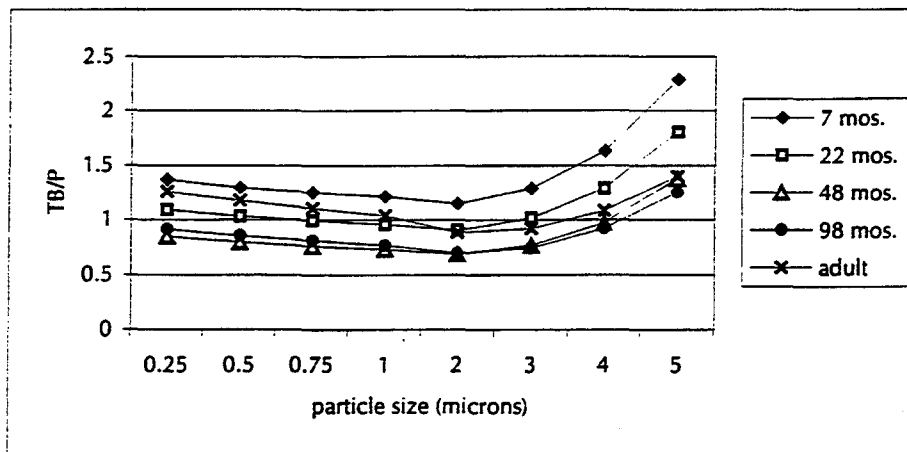


Figure 4. Comparison of TB/P ratio as a function of subject age and particle size.

percentage of the dose in the TB compartment, whereas deposition in the 48- and 98-month-olds is generally skewed toward the P region for the majority of particle sizes considered.

SUMMARY

The physiologically realistic dosimetry model used in our simulations is in agreement with experimental data from inhalation exposure experiments in adults. The model has a wide variety of input and output options. Input parameters include aerosol characteristics (e.g., particle size and density), lung morphology (e.g., human or laboratory animal, adult or child), and breathing pattern (e.g., tidal volume and frequency). Data output, in terms of aerosol deposition fractions, may be calculated at desired levels of spatial resolution; that is, total, compartmental (tracheobronchial and pulmonary), and localized (airway-by-airway).

Although lung deposition is affected by many factors, some specific observations can be made regarding the effects of subject age:

- Total (TB + P) lung deposition was generally higher in children than adults. These differences may be significant, depending on particle size, respiratory intensity, and subject age.
- Tracheobronchial deposition was a monotonically decreasing function of age under resting conditions and all particle sizes considered.
- Pulmonary deposition was highest in the 48 and 98-month-old subjects for all particle sizes examined.

These validated theoretical models may provide additional insight into PM distribution in the developing human lung, and therefore may aid in the integration of children into risk assessment protocols for particulate air pollutants.

References

- Bates, D. V. 1995. The effects of air pollution on children. *Environ. Health Perspect.* 103(Suppl. 6):49-53.
- Becquemin, M. H., Roy, M., Bouchikhi, A., and Teillac, A. 1986. Deposition of inhaled particles in healthy children. In: *2nd Int. Symposium on 'Deposition and clearance of aerosols in the human respiratory tract'*, Salzburg, ed., W. Hofmann, pp. 18-22.
- Browner, C. M. 1996. *Environmental health threats to children*. Washington, D.C., U.S. Environmental Protection Agency, EPA 175-F-96-001.
- Dunnill, M. S. 1962. Postnatal growth of the lung. *Thorax* 17:329-333.
- Hofmann, W. 1982. Mathematical model for the postnatal growth of the human lung. *Respir. Physiol.* 49:115-129.
- Hofmann, W., Martonen, T. B., and Graham, R. C. 1989. Predicted deposition of nonhygroscopic aerosols in the human lung as a function of age. *J. Aerosol Med.* 2(1):49-68.
- Koren, H. S. 1995. Associations between criteria air pollutants and asthma. *Environ. Health Perspect.* 103(Suppl. 6):235-242.
- Martonen, T. B., Graham, R. C., and Hofmann, W. 1989. Human subject age and activity level: Factors addressed in a biomathematical deposition program for extrapolation modeling. *Health Phys.* 57(Suppl. 1):49-59.
- Musante, C. J., and Martonen, T. B. 1999. Computer simulations of particle deposition in the developing human lung. *Inhal. Toxicol.*, submitted.
- National Research Council. 1998. *Research Priorities for Airborne Particulate Matter I. Immediate Priorities and a Long-Range Research Portfolio*. Washington, D.C., National Academy Press.
- Phalen, R. F., Oldham, M. J., Beaucage, C. B., Crocker, T. T., and Mortensen, J.D. 1985. Postnatal enlargement of human tracheobronchial airways and implications for particle deposition. *Anat. Rec.* 212:368-380.
- Schiller-Scotland, C. F., Hlawa, R., and Gebhart, J. 1994. Experimental data for total deposition in the respiratory tract of children. *Toxicol. Lett.* 72:137-144.
- Weibel, E. R. 1963. *Morphometry of the Human Lung*. New York, Academic Press, Inc.
- Xu, G. B., and Yu, C. P. 1986. Effects of age on deposition of inhaled aerosols in the human lung. *Aerosol Sci. Technol.* 5:349-357.

A Software Package For Multiple-Path Modeling of Particulate Matter Deposition in Human and Rat Lungs

Ravi P. Subramaniam¹, Bahman Asgharian², Leendert van Bree³, Flemming R. Cassee³, Jan I. Freijer³, Frederick J. Miller² and Peter J.A. Rombout³.

¹Sciences International, Inc. Alexandria, Virginia, USA, ²Chemical Industry Institute of Toxicology, Research Triangle Park, North Carolina, USA, ³National Institute of Public Health and the Environment, Bilthoven, The Netherlands.

Characterizing the dosimetry of particulate matter (PM) in the respiratory tract is critical to evaluating health risks due to airborne particulate matter toxicants. Lack of resolution in current dosimetry models for both animals and humans introduces uncertainty in estimates of risk to human health based on animal data. We developed a user-friendly software package, based upon a multiple-path model, developed previously by Anjilvel and Asgharian (1995). The software calculates lobar-specific and airway-specific deposition of monodisperse and polydisperse aerosols in human and rat respiratory passages. The multiple-path model is capable of incorporating asymmetries in airway branching structure if the morphometric details are available. The software provides a graphical user interface to choose among various models, to specify breathing and exposure parameters, and to obtain graphical and text outputs for various dose metrics. In this article, we provide a description of the software and some key results for regional and lobar deposition in the human lung. Further details and comparisons with experimental data will be presented in an article to be published elsewhere.

Introduction

Experimental toxicology studies of PM typically involve the use of animal models. However, there are significant interspecies differences in the PM dose that is delivered to specific regions of the respiratory tract and in the subsequent clearance of the deposited matter. Thus, the extrapolation of the results of animal studies to humans requires that dosimetry models be developed that are capable of adequate regional resolution in laboratory animals and humans. The models most commonly used for PM dosimetry (e.g. ICRP, 1994) idealize the airway structure to consist of symmetrical dichotomous branches using the lung geometry of Weibel (1963) or Yeh (1980). This leads to a typical-path description of the lung that calculates average regional deposition but fails to account for heterogeneities in deposition patterns within airways of a particular lung depth or generation. Although the lower airways of the human lung may be reasonably characterized in a symmetric fashion, there are major asymmetries, particularly in the upper few airways of the human tracheobronchial tree, that may lead to different deposition patterns in these airways as well as in the apportionment of air flow to the different lung lobes. Because of its monopodial nature, the rat lung is highly asymmetric, so a typical path characterization is likely to lead to significant errors in site-specific predictions of deposition.

To obtain an accurate and detailed assessment of particle deposition in the lung, a multiple-path model was developed previously by Anjilvel and Asgharian (1995) to simulate particle deposition in the Long Evans rat lung. In the current work, the above approach has been

extended to calculate deposition in the human lung. Detailed morphometric mapping down to the level of the terminal bronchioles was available for the Long Evans rat. For the human lung, on the other hand, such detailed data are not yet fully available, requiring a combination of multiple- and single-path analyses of the air flow in the model. The software described in this article combines deposition models for the rat and human respiratory tracts into a single package. It includes a graphical user interface that allows the user to choose among various anatomical lung models for rat and humans, to specify information on particle characteristics and breathing parameters, and to obtain graphical and text outputs based upon several available options for the dose metric. While it currently calculates only particle deposition, the program's modular feature allows for a model for clearance to be incorporated later. The software provides for an efficient way to incorporate data on exposure and activity patterns, and thus may be used to assess the dosimetric effects of various PM emission control strategies.

Methods

The multiple-path formalism (Anjilvel and Asgharian, 1995) incorporates asymmetry in the lung branching structure and calculates deposition in individual airways by using detailed information on lung geometry. Morphometric information at such a level of detail was available for the rat lung, where the entire set of airway measurements collected by Raabe et al. (1977) for the 2404 conducting airways of a Long Evans rat have been used. A symmetric 8-generation model acinus was attached to the end of each terminal bronchiole to model the acinar region in the rat lung (Yeh et al., 1979; Anjilvel and Asgharian, 1995).

For the human lung, a full multiple-path approach could not be implemented due to the lack of complete conducting airway measurements. Therefore, the option to use either a symmetric geometry or a 5-lobe symmetric but structurally different geometry has been provided. The 5-lobe symmetric geometry for the human consists of characterizing the asymmetry completely at only the level of the major segmental bronchi leading to the five lobes of the lung. Each lung lobe is then represented as a separate symmetric tree, and deposition is predicted for each generation within the individual lobes. The symmetric representation for the whole lung as well as the lobar data were obtained from Yeh and Schum (1980).

Inspiratory flow is assumed to be constant with time. At an airway entrance, uniform flow is assumed to be at the average parabolic velocity for a given volumetric flow rate at that point. The flow rate at this point is determined to be proportional to the lung volume distal to it.

Aerosol concentration at either end of an airway is determined using deposition efficiency formulae that, depending on the mechanism of deposition, are functions of the air velocity, airway dimensions, bifurcation angle, gravity angle, and particle density. The specific functional formulation for each mechanism is obtained from: Cai and Yu (1988) for impaction in rat airways, Zhang et al. (1997) for impaction in human airways, Ingham (1975) for diffusion, and Wang (1975) for sedimentation. The mass entering or exiting an airway for a given duration of time is calculated from the aerosol concentration and the flow rate at either end of the airway. The aerosol concentration within an airway is interpolated from the concentration values at the

airway ends and integrated over the airway to obtain the remaining mass at the end of inspiration. The deposition fraction for each airway is then determined using the principle of mass balance:

$$\text{Mass deposited} = (\text{Initial airborne mass}) + (\text{Airborne mass entering}) - (\text{Airborne mass exiting}) - (\text{Airborne mass remaining}).$$

Calculations may be done for monodisperse or lognormally distributed polydisperse aerosols. The regional and overall deposition fractions incorporate the filtering effect of the head using efficiency equations fitted to empirical data (see ICRP, 1994). Different equations are used depending upon nose or mouth breathing.

While deposition of coarse mode particles increases significantly with particle size because of impaction either in the head or tracheobronchial (TB) region, increased inertia poses a limitation to the ability of particles to enter the head region. This reduction in the inhaled fraction of the aerosol with increasing particle sizes may be significant for nasal breathing and more so for rats than for humans. An inhalability adjustment is made to the inhaled concentration using empirical curves derived by Menache et al. (1995).

The model was implemented for use on the Windows NT or Windows 95 environment. The program allows the user to provide as input particle characteristics, the breathing scenario and breathing parameters, the functional residual capacity, and the upper respiratory tract volume. Various breathing patterns may be simulated: endotracheal, nasal, oral, and combined nasal and oral (oronasal). Partitioning of airflow for oronasal breathing are as given by Niinima et al (1981). The exposure scenario may be per breath or for repeated breathing. For repeated breathing, the user may specify different breathing patterns either on an hourly basis during the day or activity patterns for variable time durations. The ratio of the time spent inhaling to the time spent exhaling is also allowed to vary so that specific exercise and abnormal breathing scenarios may be modeled.

Results for the deposition fraction, deposited mass flux and mass deposited per unit area are provided in the software in graphical and text formats. Simulation results are provided for total, regional and lobar deposition, and as a function of airway generation number. An advanced feature that fully exploits the capabilities of the multiple-path formalism is provided for the rat lung. This feature provides a histogram of the frequency distribution of the acini as a function of the deposition fraction per acinus.

Results

In previous work (Anjilvel and Asgharian, 1995), we reported on simulations of aerosol deposition in the rat lung; therefore, in this work, we focus only on deposition in the human lung. In Fig. 1, total and regional (tracheobronchial and alveolar) deposition for a range of monodisperse particle diameters are compared with the experimental results of Heyder et al (1986). The total deposition agrees well with experimental data. For particle diameters between 0.05 and 1 μm , the calculated tracheobronchial (TB) deposition fraction ranges between 0.1 and 0.06. On the other hand, Heyder's experiment gives zero TB deposition in this range. It is possible that because of rapid clearance, deposition in the TB region is not adequately

represented by the experiment in this range of particle size. For particle diameters greater than 1 μm , there is general qualitative agreement for alveolar deposition and good agreement for deposition in the tracheobronchial region. The peak in alveolar deposition occurs at roughly the same particle diameter (3.5 μm) in both the calculated and experimental results. However, the peak in the calculated deposition fraction is lower than the experimental data by about 30%.

The deposition fractions for the five human lung lobes are shown in Fig. 2 and compared with calculations by Gerrity et al. (1981) who used a Horsfield asymmetric model of the lung and the deposition probability equations of Landahl (1950). Gerrity et al.'s calculations were done for one particle size only, and their results are depicted by symbols in Fig. 2. In both results, deposition is highest in the lower lobes and least in the right middle lobe. The deposition in each lobe is in proportion to the lobar volume and is therefore in rough proportion to ventilation (as also concluded by Gerrity et al.). The volumes of the left and right sides of the lung are nearly equal for both the upper and lower lobes. The deposition fraction obtained by our model is less than that obtained by Gerrity et al. by roughly 0.03 for both the upper and lower lobes. In our calculation, the right and left upper lobes receive equal deposition for all particle diameters considered, and a similar conclusion applies for the lower lobes for particle diameters less than 10 μm . For particles larger than 10 μm , the right lower lobe receives a slightly greater deposition than the left lower lobe; the difference in the upper lobes is significantly less. The increase in deposition by gravitational sedimentation for larger particles is likely to be more for the lower lobes, and small differences in ventilation between these lobes are likely to affect deposition. Regional lobar deposition in the human lung has also been calculated by Yeh and Schum (1980). Our results differ significantly from theirs for particle diameters below 3 μm . This will be discussed further in a more detailed article.

In Fig. 3, the dose metric used is mass deposited per unit area of airway surface, and the logarithm of this dose is plotted as a function of airway generation number for the five lobes for a) ultrafine (0.02 μm) and b) coarse (4 μm) aerosols. Deposition is entirely diffusional for the 0.02 μm particle, while for the 4 μm particle, deposition is by impaction in the upper airways and by sedimentation in the lower airways. In the upper airways, for both particle sizes, the upper and middle lobes receive a similar dose in a given generation, while the lower lobes show significant differences. At a specific generation number in the upper airways, the dose is similar for the two particle sizes for the same lobe. In the middle airways (generation 10 to 17), all lobes receive a similar dose of the coarse aerosol with no significant difference between generations. However, for the ultrafine aerosol, there are significant differences among the lobes. The right middle lobe, which showed the least deposition per unit area in the upper airways, receives the highest dose in the middle airway. Fig. 3 shows significant differences (that increase with lung depth) between the lobes in the lower airways, except for the right upper and right middle lobes, which receive comparable doses. At generation 22, the difference between the left upper and right lower lobes is roughly 6-fold for the coarse aerosol, and is about 12-fold for the ultrafine aerosol.

Discussion

The results presented above illustrate that there are important differences in deposition between the five human lung lobes and that these differences are accentuated as one examines deposition in each generation. The software package we have developed provides an easy way of incorporating heterogeneities at both the lobar and individual airway level and can do so for both the rat and human respiratory tract, thus allowing for more accurate extrapolations across species. We are in the process of including clearance processes in the model. With such an addition, and with the options for breathing and exposure scenarios, the software provides a useful tool to relate realistic exposure patterns to the dose delivered to specific regions in the lung, and thereby to observed health effects. The software may be obtained from the Library at the Dutch National Institute of Public Health and the Environment (P.O. Box 1, 3720 BA, Bilthoven, the Netherlands. Tel: 31-30-274 3156. Fax: 31-30-274 4404).

References

- Anjilvel, S. and Asgharian, B. 1995. A multiple-path model of particle deposition in the rat lung. *Fund. Appl. Toxicol.* 28, 41-50.
- Cai, F.S. and Yu, C.P. 1988. Inertial and interceptional deposition of spherical particles and fibers in bifurcating airways. *J. Aerosol Sci.* 19, 679-688.
- Gerrity, T.R., Garrard, C.S., Yeates, D.B. 1981. Theoretic analysis of sites of aerosol deposition in the human lung. *Chest.* 80, 898-901.
- Heyder J., Gebhart, J., Rudolf, G., Schiller, C.F., Stahlhofen, W. 1986. Deposition of particles in the human respiratory tract in the size range 0.005-15 μm . *J. Aerosol Sci.* 17, 811-825.
- ICRP, 1994. Human respiratory tract model for radiological protection. ICRP Publ 66. *Annals of ICRP.* 24, 231.
- Ingham, D.B. 1975. Diffusion of aerosols from a stream flowing through a cylindrical tube. *J. Aerosol Sci.* 6, 125-132.
- Landahl, H.D. 1950. On the removal of airborne droplets by the human respiratory tract: I. The lung. *Bull. Math. Physiol.* 12:43-56.
- Menache, M.G., Miller, F.J., Raabe, O.G. 1995. Particle inhalability curves for humans and small laboratory animals. *Ann. Occup. Hyg.* 39, 317-28.
- Niinima, V., Cole, P., Mintz, S. and Shephard, R.J. 1981. Oronasal distribution of respiratory airflow. *Respir. Physiol.* 43, 69-75.
- Raabe, O.G., Yeh, H.C., Newton, G.J., Phalen, R.F., and Velasquez, D.J. 1977. Deposition of inhaled monodisperse aerosols in small rodents. In *Inhaled Particles IV* (ed. W.H. Walton), pp. 1-21, Pergamon Press, Oxford.
- Wang C.S. 1975. Gravitational deposition of particles from laminar flows in inclined channels. *J. Aerosol Sci.* 6, 191-204.
- Weibel, E.R. 1963. *Morphometry of the human lung.* Springer-Verlag, Berlin.
- Yeh HC. 1980. Respiratory tract deposition models. Report, Inhalation Tox. Res. Inst. LF-72, UC-48.

Yeh, H.C. and Schum, G.M. 1980. Models of human lung airways and their application to inhaled particle deposition. *Bull. Math. Biol.* 42, 461-80.

Yeh, H.C., Schum, G.M. and Duggan, M.T. 1979. Anatomic models of the tracheobronchial and pulmonary regions of the rat. *Anat. Rec.* 195, 483.

Zhang, L; Asgharian, B. and Anjilvel, S. 1997. Inertial deposition of particles in the human upper airway bifurcations. *Aerosol Sci. Technol.* 26, 97-110.

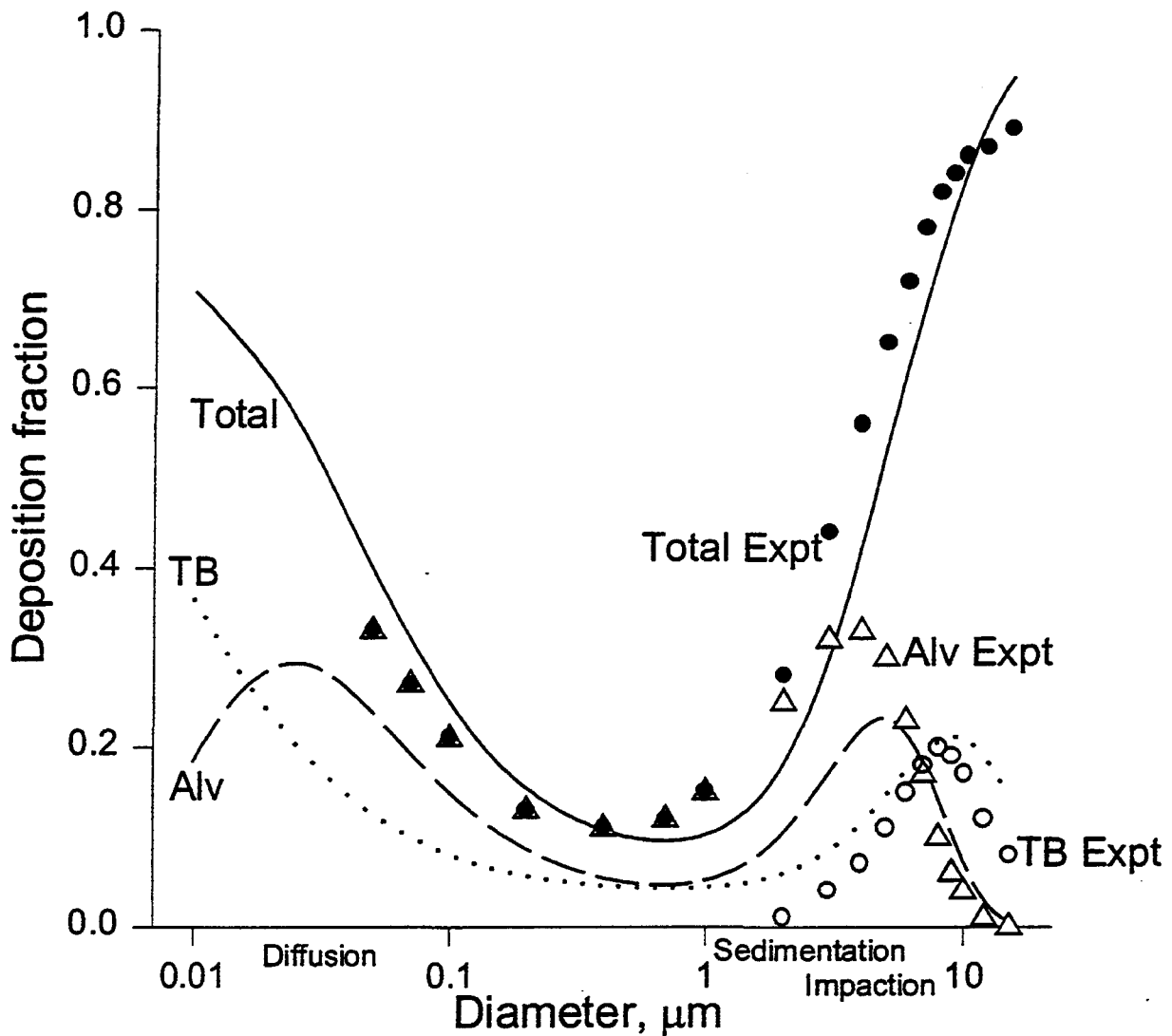


Figure 1 Calculated total, tracheobronchial (TB) and alveolar (Alv) deposition compared with experiment (Heyder et al., 1986). Lines represent simulations, solid: total, dashed: TB, dotted: Alv. Symbols represent experimental data, filled circle: total, open circle: TB, triangle: Alv. The x-axis is a logarithmic scale and ranges from 0.01 to 15 μm . Breathing is through the mouth; tidal volume is 500 ml, and breathing frequency is 15 bpm

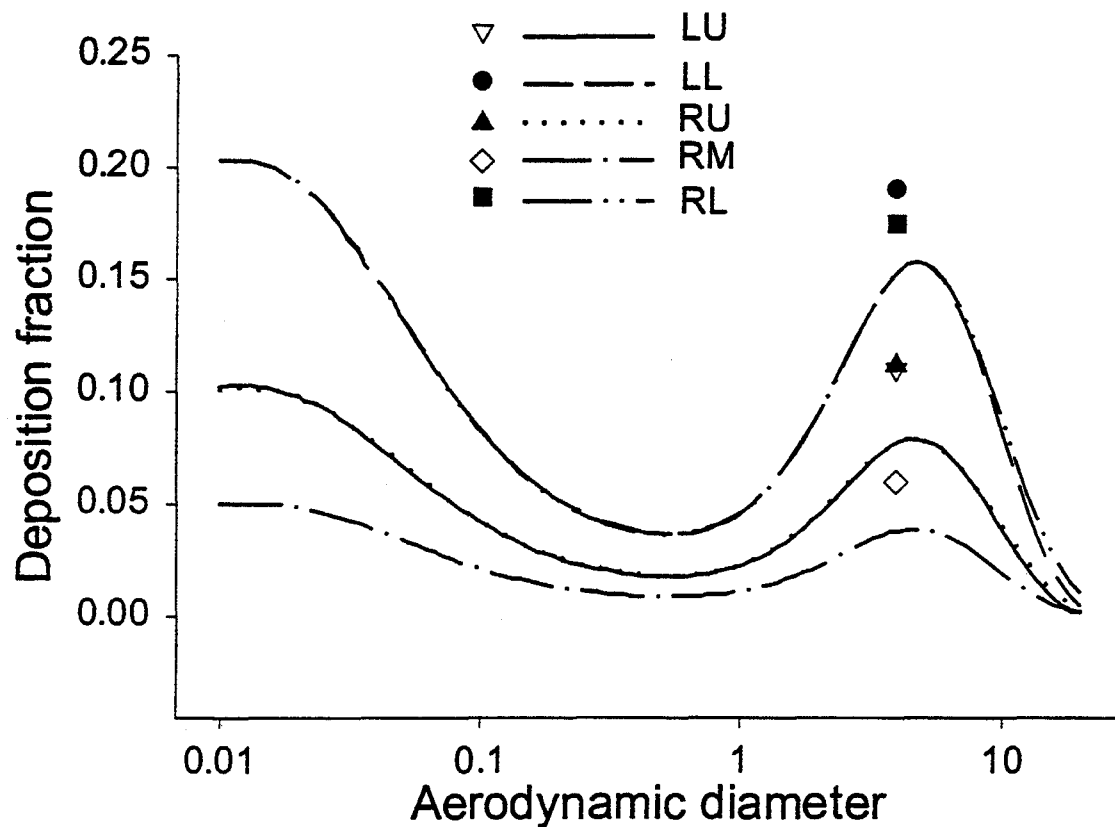


Figure 2 Lobar deposition fractions for various particle diameters. Lines are the current simulations. Symbols represent simulations by Gerrity et al. (1981). The lobes are denoted as LU, left upper; LL, left lower; RU, right upper; RM, right middle; RL, right lower. Note the overlap in the deposition curves, up to a particle diameter of 10 μm , for the RU and LU lobes, and likewise for the RL and LL lobes. Also note the overlap in results by Gerrity et al. for the RU and LU lobes. Simulations are for mouth breathing at a tidal volume of 1000 ml and a breathing frequency of 15 bpm. The x-axis is a logarithmic scale.

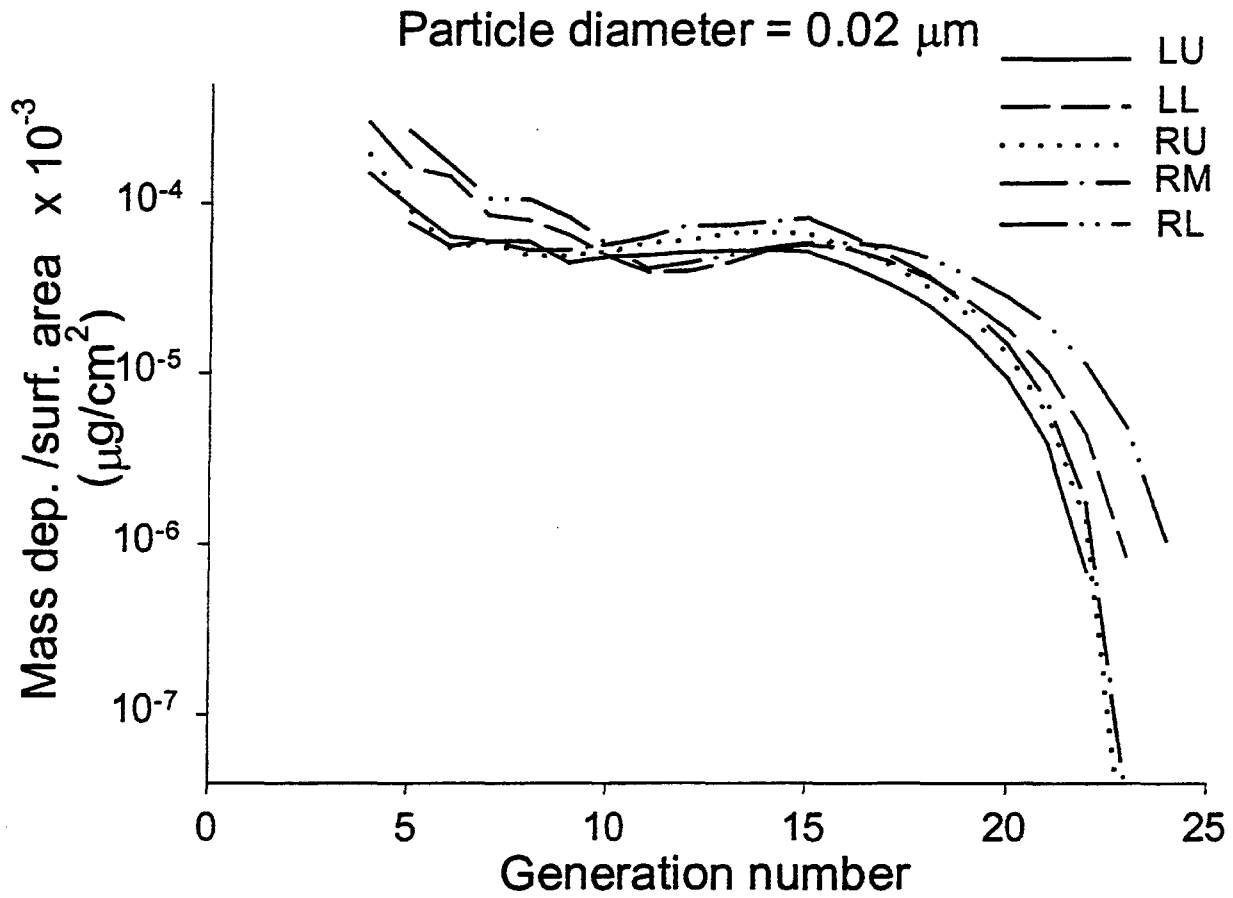


Figure 3a Mass deposited per unit airway surface area vs airway generation number for the five human lung lobes for 0.02 μm particle diameter. The scale on the y-axis is logarithmic. The lobes are denoted as LU, left upper; LL, left lower; RU, right upper; RM, right middle; RL, right lower.

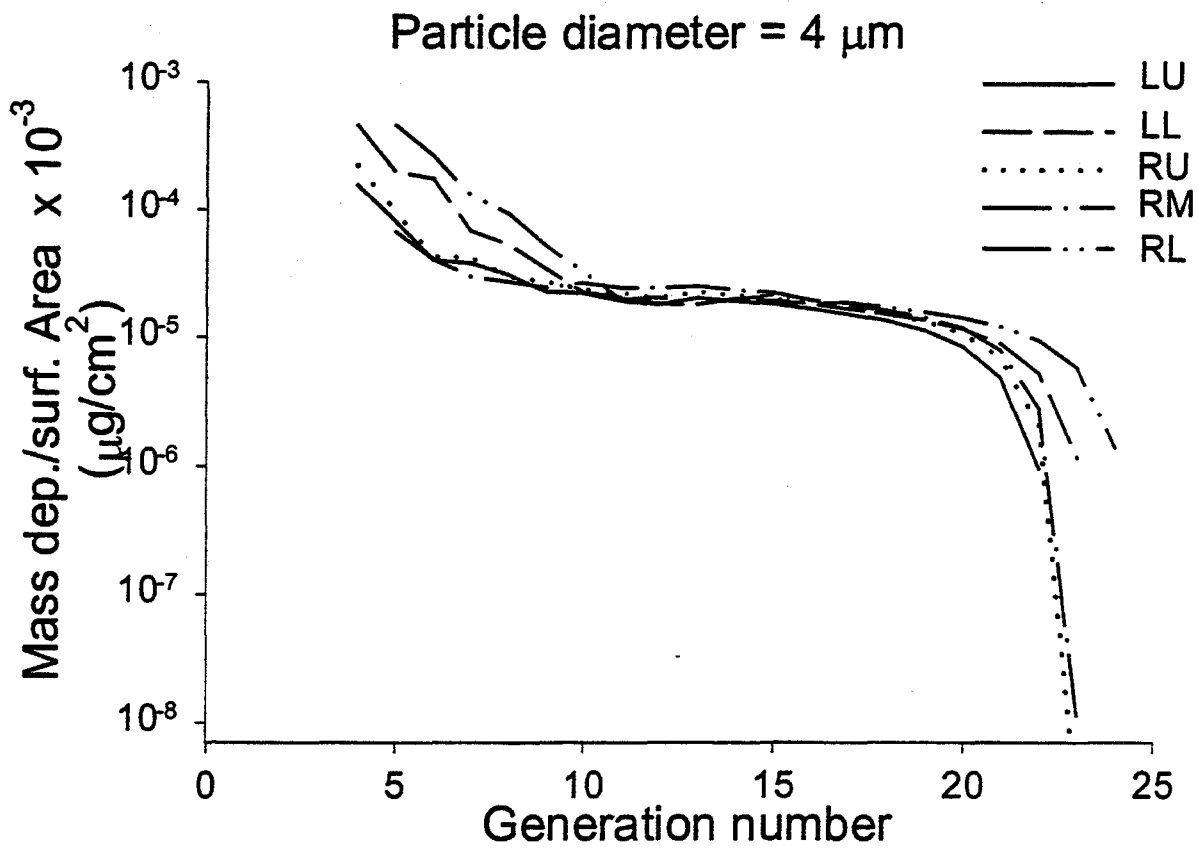


Figure 3b Mass deposited per unit airway surface area vs airway generation number for the five human lung lobes for 4 μm particle diameter.

VIII. SUSCEPTIBILITY-RELATED PAPERS (SESSION 5)

Lung Pathology Associated with Fine Particle Air Pollution (PM) in the Great London Smog of 1952: Metals and Ultrafine PM in Human Lungs

JL Abraham, A Hunt, CL Berry, Departments of Pathology, SUNY HSC, 750 East Adams St., Syracuse, NY, 13066, USA and Royal London Hospital (RLH), UK.

ABSTRACT

During the great London Smog of December 5-9, 1952, London daily mortality rose from <250/day to >900/day, with >4000 estimated excess deaths recorded over a period of several weeks. This episode has served as one of the sentinel events leading to recognition of the relationship of PM to daily mortality. The daily mortality observed in the 1952 episode fits on the dose-response curve derived from contemporary epidemiological studies of many diverse locations. However, the absolute increases in human mortality with current levels of PM are so low that collection of contemporary autopsy materials from deaths known to result from PM is not feasible. Therefore, we have investigated autopsies in archives from before, during and after the Great London Smog of December 5-9, 1952. We observed the total number of autopsies increasing with a monthly peak paralleling previously reported daily/weekly mortality from death certificates -- which have shown the major peak increases to be from pulmonary and cardiovascular deaths. Autopsies which listed Bronchitis and/or Emphysema (COPD) among major diagnoses showed the sharpest peak, as did death certificate data. The steepest dose-response curve for PM and daily mortality is also for respiratory causes. The 1952-53 winter COPD autopsy peak lagged, and was much broader than the death certificate peak. This reflected deaths among people initially hospitalized during the Smog, or whose COPD worsened then. Daily and weekly autopsy numbers were too few for analysis. Cardiovascular sudden deaths, identified in the death certificate data, were less clearly reflected in hospital autopsies. Lung tissues revealed retention of the respirable PM in large airways, small airways and air spaces. Particulates in macrophages were associated with immunohistochemical evidence of inducible nitric oxide synthase and nitro-tyrosine -- both markers of reactive oxygen species injury. Particle numbers, size and chemical composition characterized using scanning electron microscopy and energy-dispersive x-ray spectroscopy reveal predominately fine and ultrafine carbonaceous PM, with numerous sulfur and metal containing particles. The occurrence of metallic elements (Fe,Pb,Sn,Zn,Cu,Mn,Cd,Sb,Al,Ti) is similar to that in contemporary aerosol samples of PM from combustion sources. Analysis of these historic autopsy tissues supplements contemporary PM studies.

INTRODUCTION

Extant epidemiological data argues for a consistent link between elevated mass concentration of ambient PM and increased morbidity and mortality in the exposed population. This association is largely independent of geographical locale. However, the epidemiological studies are linked by a common urban setting and the possibility that adverse health impacts are the result of inhaling fine particles produced by urban-industrial combustion processes. While animal studies have established the biological plausibility of PM caused health effects, to extrapolate from animal studies in which

ambient, or specific combustion products, are administered at levels in excess of what might be considered environmentally normal requires further data on the human exposure-dose-response relationship.

The most direct evidence linking exposure to increased risk is to be obtained from correlating the composition of the exposure aerosol with a recorded increase in mortality. The PM exposure-dose-response relationship is best clarified by identifying and quantifying the inhaled PM in (the lung tissue of) individuals who expired as a consequence of the PM exposure. *However, the absolute increases in human mortality with current levels of ambient PM in Western Europe and North America are so low, that the collection of contemporary autopsy materials from deaths known to result from PM is not feasible.* But, there exists archived autopsy material which was collected during periods when major air pollution episodes were more commonplace. Therefore, it is possible to examine actual human lung and other tissues from persons who expired during these episodes, when mortality was so greatly increased that one can be fairly certain that one will be examining tissues from actual PM-induced human deaths. Here, we present initial data from autopsy material which was archived at the time of the Great London Smog event of the 1952. As of this date, it appears that no ambient aerosol samples collected during the Great London Smog of 1952 are available for analysis. *By investigating the lung particle burden from this and other cases, the principal objective of our investigation is to determine the composition of the PM phases in the London smog aerosol during this increased mortality episode.*

LONDON SMOGS

The city of London has a long history of air pollution problems [Brimblecombe, 1987]. Episodic smogs associated with increases in human mortality can be traced back to the seventeenth century [Brimblecombe, 1987]. Although the frequency of smog events has declined to a fraction of the number which occurred during the peak periods at the end of the nineteenth century, during this century there have been several 'great' smog episodes which have had a major impact on the health of the population of London. During the twentieth century, events of this type which resulted in excess mortality occurred in 1948, 1952, 1956, 1957 and 1962.

The Great Smog of 1952 was, in terms of human health impact, the most calamitous of the twentieth century. The estimated number of deaths in December 1952 (the time of the smog) totaled 4,000 in excess of that normally expected [Beaver, 1953]. It was further estimated that following the initial acute exposure there were an additional 8,000 excess deaths before the mortality rate returned to the comparable 1951/52 levels [Beaver, 1953]. The smog lasted 5 days (5th to 9th December) when a slow-moving high pressure system became stationary over London and persisted for several days. Almost immediately the SO₂ and smoke concentrations began to rise. Particulate emissions from domestic fires and industrial process provided condensation nuclei for the moist air to form a dense smog. With little atmospheric dispersion the SO₂ and smoke levels climbed to peak values of 3.83 mg m⁻³ and 4.46 mg m⁻³ respectively. The typical winter situation was compounded by increased emissions from domestic heat sources and power plants, which responded to the atypical low temperatures (daily mean temperatures were below the 80-year average). The most important causes of death during the week at the episode's height (7th December to 14th December) according to death certificate data were: bronchitis (a 14-fold increase over the November weekly average), influenza (a 12-fold increase) pneumonia (a 5-fold increase) other respiratory disease (a 9-fold increase) and heart disease (a 3-fold increase). Several hundred coroner's autopsies were performed, but apparently have not been reported in any discoverable detail.

METHODS

Case Selection. The increase in autopsies listing COPD among major diagnoses occurred during and following the Great Smog of 1952. Acute cardiovascular deaths were not reflected in this inpatient autopsy population; there was no observable peak in autopsies listing cardiovascular causes of death. Also, the number of autopsies was too few to examine daily or weekly rates. Cases were retrieved from the autopsy archives of the RLH, with the initial group presented here selected for further study by availability of lung parenchymal tissue block(s), date of death, age and major autopsy diagnoses.

Tissue Preparation. Standard pathology laboratory methods for light microscopy (LM) and electron microscopy (EM) were utilized. For pre-existing specimens, paraffin blocks of formalin fixed tissues were sectioned at 5 micrometers and sections stained with Hematoxylin and Eosin for routine pathologic evaluation. Representative photomicrographs illustrate the pulmonary parenchymal reaction and exogenous particulate material present in the stained tissue sections from our index case, a 76 year old woman with history of COPD and congestive heart failure dying acutely on Dec 7, 1952. The H&E sections illustrate examples of particulate material of contemporary exposure origin (i.e., at the time of the smog) found in bronchial and bronchiolar exudate, alveolar edema, and airspace macrophages.

Electron Microscopy. Sections for SEM/EDS analysis were mounted on (pure) carbon planchets and the paraffin removed with xylene prior to analysis in the SEM. The data presented here were collected using an RJ Lee PSEM, Hitachi S-520 and 4700 SEMs (the latter courtesy of Hitachi instruments), and Phillips 201 TEM. Imaging was performed in the secondary electron (SE) and backscattered electron (BE) imaging modes. The BE signal was tuned to reveal higher atomic number PM as bright features against the darker (lower atomic number) matrix. The high magnification shows the soot aggregate to be composed largely of clusters of ultrafine carbonaceous particles – typical of combustion processes – in what appear to be layers of amorphous material, consistent with the apparent entrapment of PM in layers of mucus in the airways, gradually accumulating the large aggregates easily seen by light microscopy. For Transmission Electron Microscopy (TEM), a portion of a paraffin section containing the soot aggregate was dissected out, embedded in epoxy resin and sectioned with a diamond knife, with thin sections collected on copper slotted grids (courtesy of M. Barcza, SUNY HSC). TEM reveals many of the ultrafine particles seen by high resolution SEM, and additional ultrafine particles as small as 10nm or less diameter.

X-Ray Microanalysis. Microanalysis of individual particles utilized automated analysis as much as possible, with review of the data and follow up manual analysis of selected particles of interest. The methodology for *in situ* quantitative IPA has been developed and utilized extensively by our laboratory [Abraham et al, 1983, 1991]. Basically, selected fields of view of the section of tissue are searched using the backscattered electron (BE) image to detect particles of atomic number higher than that of the substrate and tissue. With carbon support media, particles with atomic number greater than carbon can be detected. Correlation of the particle burden with location of particles in specific cells and tissues is possible with *in situ* analysis but not with destructive methods such as ashing or digestion. The high atomic number particles appear brighter than the carbonaceous matrix (some of which contains detectable calcium and sulfur).

Cellular Activation. We have attempted to identify (for subsequent correlative *light microscopy-scanning electron microscopy* of particle associations with) activated macrophages and other cells in which reactive oxygen species have been active, as marked by immunohistochemical staining for CD68(KP-1) (a macrophage marker), inducible Nitric Oxide Synthase (iNOS) (an activation marker) and NO-Tyrosine (NT) (a marker of nitric oxide reaction). NOS can be induced (by gene transcription) in macrophages after they have been exposed to certain stimuli (e.g., inflammatory cytokines (IL-1 β , TNF- α)). It has been shown that alveolar macrophages when exposed *in vitro* to dust particles can release oxygen radicals, and can secrete a large panel of cytokines. Immunohistochemical stained tissue sections show iNOS activity in several neutrophils and in some macrophages and bronchiolar epithelium (which has constitutively active iNOS production). The NT staining of endothelium and fibrin indicates the reaction product of Nitric Oxide and nearby tyrosine groups. These findings indicate adequate tissue preservation to allow pursuit of these and other immunohistochemical markers to examine the relationship of specific particle types to cellular activation.

RESULTS AND DISCUSSION

In addition to the PM analyzed in the large soot aggregate in the airway of the 76 year old woman dying on Dec. 9, 1952, similar fine PM was visible in many intact cells in the adjacent exudate and in other airways and airspaces in this and other cases. As a result of the overwhelming number of carbonaceous particles, however, the number of non-carbonaceous particles characterized in individual cells is, to date, limited. Most particles are on the order of 100nm diameter or less. Aggregates resembling contemporary diesel PM emissions are notable.

It is our intention to collect additional data on the fine PM in the airways of additional cases dying during the peak of the Great Smog, and this will serve as a library of 'source' PM, since no actual samples from the 1952 episode are apparently available for analysis. Also, the fine PM found in the lungs is, without dispute, at least a partial if not total sample of the insoluble and respirable PM during this sentinel event in air pollution history.

In contrast to the extracellular very fine PM in the airways and airspaces (representing recent exposure prior to death), the interstitial macrophages in perivascular and peribronchiolar locations are the 'sump' of regional clearance, and the PM in these areas is much more heterogeneous, and contains a mixture of many non-combustion source particles as well as some of the fine PM as seen in the airways in some persons.

Our initial studies show the feasibility of utilizing archival human autopsy tissues to study actual PM and tissue and cellular reactions in persons with high probability of death resulting from major PM pollution episodes. This provides further support for the ongoing contemporary analysis of ambient PM and experimental studies to investigate mechanisms.

The diversity of fine PM and the relative uniformity of epidemiologic dose-response relationships for PM and daily mortality suggests that *size and concentration may be more important than chemical composition, or that composition of ultrafine and fine PM may be more similar, both spatially and temporally, than previously expected.* Our results from the 1952 London epidemic reveal most particles less than 200nm diameter, and many in the <100nm range. This is in keeping with diverse studies of PM: e.g., from coal burning power plants, which have shown a peak in PM of <100nm diameter [Mohr, 1996]; the same authors [Mohr, 1996] also point out that although ultrafine particles do not contribute significantly to the mass based outlet emission of an Electrostatic Precipitator (ESP)

they may become more important in upcoming regulations like $PM_{2.5}$; and PM from municipal incinerators [Greenberg, 1978], in which size distributions of emitted PM in Nicosia are similar to those from incinerators in the Washington, DC area. In these studies, the fraction of elemental mass less than 0.6 μm aerodynamic diameter was approximately 90% for Pb, 80% for Cu, 80% for Cd and 70% for Zn. The reported relative frequencies of major metallic elements is similar to our observations based on individual particle analysis.

Similar observations were made using SEM analytical techniques with ambient PM in Syracuse, NY, in which the concentration of metal-bearing particles (primarily Fe and Pb, less Zn, Mn, Cr, Cu and Sn) were 0.05 to 0.2 particles/cm³, approximately two orders of magnitude below the total inorganic (primarily sulfates) particle concentrations. The inorganic-to-total fine particle concentration ratio was close to 0.2 across all indoor and outdoor samples. [Abraham, ME, 1998]. The size distribution of ambient aerosols are similar to those PM retained in the lungs also, thus not only potentially relevant to acute but also to chronic health effects.

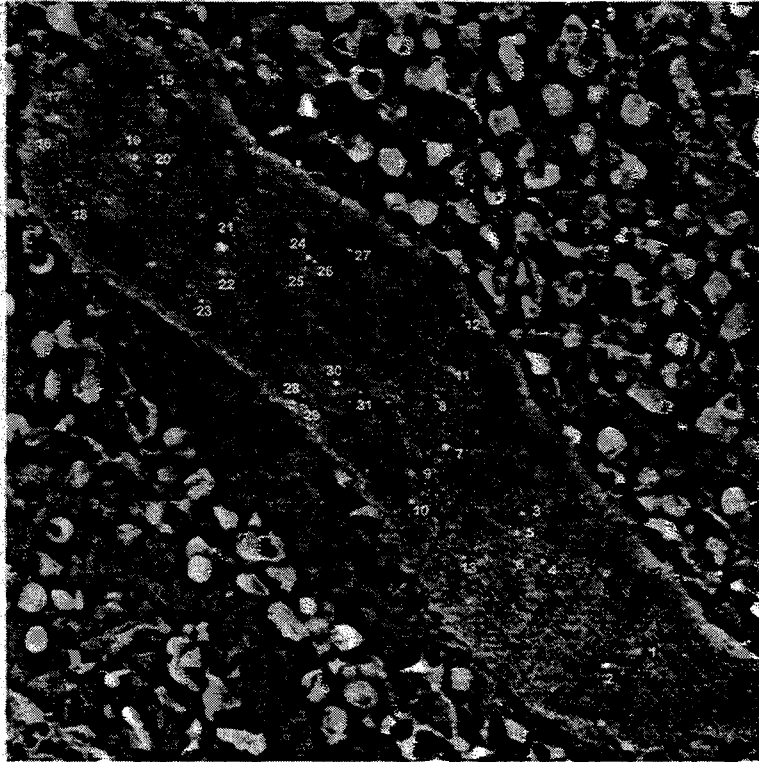
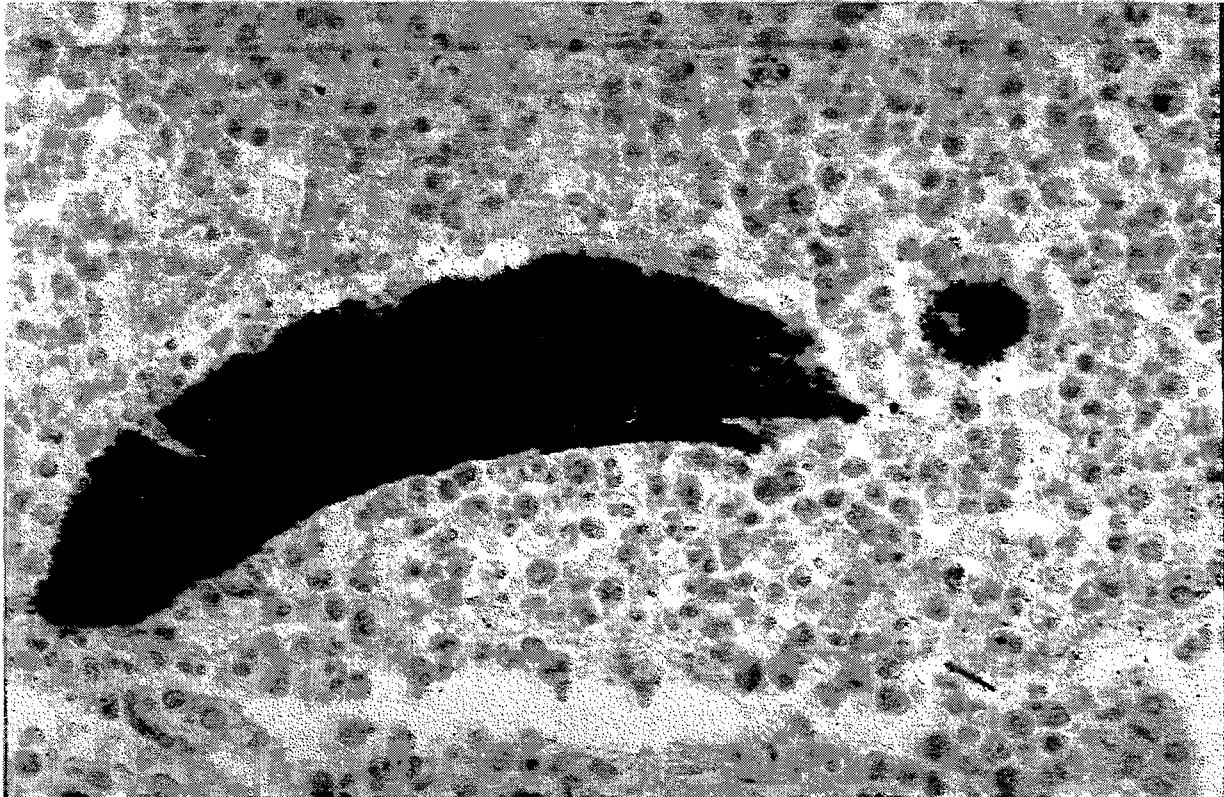
The relative uniformity of distributions of metal-containing fine PM across these diverse studies (both geographically and methodologically), and the similarity of our results on metal PM types in the lung tissue from the London 1952 cases (Table I) also supports the relevance of continued analysis of effects of fine PM and metal contents.

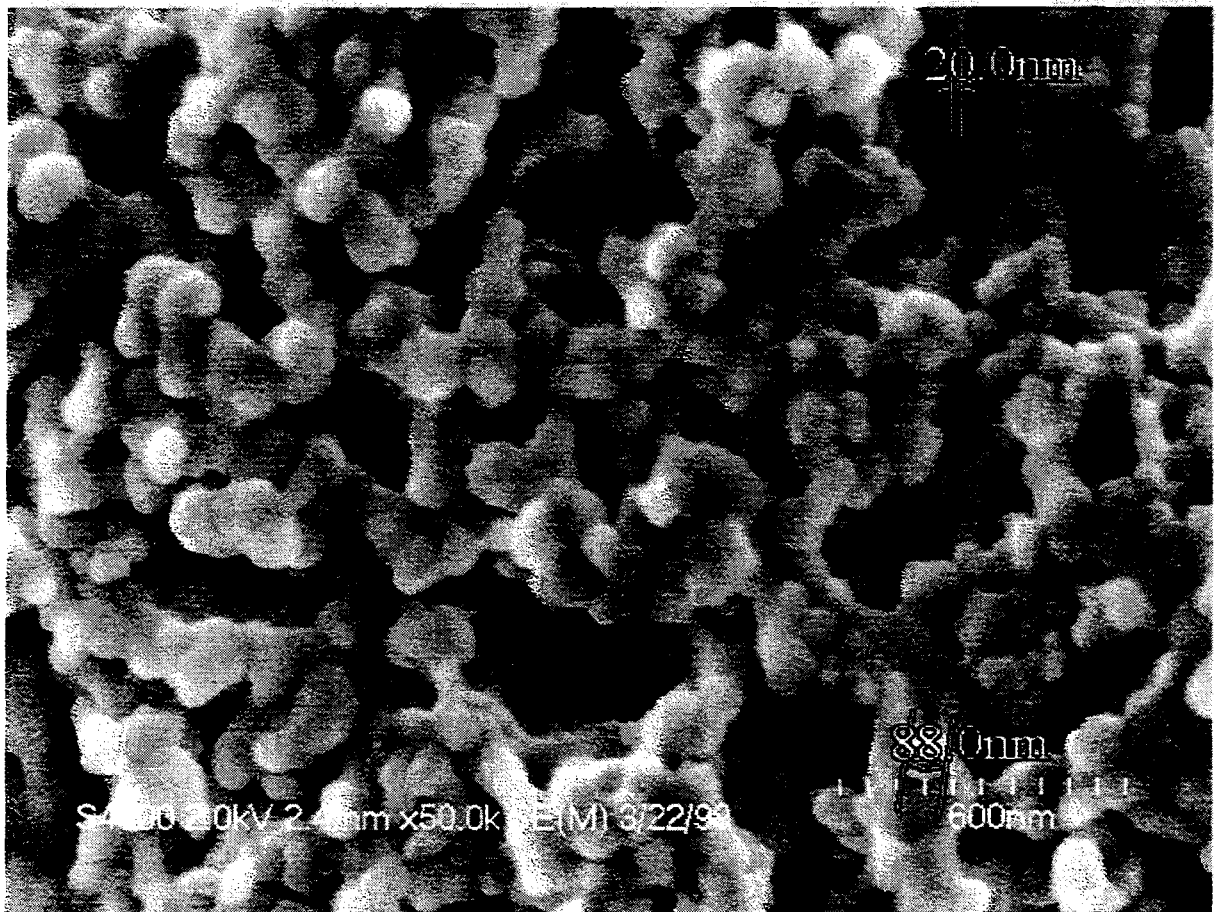
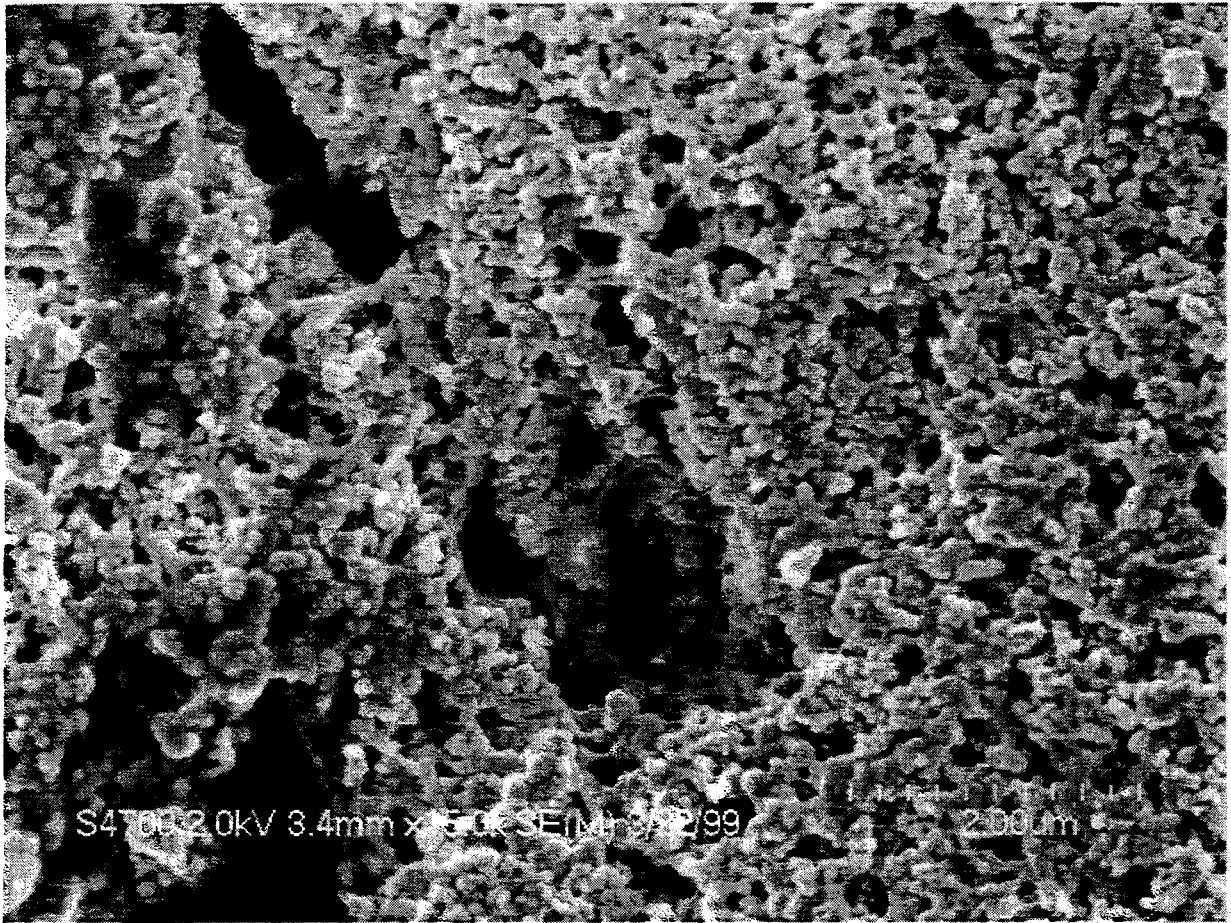
The ratio of carbonaceous (low backscattered electron yield) particles to higher atomic number metallic fine PM in the 1952 London fine PM [several hundred or more to one] is similar to what has been measured in contemporary submicrometer PM in ambient air in Syracuse, NY [Abraham, ME, 1998], and to what is being described at this meeting in lungs from heavily polluted Mexico City. These findings which are concordant over many years and locations support the need for further investigation of the very fine PM in many locations around the world, and attempts to elucidate specific composition of fine PM and mechanisms of toxicity. These results do not (yet) allow conclusion about whether one specific type of fine PM or ultrafine PM is "the" most likely candidate for causal relationship to mortality and morbidity observed in epidemiologic studies, but they do suggest more focus on submicrometer PM is indicated. *If the particle size most relevant to acute health effects is in the <200nm range, measurements of PM_{10} and even $PM_{2.5}$ or $PM_{1.0}$ may be insensitive to important fluxes in the 'relevant' PM for health effects.* The rationale of monitoring of $PM_{1.0}$ (or smaller) as opposed to $PM_{2.5}$ should be the subject of serious consideration.

REFERENCES

- Abraham, J.L. and Burnett, B.R.: Quantitative analysis of inorganic particulate burden in situ in tissue sections. *Scanning Electron Microscopy/1983*, 2:681-696, 1983.
- Abraham, JL, Burnett, BR and Hunt, A. Development and use of a pneumoconiosis database of human pulmonary inorganic particulate burden in over 400 lungs. *Scanning Microscopy*, 5:95-108, 1991.
- Abraham, ME, Physico-chemical characterization of submicrometer Indoor/Outdoor aerosols. in *PM_{2.5}: A fine particle standard*. Air&Waste Management Assoc., 1998, p.862
- Beaver, H. Committee on Air Pollution: Interim Report. HMSO Cmd.9011, 1953.
- Brimblecombe, P. The Big Smoke. 1987. Routledge, London.
- Greenberg, RR, et al. Composition of particles emitted from the Nicosia Municipal Incinerator. *EST* 12:1329, 1978.
- Mohr, M et al. Submicron Fly Ash Penetration Through Electrostatic Precipitators at Two Coal Power Plants. *Aerosol Sci Tech* 24:191, 1996

FIGURES: Top: light micrograph showing soot in mucopurulent exudate in bronchiole. Bottom: BE image showing numerous higher atomic number particles within the carbonaceous soot aggregate. Next page: High resolution (field emission) SEM images of soot aggregate, showing innumerable ultrafine particles in mucus.





**CARDIAC AND THERMOREGULATORY TOXICITY OF RESIDUAL OIL FLY ASH
IN CARDIOPULMONARY-COMPROMISED RATS**

Matthew J. Campen¹, Daniel L. Costa², and William P. Watkinson²

¹ Department of Environmental Sciences and Engineering
School of Public Health and Curriculum in Toxicology
University of North Carolina
Chapel Hill, North Carolina 27599

² Pulmonary Toxicology Branch, Experimental Toxicology Division
National Health and Environmental Effects Research Laboratory
U.S. Environmental Protection Agency
Research Triangle Park, North Carolina 27711

Running Title: Toxicity of Residual Oil Fly Ash in Rats

Address Correspondence To: William P. Watkinson, Ph.D.
MD-82; Pulmonary Toxicology Branch
Experimental Toxicology Division
National Health and Environmental Effects Research Laboratory
Research Triangle Park, N.C. 27711
#919-541-4018 (Office)
#919-541-0026 (FAX)
watkinson.william@epamail.epa.gov

This paper has been reviewed by the National Health and Environmental Effects Research Laboratory, U.S. Environmental Protection Agency, and approved for publication. Mention of trade names or commercial products does not constitute endorsement or recommendation for use.

ABSTRACT

Cardiac And Thermoregulatory Toxicity Of Residual Oil Fly Ash In Cardiopulmonary-Compromised Rats. Campen, M. J., Costa, D. L., and Watkinson, W. P. (1999) *Inhal. Toxicol.* __, __-__. Recent epidemiological studies have reported a positive association between levels of ambient particulate matter (PM) and daily morbidity and mortality due to respiratory or cardiovascular causes; however, toxicological evidence supporting these findings is limited. The present study compared cardiac and thermoregulatory responses to intratracheal instillations of residual oil fly ash (ROFA) in normal and cardiopulmonary-compromised male Sprague-Dawley rats. Animals (n=64) were implanted with radiotelemetry transmitters capable of continuously monitoring heart rate, core body temperature, and electrocardiographic waveforms. Comparisons of particulate matter toxicity were conducted between 1) healthy rats and rats with cardiopulmonary stress or disease, including 2) rats exposed to an ambient temperature of 10°C, 3) rats preexposed to ozone to induce pulmonary inflammation, and 4) rats pretreated with monocrotaline (MCT) to induce pulmonary hypertension and vasculitis. Animals from each regimen were instilled with one of four doses of ROFA (0, 0.25, 1.0, 2.5 mg) and telemetry data were acquired for 96 hours following ROFA instillation. Dose-related hypothermia and bradycardia were observed in healthy animals following exposure to ROFA; the magnitude and duration of these responses were potentiated in all compromised models. Delayed hypothermic and bradycardic responses occurred in healthy animals receiving 2.5 mg ROFA up to 48 hours following instillation. These delayed responses were exacerbated in the MCT- and 10°C-exposure models, but attenuated in the O₃-preexposed group. Additional observed effects of ROFA included induction of cardiac arrhythmias and increased mortality. These results demonstrate a distinct cardiac component to ROFA toxicity that agrees with epidemiological findings of PM-related excess mortality. Furthermore, the observed dose-related hypothermia and bradycardia may confound the interpretation of results from air pollution toxicology studies in rodents.

KEYWORDS

| | |
|--------------------|-------------|
| radiotelemetry | temperature |
| monocrotaline | arrhythmia |
| hypothermia | heart rate |
| ozone | |
| particulate matter | |

INTRODUCTION

Recent epidemiological studies (Lyon *et al.*, 1995; Pope *et al.*, 1992; Schwartz, 1994) have reported excess daily morbidity and mortality associated with increases in the levels of ambient particulate matter (PM). This association is strengthened when analyses are limited to hospital admissions for cardiovascular or respiratory disease (Burnett *et al.*, 1995; Ponka and Virtanen, 1996; Schwartz and Morris, 1995), suggesting that these organ systems may be particularly sensitive to the effects of PM. However, toxicological confirmation of such adverse PM health effects is obfuscated by several factors, including the variability of PM composition, the inherent complications with the extrapolation of relatively high-dose animal data to the low-dose human situation, and the likely enhanced susceptibility associated with preexisting disease.

The most compelling evidence linking the reported epidemiological PM-associated increases in mortality with PM toxicity in animals comes from rodent studies (Dreher *et al.*, 1997; Killingsworth *et al.*, 1997; Nadziejko *et al.*, 1997). Laboratory rodents, however, have an innate response to many toxins, including pulmonary irritants, which may confound the examination of cardiopulmonary toxicity. Decreases in heart rate (HR) and core body temperature (T_{co}) have been demonstrated in rats and mice following exposure to a number of toxic agents, including ozone, chlordimeform, chloroform, and carbon monoxide (Gautier and Bonora, 1994; Terrell *et al.*, 1997; Watkinson and Gordon, 1993; Watkinson *et al.*, 1995). This *hypothermic response*, as defined by Watkinson and Gordon (1993), is characterized by dose-related decreases in the above parameters, as well as in other physiological and metabolic indices, such as minute ventilation, tidal volume, and oxygen consumption. It was further proposed that such a reduction in metabolism could serve to modulate the toxic effects of a given compound. With respect to inhaled toxic agents, a reduced metabolism may also lead to a decrease in

minute ventilation and, therefore, dose. However, complications in other organ systems may arise if the magnitude of the T_{co} decrease is too severe. Results of previous research from this laboratory suggest that a T_{co} reduction of approximately 1.5–2.5°C appears to decrease toxicity and increase survival, while more severe decreases (>3°C) create an additional stress on the rodent and may actually potentiate toxicity (Watkinson and Gordon, 1993). Importantly, this hypothermic response to toxic agents commonly seen in rodents has not been reported for humans, thus complicating the extrapolation of rodent data to humans for regulatory purposes.

The present study investigated the effects of residual oil fly ash (ROFA), a fugitive-derived airborne particulate matter, on cardiac and thermoregulatory responses in conscious, unrestrained adult rats. The origin and characteristics of ROFA are described in detail elsewhere (Dreher *et al.*, 1997; Hatch *et al.*, 1985). Briefly, ROFA is a highly soluble PM sample, containing relatively large concentrations of certain transition metals, including iron, nickel, and vanadium. Rodent models of cardiopulmonary stress or disease were used to study potential risk factors and examine their role(s) in modulating the toxicity of ROFA. Consequently, effects of ROFA could be compared among 1) healthy rats and a variety of animal models that simulated 2) cardiovascular and thermoregulatory stress via cold-exposure, 3) pulmonary inflammation induced by pretreatment with ozone, or 4) pulmonary hypertension with concomitant vasculitis and right ventricular hypertrophy induced by monocrotaline (MCT).

METHODS

Animals. Male Sprague-Dawley rats (Charles River Laboratory, Raleigh, NC; 60-day-old at the beginning of study) were used in all protocols. Rats were isolated in an animal housing facility for one week following delivery to ensure that all animals were pathogen-free and to allow recovery of normal circadian rhythm. Following telemeter implantation, rats were individually housed in plexiglas cages (28×17×12 cm) within a specially designed, climate-controlled exposure chamber. The T_a was controlled at $22\pm 1^\circ\text{C}$ unless otherwise noted and the relative humidity was maintained from 40–65%. A 12-h light:12-h dark cycle was imposed with food and water provided *ad libitum* throughout the experiment. All protocols were approved by the Institutional Animal Care and Use Committee of the U.S. EPA.

Experimental Preparation. Animals were anesthetized with pentobarbital sodium (Nembutal, Abbott Laboratories, North Chicago, IL; 50 mg/kg, i.p.) and implanted with a radiotelemetry transmitter (Model TA11CTA-F40; Data Sciences International, Inc.) using aseptic surgical procedures (Watkinson *et al.*, 1995). Warm water bottles were placed within the cages for 1–2 hours post-surgery to facilitate return to normothermia and speed recovery from anesthesia. Animals were allowed a minimum of five days for recovery from surgery and the reestablishment of circadian rhythm. At the time of ROFA instillation, rats ranged in body weight from 320–410g.

Experimental Protocol. The study was conducted using four treatment regimens (Table 1). Unless otherwise noted, animals within each regimen were matched by weight, order of exposure, and position within the chamber, then randomly assigned to one of four groups ($n=4/\text{group}$) receiving intratracheally-instilled doses of ROFA. ROFA was suspended in saline such that all instillates were

0.3 cc in volume, and all doses were administered while the rats were under light halothane anesthesia (Costa *et al.*, 1986).

REGIMEN 1: ROFA Exposure in Healthy Rats.

Animals were allowed twelve days to recover from the surgery, after which they were divided into four groups ($n = 4/\text{group}$) and intratracheally-instilled with one of four doses of ROFA (0.0, 0.25, 1.0, or 2.5 mg). Animals were maintained at an T_a of $22 \pm 1^\circ\text{C}$ and monitored telemetrically for 96 hours. At the end of the monitoring period, rats were anesthetized (pentobarbital sodium, 60 mg/kg, i.p.) and euthanized via exsanguination. Whole lung and heart tissues were dissected and treated as described below.

REGIMEN 2: ROFA Exposure in Rats Housed at a Cold T_a .

The protocol for the second regimen was essentially identical to that of the first with the exception of a lower T_a . For this regimen, animals were allowed five days to recover from surgery, after which chamber T_a was lowered to 10°C . Five additional days were allowed for the animals to adapt to the cold temperature. ROFA was administered on the tenth day post-surgery according to the above protocol and the animals were maintained at an T_a of 10°C throughout the 96-h monitoring period. The remainder of this study was conducted identically to that of Regimen 1.

REGIMEN 3: ROFA Exposure in Rats with Ozone-Induced Pulmonary Inflammation.

Using a 2×2 study design, rats were exposed in a whole-body chamber to either ambient O_3 (1 ppm \times 6 hours) or filtered air 18 hours prior to either ROFA (2.5 mg) or saline instillation. Dosing

groups were divided as follows: Air/Saline (n=3), Ozone/Saline (n=4), Air/ROFA (n=4), Ozone/ROFA (n=4). Animals for this regimen were given 31 days to recover from surgery. Data acquisition and tissue collection were carried out as described below.

REGIMEN 4: ROFA Exposure in Rats with MCT-Induced Pulmonary Vasculitis and Pulmonary Hypertension.

MCT (60 mg/kg, i.p.) was administered to all rats in this regimen at twelve days following surgery. Twelve additional days were allowed to establish a general pulmonary vasculitis and mild pulmonary hypertension (Reindel *et al.*, 1990) before ROFA instillations were conducted (as described in Regimen 1). At the end of the 96-h monitoring period, surviving animals were anesthetized, as described above, for tissue retrieval. Lungs and heart ventricles from all animals were dissected and weighed.

Telemetry Data Acquisition and Analysis. High speed (50 mm/s \times 10s) chart recordings (Model MT95K2; AstroMed, West Warwick, RI) of the telemetric ECG signals from all animals were acquired at 4-h intervals for 48 hours prior to ROFA administration. Following ROFA instillation, ECG rhythm strips were obtained at 5-min intervals for the first hour, at 10-min intervals for the next five hours, and at 30-min intervals for the remainder of the 96-h monitoring period. T_{co} and HR data for all rats were collected by a computerized acquisition system (Dataquest IV, Data Sciences International Inc., St Paul, MN) at 10-min intervals and stored on disk for 48-h before and 96-h following ROFA instillation.

Tissue Sample Collection and Analysis. At the conclusion of each 96-h monitoring period, surviving rats were euthanized and their hearts were excised, trimmed of atrial and vascular tissue, washed twice with saline to remove excess blood, and blotted dry. The right ventricle was dissected

away from the left ventricle and septum and both sections were weighed and recorded as the ratio of the weights ($\frac{\text{Right Ventricle}}{\text{Left Ventricle} + \text{Septum}}$). The lungs and trachea were dissected at the base of the larynx, cleared of any residual external tissue, and weighed.

Statistics. HR and T_{co} data were averaged within dose groups and analyzed by Tukey's fixed effects ANOVA. All endpoints were averaged by group and compared via Student's t-test. Arrhythmia frequency was analyzed by standard ANOVA. Probability values of < 0.05 were considered significant.

RESULTS

Core Temperature. The T_{CO} of control animals in all regimens demonstrated a robust circadian rhythm with an amplitude of approximately 1°C . Additionally, control animals displayed an *increase* in T_{CO} that was both brief (<1 h) and moderate ($<0.5^{\circ}\text{C}$) immediately following saline instillation. ROFA instillation elicited a transient dose-dependent decrease in T_{CO} in animals housed at an T_a of 22°C . The maximum T_{CO} decrease of high dose animals was 2.2°C (all T_{CO} and HR data are presented as dose-group mean difference from control group values); T_{CO} returned to preexposure values within 6 hours post-instillation (Figure 1A). Medium and low dose rats displayed less severe T_{CO} decreases (1.5°C and 0.6°C , respectively), with durations considerably shorter than those of the high dose animals. Additionally, high dose rats exhibited a delayed hypothermia of $\approx 1.0^{\circ}\text{C}$ below control levels that was most pronounced from 24–36 hours post-instillation.

The T_{CO} response of animals housed at an T_a of 10°C was similarly dose-related, but potentiated compared to that of the animals housed at 22°C . The T_{CO} of high dose cold-exposed rats decreased 3.5°C and returned to control values after approximately 6 hours following ROFA administration (Figure 1B). The T_{CO} of medium and low dose rats in the low temperature regimen showed decreases of 2.9°C and 0.5°C , respectively. A delayed hypothermia of $\approx 1.0^{\circ}\text{C}$ below control was again observed in high dose rats. The duration of this response was prolonged in comparison to the rats in Regimen 1, spanning 12–72 hours post-instillation.

Pretreatment with O_3 caused hypothermia which was rapidly resolved following cessation of exposure. The T_{CO} of all O_3 -preexposed animals returned to control values prior to ROFA instillation. The T_{CO} of animals with ozone-induced pulmonary inflammation demonstrated a maximum decrease of 4.0°C following ROFA instillation (2.5 mg), a value 1.8°C lower than air-exposed animals

administered the same dose of ROFA (Figure 1C). This hypothermic response lasted approximately 18 hours before returning to preexposure values. No delayed hypothermia was observed in O₃-preexposed animals.

Animals with MCT-induced pulmonary vasculitis and mild pulmonary hypertension displayed T_{co} decreases in a dose-dependent manner immediately following ROFA administration (Figure 1D). The T_{co} of low dose rats decreased 1.0°C following ROFA administration, but returned to pre-exposure levels within 2 hours. Significant deviations from control values (up to 0.5°C) were observed in this low dose group sporadically over a range of 30–42 hours after instillation. As stated, the immediate T_{co} decrease was dose-dependent (3.0°C and 3.5°C below control in medium and high dose groups, respectively); however, the high dose group returned briefly to control values while the medium dose group steadily decreased throughout the study. At 24 hours post-instillation, the high dose group also began a gradual decline in T_{co}, which remained 1.0°C below that of the time-paired saline controls at the end of the study. It should be noted that there were a number of lethalties in the MCT-treated rats following ROFA instillation (n=2, 3, and 1 in the high, medium, and low dose groups, respectively) that contributed to the large variability and precluded statistical analysis of these data. Data from lethalties were excluded in the above analysis, thus reducing the group numbers.

Heart Rate. In general, HR response patterns were very similar to T_{co} responses across all groups. In all regimens, HR of saline-instilled animals increased slightly for a few minutes following handling. In Regimen 1, HR of high dose animals decreased 95 bpm below control for a 4-h duration immediately following instillation (Figure 2A). The HR of medium dose rats decreased 75 bpm below control for 1 hour, while the HR of low dose rats did not significantly deviate from that of saline-treated animals. High and medium dose rats demonstrated a delayed bradycardia spanning from

approximately 12–48 hours after instillation. A slight rebound effect of elevated HR was observed over the last 24 hours of the study in high dose animals.

Rats housed in cold T_a demonstrated a two-fold potentiation of this HR response, with HR of high dose rats decreasing 175 bpm and that of medium dose rats decreasing 160 bpm (Figure 2B). Low dose rats housed at 10°C also demonstrated a brief but significant decrease over controls (63 bpm), driven in part by the transient HR *increases* observed in control animals following handling and increased activity. HR of high dose animals did not return to control levels following the immediate response and demonstrated significant differences (up to 160 bpm) from control values for over 48 hours post-instillation.

Ozone-induced inflammation potentiated the immediate decrease in HR over air-exposed rats receiving the same dose of ROFA (124 bpm versus 95 bpm); however, no delayed response was observed in the ozone-pretreated rats (Figure 2C). The delayed response (\approx 50 bpm) was observed in air/ROFA-exposed animals from 36–48 hours post-instillation. As expected, HR was markedly decreased following ozone exposure but returned to control values before ROFA administration occurred. HR in ozone-treated rats appeared to display a rebound effect on day 3, rising \approx 50 bpm above control.

Animals with MCT-induced pulmonary vasculitis and hypertension demonstrated immediate decreases in HR in response to all doses of ROFA (122, 107, and 55 bpm in high, medium, and low dose groups, respectively; Figure 2D). High dose rats returned to control levels at 24 hours following instillation, but demonstrated a progressive bradycardia for the remainder of the monitoring period. Medium dose rats showed a similar delayed response compared to the high dose rats, although they displayed a greater overall decrease in HR. The HR of surviving low dose rats quickly returned to

control values, but demonstrated significant decreases compared to control animals during dark periods when activity and T_{co} are normally elevated. The HR of lethalties increased ~100 bpm within 2 hours before death. Again, due to mortalities following ROFA instillation in the MCT-treated rats, HR data could not be analyzed with the statistical models available for the other groups.

Arrhythmias and Electrocardiographic Changes. In all studies, exposure to ROFA was weakly ($p=0.15$) associated with a dose-dependent increase in the frequency of observed cardiac arrhythmias. Interestingly, correlational analysis showed a stronger relationship between the maximal T_{co} decrease for individual animals and their arrhythmia frequency ($r^2=0.54$) than between dose and arrhythmia frequency ($r^2=0.46$). Arrhythmias observed in control animals were generally infrequent and benign (e.g., sinus arrhythmia, isolated premature contractions). In contrast, ROFA-treated rats demonstrated a range of dysrhythmias from relatively innocuous premature contractions and R-R interval changes to more serious conduction deficits such as prolonged AV blockade and bundle branch blocks.

In rats housed at an T_a of 22°C, the frequency of arrhythmias was increased in high and medium dose groups for the first 24 hours, but slowly subsided thereafter (Figure 3A). In Regimen 2, the medium dose animals behaved similarly to those in Regimen 1, but the frequency of arrhythmic events in the high dose rats did not diminish over the second 24-hour period (Figure 3B). In Regimen 3, the arrhythmogenic effects of ROFA were abrogated in O_3 -preexposed rats (Figure 3C). These results stand in contrast to the potentiated hypothermia and bradycardia elicited by this model of pulmonary inflammation.

MCT-treated animals displayed marked increases in the frequency and severity of arrhythmic events following all doses of ROFA, and the frequency of arrhythmias remained elevated at the end of

the 96-h monitoring period for all three groups receiving ROFA (Figure 3D). Depression of the S-T segment area and general morbidity were observed in several of the surviving animals. Lethalities occurred in all dose groups except control and were preceded by severe hypothermia and bradycardia, as well as distinct ECG abnormalities. These aberrant ECG patterns were expressed in one of two ways: 1) prolonged depression of the S-T segment area accompanied by gradual myocardial failure; or 2) sudden myocardial failure with associated conduction abnormalities. For a more complete description of the particle-associated arrhythmogenesis, see Watkinson *et al.* (1998).

Organ Weight Analysis. In all studies, ROFA caused a dose-dependent increase in lung wet weight and produced macroscopic inflammation, necrosis, and focal edema of the lung. The RV/LVS ratio was not affected by ROFA in any study, although MCT-treated rats displayed significant ($p < 0.01$) hypertrophy of the right ventricle ($RV/LVS = 0.35 \pm 0.06$) compared to rats not receiving MCT (0.26 ± 0.05). Euthanized MCT-treated rats had a significantly higher RV/LVS ratio ($p < 0.01$) than rats that died during the study (0.31 ± 0.03).

DISCUSSION

These studies were designed to investigate the adverse cardiovascular health effects caused by PM in healthy and cardiopulmonary-compromised rats. These results clearly demonstrate that ROFA induced robust cardiac and thermoregulatory responses in rats, characterized by both immediate and delayed reductions in HR and T_{co} , increases in the frequency and severity of cardiac arrhythmias, and increased cardiac-related mortality. Most observed effects were potentiated in all animal models of cardiopulmonary stress or disease. Hypothermic and bradycardic effects induced by other pulmonary irritants suggest that the observed response to ROFA instillation was not unexpected in rodents (Watkinson *et al.*, 1995; Watkinson *et al.*, 1997). However, the biphasic nature of the bradycardia and hypothermia following ROFA exposure was unlike the previously reported exposure-dependent monophasic responses to other inhaled toxins.

The immediate hypothermic response is similar to that seen following treatment with ozone or chloroform (Terrell *et al.*, 1997; Watkinson *et al.*, 1995). Both of these toxic agents are pulmonary irritants thought to induce nervous system reflex response via interaction, directly or indirectly, with pulmonary C-fibers (Kwong *et al.*, 1998; Lai and Kou, 1998). Detailed physiologic and biochemical mechanisms underlying the hypothermic response pathway in rodents are only partially understood. Irritant-induced decreases in physiological and metabolic parameters (HR, T_{co} , tidal volume, O_2 consumption), as well as the increased incidence of cardiac arrhythmias that appear to be similar to those induced by cholinergic substances, implicate the parasympathetic nervous system as a possible mediator of this response. The results of the present study are consistent with this hypothesis.

High doses of ROFA elicited a delayed hypothermia previously unreported for other pulmonary toxins. This delayed response coincided with reported time points for the development of

pulmonary inflammation following particulate exposure (Adamson and Bowden, 1978; Dreher *et al.*, 1997). Interestingly, ozone-induced pulmonary inflammation, which peaks 18–24 hours after exposure (Pino *et al.*, 1992), does not produce a delayed hypothermia similar to that seen in response to ROFA. Decomposition and detoxification of O₃ occurs rapidly at the surfactant layer of the lungs, while particles and particle constituents may have significantly longer pulmonary residence times, resulting in a continued oxidative burden in the lungs. Whether such kinetic differences in the airways could be responsible for the disparity of the delayed physiological responses is unclear. However, given the highly soluble nature of the ROFA dust (Dreher *et al.*, 1997), it is unlikely that a significant amount of material resides in the lung after 24 hours.

Animals housed at 10°C demonstrated a potentiated hypothermic response following ROFA administration compared to animals housed at an T_a of 22°C. The cold-exposed rat was selected to provide a non-pathologic animal model of cardiopulmonary stress. Acclimating to colder temperatures involves numerous physiological and metabolic changes that can tax the cardiovascular system as it attempts to maintain homeostasis and normothermia, leading to significant increases in cardiac work (Fregly *et al.*, 1989). At the time of instillation, the initial HR for all cold-exposed rats was significantly higher than the HR for animals in any other regimen (~ 425 bpm versus ~ 325 bpm, respectively). While the magnitude of the HR decrease was much greater in cold-exposed rats, the minimum HR following ROFA instillation did not differ from that of the ROFA-exposed animals housed at T_a=22°C.

Pulmonary inflammation has been proposed to be an important factor in susceptibility to PM toxicity. Exposure to O₃ causes a pulmonary inflammation that is most severe between 18-24 hours following exposure (Pino *et al.*, 1992). As anticipated, rats exposed to O₃ displayed an immediate hypothermic response. However, by the time of instillation (24 hours post-exposure), the HR and T_{co}

of O₃-treated animals had returned to control values. Preexposure to O₃ led to a significant exacerbation of the immediate hypothermic response, but attenuated the delayed response. However, O₃-exposed rats displayed no increase in arrhythmia frequency following ROFA instillation, unlike animals preexposed to filtered air or animals from the first two regimens.

When injected intraperitoneally, MCT leads to a variety of cardiopulmonary pathologies, including pulmonary inflammation, pulmonary hypertension, and right ventricular hypertrophy (Lipke *et al.*, 1993; Reindel *et al.*, 1990). This model has been used in a number of rodent studies and is known to increase sensitivity to PM toxicity (Killingsworth *et al.*, 1997; Kodavanti *et al.*, 1999). In the present study, rats pretreated with MCT displayed exacerbated immediate and delayed hypothermic responses to instilled ROFA. Lethalities were observed in the MCT-treated animals exposed to ROFA (50%), but not in animals receiving saline. Previous studies have reported similar mortality rates (42%) following exposure to PM with this model of cardiopulmonary disease (Killingsworth *et al.*, 1997). While bradycardia was evident in all ROFA-exposed rats, lethalities displayed an abrupt increase in HR immediately prior to death. Killingsworth *et al.* (1997) observed a lowered right ventricular systolic pressure in ROFA-exposed lethalities as compared with that of surviving animals. Taken together, these data are consistent with right ventricular heart failure as a mechanism of mortality. While right ventricular heart failure is a typical outcome of MCT treatment in rats, the absence of lethalities in saline-instilled rats suggests that ROFA may hasten or otherwise exacerbate the MCT pathology.

Many of the arrhythmias observed in the present studies, including type 2 AV-node block and premature contraction, may be related to hypothermia and increased parasympathetic activity rather than a direct toxic response to ROFA. Although ROFA contains several transition metals that are

reported cardiotoxins, including nickel, vanadium, and iron, the translocation of such metals in biologically relevant concentrations from the lungs to the myocardium has not been reported. Arrhythmia frequency in individual animals demonstrated a higher correlation with their maximum T_{CO} decrease ($r^2=0.54$, Pearson's coefficient) than with the dose model ($r^2=0.46$) and ANOVA revealed only a weak association between ROFA dose and the frequency of arrhythmias. This suggests that the observed arrhythmias are a further complication of hypothermia and/or increased parasympathetic activity. The types of arrhythmias observed, primarily AV node blockade or premature ventricular contraction, are characteristic of increased parasympathetic activity and therefore potentially nonspecific to the compound administered. ECG patterns in humans following acute accidental hypothermia often demonstrate similar arrhythmias. On the other hand, the O_3 -pretreatment appeared to abrogate ROFA-induced arrhythmogenesis, despite a potentiated immediate hypothermic response. This may be at least partially attributable to increases in antioxidant enzymes or adaptive alterations in lung biochemistry and cell signaling capacity induced by exposure to ozone.

Despite the absence of dose-response effects on mortality following ROFA exposure, abnormal ECG patterns observed in lethalties may help elucidate possible mechanisms of cardiac toxicity. As previously reported (Watkinson *et al.*, 1998), mortalities occurred only in the MCT-treated animals following exposure to ROFA (0, 25, 75, and 50% lethalties in control, low, medium and high dose groups, respectively). Examination of the ECG recordings for those animals suggested two distinct scenarios: 1) a relatively slow failure of the myocardium potentially due to hypoxemia leading to myocardial ischemia, or 2) an abrupt failure of the heart due to a fatal conduction-related arrhythmia. The first scenario demonstrated severe morphological alterations that suggest ischemia or acidosis, potentially caused by an edema-related respiratory insufficiency. The latter scenario was characterized

by a relatively stable rhythm with considerable signal noise and/or myocardial irritability. This irritability may indicate electrophysiological disturbances possibly caused by hypoxemia, metal toxicity, or cytokine-induced myocarditis. Both ECG patterns support epidemiological findings that suggest that individuals with coronary artery disease, heart failure, or cardiac dysrhythmia are more susceptible to the adverse effects of PM exposure (Burnett *et al.*, 1995; Ponka and Virtanen, 1996; Schwartz and Morris, 1995).

The results of this study, in addition to clearly demonstrating a cardiac component of ROFA toxicity, reemphasize the toxicokinetic importance of the previously reported hypothermic response. These data indicate that rodents undergo unique physiological changes following exposure to ROFA that may significantly alter toxicological endpoints and confound the analysis, interpretation, and extrapolation of results. Dose-related reductions in T_{co} may produce differentiated physiological models that may, in turn, alter toxicokinetic parameters. For example, in whole body exposures, minute volume may be lowered during hypothermia, leading to a decreased uptake of inhaled toxins. Also, the kinetics of enzymatic activation/inactivation of the compound and/or the production of radicals or reactive intermediates can be modulated by changes in body temperature. The present study, which administered discrete doses by instillation rather than inhalation, was able to control for the first potential confounder, but not the latter. Enzyme kinetics and production of biochemical intermediates are mediated in part by T_{co} (McMorn *et al.*, 1998; Puntarulo and Cederbaum, 1989). If the temperature of the alveoli decreases, the quantity of radicals or intermediates generated upon contact of the particles with the surfactant could be reduced. As noted earlier, moderate hypothermia appears to afford some protection in terms of surviving toxic insult, while more severe hypothermia is thought to eventually compromise organ systems. Indeed, results from this study suggest that cardiac

arrhythmias may develop when hypothermia becomes severe.

In summary, the results of the present study demonstrate substantial adverse cardiovascular effects following intratracheal instillation of a fugitive-derived PM. The conclusions of this study must be tempered with the potential confounding associated with the observed hypothermic response, which may contribute in part to the cardiac anomalies seen following instillation of ROFA. The cardiac arrhythmias, which appeared to be predominantly of a parasympathetic nature, are a possible consequence of this response. However, the lethal ECG patterns, which were consistently accompanied by increases in HR, appear independent of T_{co} changes and implicate plausible mechanisms for adverse cardiovascular effects of PM secondary to pulmonary insult. These results support epidemiological findings of PM-associated morbidity and mortality in cardiopulmonary disease patients and furthermore suggest physiological pathways by which the heart might be subject to indirect PM toxicity via pulmonary inflammation-related impairments of gas exchange.

ACKNOWLEDGEMENTS: The authors thank Dr. Urmila P. Kodavanti, Ms. Julie P. Nolan, and Mr. James A. Raub for their thoughtful reviews of this manuscript. Further gratitude is extended to Ms. Judy H. Richards, Mr. James R. Lehmann, Mr. Edwin R. Lappi, and Ms. Sarah P. Watkinson for their superb technical assistance on this project. This study was supported by EPA and EPA/UNC T901915 research training grant.

REFERENCES

- Adamson, I. Y. R., and Bowden, D. H. 1978. Adaptive responses of the pulmonary macrophagic system to carbon. II. Morphologic studies. *Lab. Invest.* 38:430-438.
- Burnett, L. H., Dales, R., Krewski, D., Vincent, R., Dann, T., and Brook, J. R. 1995. Associations between ambient particulate sulfate and admissions to Ontario hospitals for cardiac and respiratory disease. *Am. J. Epidemiol.* 142:15-22.
- Costa, D. L., Lehmann, J. R., Harold, W. M., and Drew, R. T. 1986. Transoral tracheal intubation of rodent using a fiberoptic laryngoscope. *Lab. Animal Sci.* 36:256-261.
- Dreher, K. L., Jaskot, R. L., Lehmann, J., Richards, J. R., and McKee, J. G. 1997. Soluble transition metals mediate residual oil fly ash induced acute lung injury. *J. Toxicol. Environ. Health* 50:285-305.
- Fregly, M. J., Kikta, D. C., Threarte, R. M., Torres, J. L., and Barney, C. C. 1989. Development of hypertension in rats during chronic exposure to cold. *J. Appl. Physiol.* 66:741-749.
- Gautier, H., and Bonora, M. 1994. Ventilatory and metabolic responses to cold and CO-induced hypoxia in awake rats. *Respir. Physiol.* 97:79-91.
- Hatch, G.E., Boykin, E., Graham, J.A., Lewtas, J., Pott, F., Loud, K., and Mumford, J.L. 1985. Inhalable particles and pulmonary host defense: in vivo and in vitro effects of ambient air and combustion particles. *Environ. Res.* 36:67-80.
- Killingsworth, C. R., Alessandrini, F., Murthy, G. G. K., Catalano, P. J., Paulauskis, J. D., and Godleski, J. J. 1997. Inflammation, cytokine expression and death in monocrotaline-treated rats following fuel oil fly ash inhalation. *Inhalation Toxicol.* 9:541-565.
- Kodavanti, U. P., Jackson, M. C., Ledbetter, A.D., Gardner, S. Y., Watkinson, W. P., Campen, M. J.,

- and Costa, D. L.. 1999. Lung injury from intratracheal and inhalation exposure to residual oil fly ash in a rat model of monocrotaline-induced pulmonary hypertension. *J. Toxicol. Environ. Health part A* 57:101-121.
- Kwong, K., Hong, J-L., Morton, R. F., and Lee, L-Y. 1998. Role of pulmonary C fibers in adenosine-induced respiratory inhibition in anesthetized rats. *J. Appl. Physiol.* 84:417-424.
- Lai, C. J., and Kou, Y. R. 1998. Stimulation of vagal pulmonary C fibers by inhaled wood smoke in rats. *J. Appl. Physiol.* 84:30-36.
- Lipke, D.W., Arcot, S.S., Gillespie, M.N., and Olson, J.W. 1993. Temporal alterations in specific basement membrane components in lungs from monocrotaline-treated rats. *Am. J. Resp. Cell Mol. Biol.* 9:418-428.
- Lyon, J. L., Mori, M., and Gao, R. 1995. Is there a causal association between excess mortality and exposure to PM10 air pollution? Additional analyses by location, year, season, and cause of death. *Inhalation Toxicol.* 7:603-614.
- McMorn, S. O., Harrison, S. M., and Boyett, M. R. 1998. The effect of temperature on the rate-dependent decrease of the rat ventricular calcium current. *Exp. Physiol.* 83:49-63.
- Nadziejko, C., Chen, L. C., Zelikoff, J. T., and Gordon, T. 1997. Hematological and cardiovascular effects of acute exposure to ambient particulate matter (PM). *Am. J. Resp. Crit. Care Med.* 155:A247
- Pino, M. V., Levin, J. R., Stovall, M. Y., and Hyde, D. M. 1992. Pulmonary inflammation and epithelial injury in response to acute ozone exposure in the rat. *Toxicol. Appl. Pharmacol.* 112:64-72.
- Ponka, A., and Virtanen, M. 1996. Low-level air pollution and hospital admissions for cardiac and

- cerebrovascular diseases in Helsinki. *Am. J. Public Health* 86:1273-1280.
- Pope, C. A., Schwartz, J., and Ronson, M. 1992. Daily mortality and PM10 pollution in Utah Valley. *Arch. Environ. Health* 42:211-217.
- Puntarulo, S., and Cederbaum, A. I. 1989. Temperature dependence of the microsomal oxidation of ethanol by cytochrome P450 and hydroxyl radical-dependent reactions. *Arch. Biochemistry Physics* 269:569-575.
- Reindel, J. F., Ganey, P. E., Wagner, J. G., Slocombe, R. F., and Roth, R. A. 1990. Development of morphologic, hemodynamic, and biochemical changes in lungs of rats given monocrotaline pyrrole. *Toxicol. Appl. Pharmacol.* 106:179-200.
- Schwartz, J. 1994. Air pollution and daily mortality: a review and meta-analysis. *Environ. Res.* 64:36-52.
- Schwartz, J., and Morris, R. 1995. Air pollution and hospital admission for cardiovascular disease in Detroit, Michigan. *Am. J. Epidemiol.* 142:23-35.
- Terrell, D., McGee, J. K., Mansfield, J. L., Stevens, M. A., Watkinson, W. P., Campen, M. J., and Evans, M. V. 1997. Application of a closed inhalation exposure system for simultaneous measurement of metabolic and physiological variables during chloroform (CHCl₃) exposure in rats. (Abstract) *Toxicologist* 36:A327.
- Watkinson, W. P., and Gordon, C. J. 1993. Caveats regarding the use of the laboratory rat as a model for acute toxicological studies: Modulation of the toxic response via physiological and behavioral mechanisms. *Toxicology* 81:15-31.
- Watkinson, W. P., Wiester, M. J., Highfill, J. W., Aileru, A. A., Campen, M. J., Tepper, J. S., and Costa, D. L. 1994. Thermoregulatory considerations affecting both acute and prolonged

- exposures to ozone in rodents. In: *Thermal Balance in Health and Disease*, eds. E. Zeisberger, E. Schönbaum, and P. Lomax, pp. 509-514. Birkhauser-Verlag, Berlin.
- Watkinson, W. P., Wiester, M. J., and Highfill, J. W. 1995. Ozone toxicity in the rat: I. Effect of changes in ambient temperature on extrapulmonary physiological parameters. *J. Appl. Physiol.* 78:1108-1120.
- Watkinson, W. P., Campen, M. J., Lyon, J. Y., Highfill, J. W., Wiester, M. J., and Costa, D. L. 1997. Impact of the hypothermic response in inhalation toxicology studies. *Ann. NY Acad. Sci.* 813:849-863.
- Watkinson, W. P., Campen, M. J., and Costa, D. L. 1998. Cardiac arrhythmia induction after exposure to residual oil fly ash particles in a rodent model of pulmonary hypertension. *Toxicol. Sci.* 41:209-216.

FIGURE LEGENDS**Figure 1A, B, C, D.**

Changes in T_{co} for healthy and compromised, unanesthetized, adult male Sprague-Dawley rats before and after intratracheal instillation of residual oil fly ash (ROFA): (A) healthy animals ($n=16$) housed at 22°C , (B) healthy animals ($n=16$) housed at 10°C , (C) ozone-treated animals ($n=16$) housed at 22°C , and (D) monocrotaline (MCT)-treated animals ($n=16$) housed at 22°C . For Figures A, B, and D, the control, low, medium, and high dose groups ($n=4/\text{group}$) are designated by the blue, green, yellow, and red lines, respectively. In Figure C, the air/saline-treated animals are designated by the blue line, the ozone/saline by the green line, the air/ROFA by the yellow line, and the ozone/ROFA by the red line. Data were collected at 10-min intervals and averaged to 30-min time points for presentation purposes. Dashed vertical lines represent times of ROFA instillation. Bars at the bottom of each figure indicate periods of significant difference from control animals, matched to the appropriate color of the dose group, i.e., red for high dose.

Figure 2A, B, C, D.

Changes in HR for healthy and compromised, unanesthetized, adult male Sprague-Dawley rats before and after intratracheal instillation of residual oil fly ash (ROFA): (A) healthy animals ($n=16$) housed at 22°C , (B) healthy animals ($n=16$) housed at 10°C , (C) ozone-treated animals ($n=16$) housed at 22°C , and (D) monocrotaline (MCT)-treated animals ($n=16$) housed at 22°C . For Figures A, B, and D, the control, low, medium, and high dose groups ($n=4/\text{group}$) are designated by the blue, green, yellow, and red lines, respectively. In Figure C, the air/saline-treated animals are designated by the blue line, the ozone/saline group by the green line, the air/ROFA group by the yellow

line, and the ozone/ROFA group by the red line. Data were collected at 10-min intervals and averaged to 30-min time points for presentation purposes. Dashed vertical lines represent times of ROFA instillation. Bars at the bottom of each figure indicate periods of significant difference from control animals, matched to the appropriate color of the dose group, i.e., red for high dose.

FIGURE 3A, B, C, D.

Frequencies of arrhythmias in unanesthetized, adult male Sprague-Dawley rats following intratracheal instillation of residual oil fly ash (ROFA). (A) Healthy animals housed at 22°C. (B) Healthy animals housed at 10°C. (C) Ozone-pretreated animals housed at 22°C. (D) MCT-pretreated animals housed at 22°C. Each bar represents averages of four animals. Low, medium, and high dose groups received 0.25, 1.0, and 2.5 mg ROFA, respectively (Figures A, B, and D). Animals in the third study (Figure C) received saline or 2.5 mg ROFA. Following instillation, ECG rhythm strips were obtained at 5-min intervals for the first hour, 10-min intervals for the next five hours, and 30-min intervals for the remainder of the 96-h monitoring period. Arrhythmias (predominantly AV-node block and premature contractions) were counted from these printouts and frequencies were determined based on the total sampling time.

Table 1.

| SUMMARY OF PROTOCOLS FOR INSTILLED ROFA PARTICLES STUDY using RODENT MODELS OF CARDIOPULMONARY DISEASE | | |
|---|--|---|
| Experimental Regimen | Experimental Conditions | Procedure and Endpoints |
| 1) ROFA in Healthy Rats | N=16, male 60 d rats; T _a =22°C ROFA (0, 0.25, 1.0, 2.5 mg) | <ul style="list-style-type: none"> • Implant transmitters • Recovery period (7 d) • Initiate stress/disease model <ul style="list-style-type: none"> - Expose to T_a=10°C (4 d), - O₃ (1 d), or - MCT (12 d) • Instill particles intratracheally • Monitor ECG, HR, T_{co}, arrhythmias, lethalties for 48 h before and 96 h following instillation • Sacrifice animals, dissect and weigh heart and lungs |
| 2) ROFA in Cold-Exposed Rats | N=16, male 60 d rats; T _a =10°C ROFA (0, 0.25, 1.0, 2.5 mg) | |
| 3) ROFA in O ₃ -Preexposed Rats | N=16, male 90 d rats; T _a =22°C 1.0 ppm O ₃ or filtered air × 6h, ROFA (0, 2.5 mg) | |
| 4) ROFA in MCT-Treated Rats | N=16, male 60 d rats; T _a =22°C 60 mg/kg MCT i.p., ROFA (0, 0.25, 1.0, 2.5 mg) | |

Figure 1.

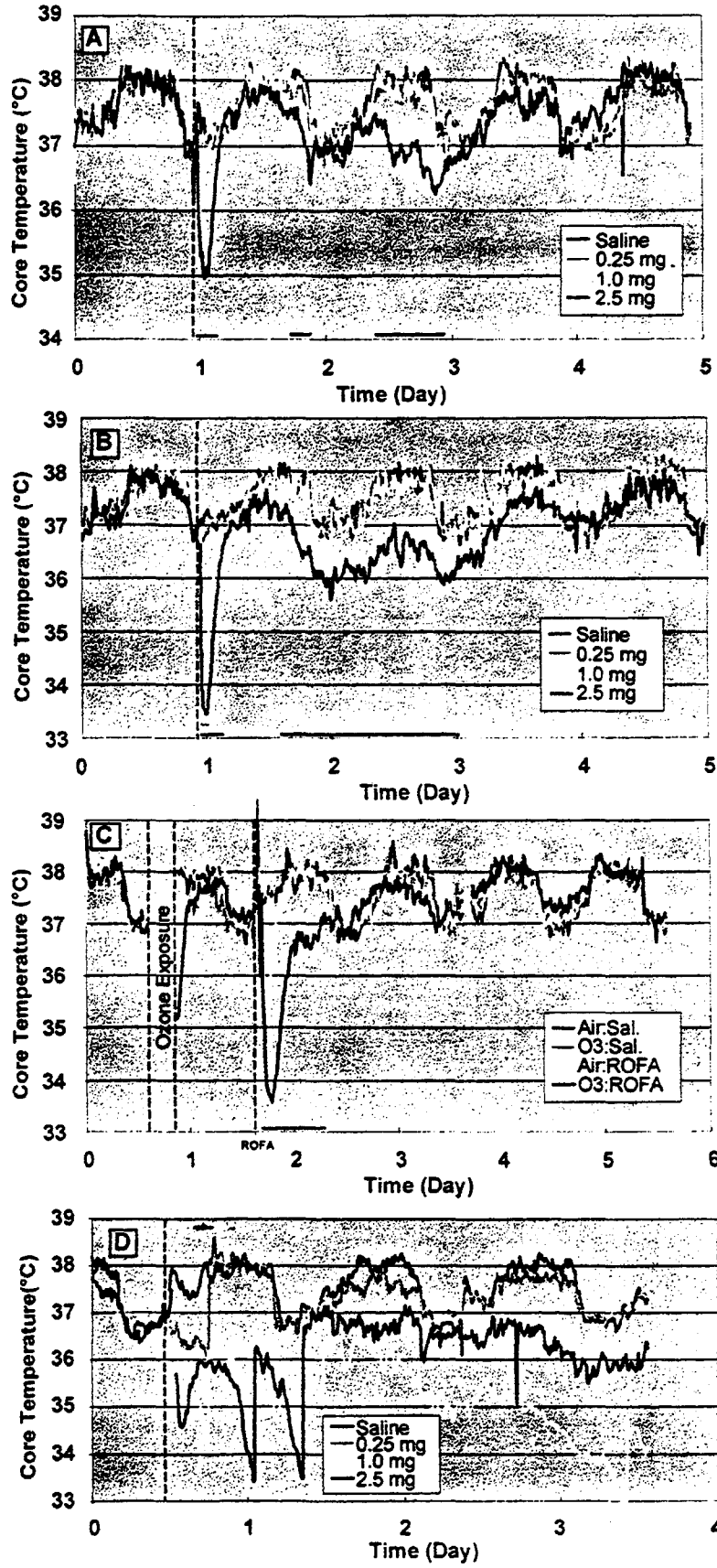


Figure 2.

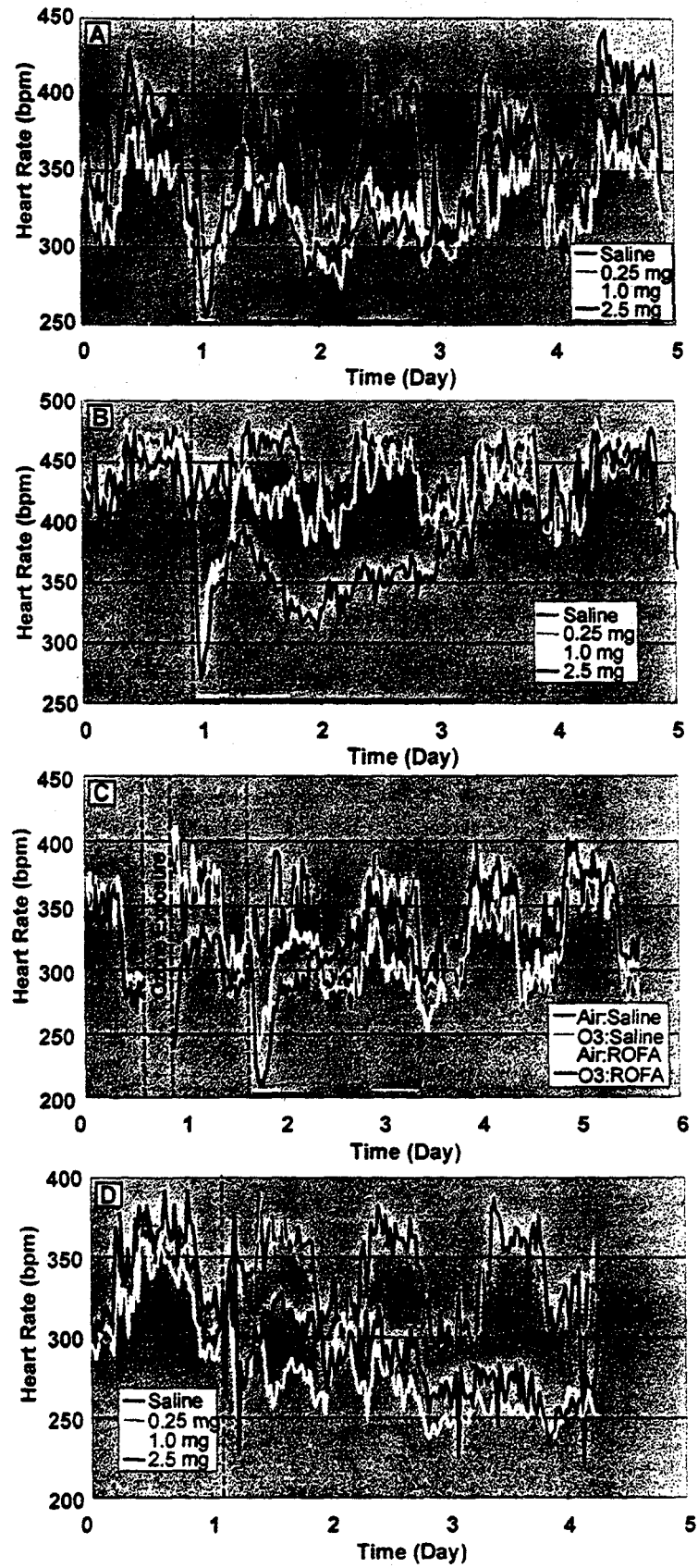
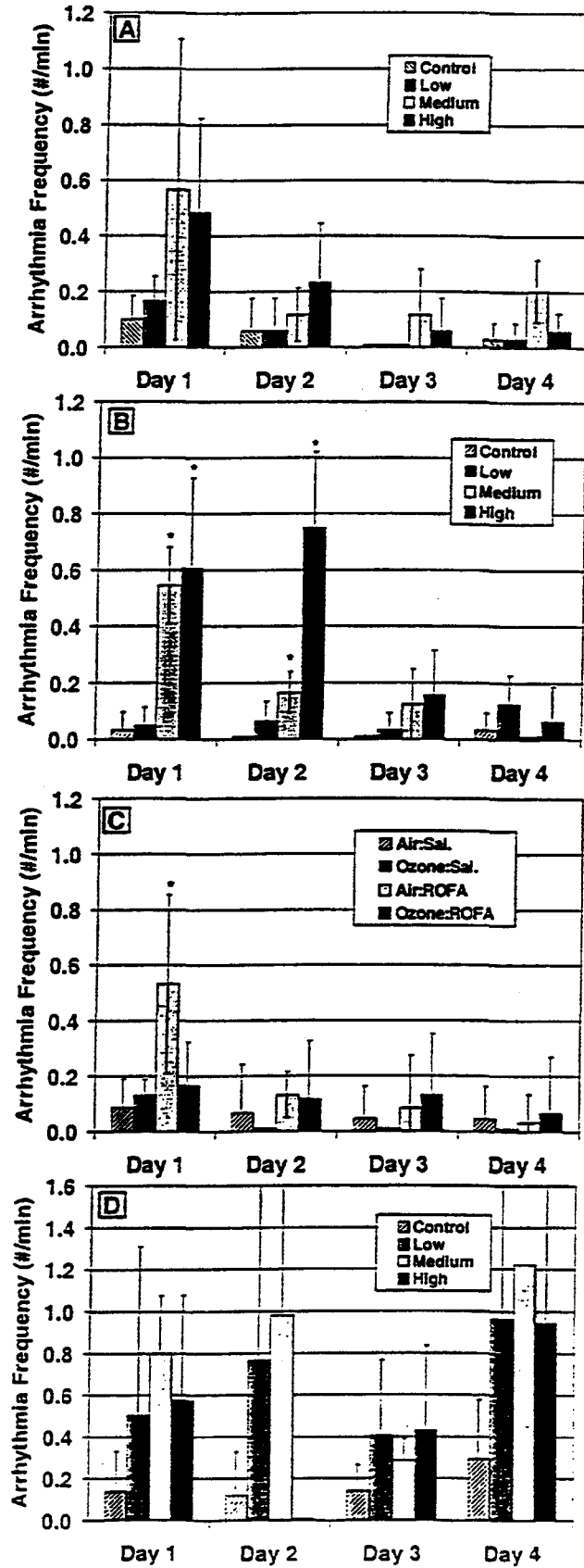


Figure 3.



Age-Related Responses To Concentrated Urban Air Particles (CAPs).

RW Clarke, P Catalano¹, B Coull¹, P Koutrakis, GG Krishna Murthy, T Rice and JJ Godleski. Departments of Environmental Health and Biostatistics¹, Harvard School of Public Health, Boston, MA, USA.

Abstract

Epidemiological studies have reported that elderly individuals have a higher risk of detrimental responses following exposure to elevated levels of ambient particulate matter. To investigate this finding in a toxicological model, aged Fisher rats were exposed for three days to concentrated urban air particles (CAPs) from Boston. Based on results from previous work, we tested the hypothesis that older animals would exhibit more severe pulmonary inflammation and hematological changes following the CAPs exposure when compared to young, normal animals (Gordon et al, 1998; Clarke et al, 1999). Aged Fisher rats (>17 months) and juvenile Fisher rats (4-6 weeks) were obtained and observed in a virus-antigen free facility for 3 months prior to exposure. Following observation, animals (10 rats/group X 4 groups total = 40 rats) were exposed to CAPs or filtered air (FA) for 5 hours/day for three consecutive days. Daily integrated CAPs concentrations were approximately 80, 170, and 50 $\mu\text{g}/\text{m}^3$ on day 1, 2, and 3, respectively. None of the animals died throughout the duration of exposure. Twenty-four hours following the last day of exposure, blood was collected by cardiac puncture, and bronchoalveolar lavage (BAL) was performed. Old rats exhibited a small, but significant, increase in BAL polymorphonuclear leukocytes (PMN) following exposure to CAPs ($0.58 + 0.16 \times 10^5$ cells (FA) versus $1.47 + 0.39 \times 10^5$ cells (CAPs)). There were no CAPs-related significant changes in aged animals in total BAL cell counts, BAL lactate dehydrogenase, total white blood cell (WBC) counts, or the percent of WBC PMN, lymphocytes, and monocytes. Young rats exhibited significantly higher total BAL cell counts marked by a significant increase in BAL PMN ($0.29 + 0.20 \times 10^5$ cells (FA) versus $5.69 + 1.52 \times 10^5$ cells (CAPs)) following CAPs exposure. When comparing aged versus young (CAPs- or filtered air-exposed) animals, advanced age was associated with significant decrements in the total BAL cell counts, total WBC counts, percent of blood lymphocytes, and blood hemoglobin; a significant increase in the percent of blood PMN was also observed. The above results suggest 1) young Fisher rats may represent a sensitive model for the examination of pulmonary inflammatory responses following CAPs exposure and 2) the lack of an inflammatory response in the aged rats, despite the presence of a higher percentage of circulating neutrophils, may reflect decreased sensitivity to inhaled particles and pathogens.

Acknowledgements

The authors wish to acknowledge the excellent technical assistance of Marshall Katler, Victoria Hatch, and Rebecca Stearns on the present work. This work was partially funded by National Institutes of Health Grants #ES08129 and #ES00002.

Introduction

Epidemiological studies have reported increased mortality and morbidity in populations exposed to increased levels of ambient particulate matter (Schwartz and Dockery, 1992; Dockery et al, 1993; Dockery and Pope, 1994; Pope et al, 1995). It is estimated that 60,000 U.S. deaths per year may be related to particulate matter exposure (Schwartz et al, 1991). Morbid responses including increased onset of acute respiratory illness (Pope et al, 1991) have also been reported in association with increased

particulate matter levels. Prospective studies have reported significantly increased mortality associated with airborne particulate exposures (Schwartz and Dockery, 1992; Dockery et al, 1993; Pope et al, 1995); mortality effects have been related to incremental particle concentration increases of $10 \mu\text{g}/\text{m}^3$ (Schwartz and Dockery, 1992; Dockery et al, 1993). In addition to the findings cited above, elderly populations are reported to be more susceptible to increased atmospheric particle levels than normal populations (Pope et al, 1995; Saldiva et al, 1995). These epidemiological results, when integrated with the increased incidence of pulmonary infection in elderly populations (Gyetko and Toews, 1993; Zissel et al, 1999), suggest that alterations in pulmonary immune status may play an important role in the biological response to inhaled ambient particulate matter.

Despite the epidemiological findings, pathophysiological mechanisms and effects due to inhaled particulate matter responsible for the observed mortality and morbidity in normal and elderly populations have not been well-defined. There have been few studies to date investigating the effects of inhaled CAPs on pulmonary responses. Clarke (et al, 1999a) reported dose-dependent, CAPs-related significant increases in pulmonary inflammation marked by neutrophil influx in both normal and chronic bronchitic rats; chronic bronchitic rats also exhibited increased vascular permeability following exposure to CAPs. Another study reported increases in the percentage of circulating neutrophils and significant, persistent increases in heart rate in normal and monocrotaline-injured rats following a single 3 hour exposure to CAPs (Gordon et al, 1998). More interestingly, this study reported significant pulmonary inflammatory responses in older (> 6 months) rats with pre-existing pulmonary injury (monocrotaline-induced) following CAPs inhalation when compared to healthy normal animals and young animals with monocrotaline injury. These results indicate that inhalation of CAPs can induce pulmonary injury and that age may be a significant susceptibility factor for alterations in pulmonary responses to inhaled particles. Based on the epidemiological and toxicological evidence cited above, we tested the hypothesis that older animals would exhibit more severe pulmonary inflammation and hematological changes following the CAPs exposure when compared to young, normal animals.

Methods

Animal Model And Exposure: Twenty young male Fisher rats (6-8 weeks; 150-200 grams; Harlan Laboratories) and twenty aged male Fisher rats (17 months; 500-600 grams; Harlan Laboratories) were obtained and managed in accordance with National Institutes of Health guidelines for the care and use of laboratory animals. The animals were divided at random into four experimental groups: 1) young, filtered air (sham)-exposed, 2) young, concentrated air particle (CAPs)-exposed, 3) aged, sham-exposed, and 4) aged, CAPs-exposed. Animals were exposed to filtered air or CAPs for six hours/day for three consecutive days in stainless steel wire-mesh holding units placed inside a custom-designed rodent exposure unit (Clarke et al, 1999a). Ten young and ten aged animals were exposed at each time (40 animals total). The sealed rodent unit had a volume of 142 L and was placed inside a 1000-L stainless steel and glass exposure unit for the duration of the exposure. Temperature and humidity inside the unit were measured throughout exposure and ranged between 25.0-30.0 °C and 30-50%, respectively.

CAPs Generation: The Harvard Ambient Particle Concentrator (HAPC) aerosol generation and delivery system has been previously described in detail elsewhere (Sioutas et al, 1995; Clarke et al, 1999). The pressure drop as air passes through the HAPC is a maximum of 15 inch H_2O . In order to account for possible effects of this negative pressure on the control filtered air exposures, a valve was used at the inlet to create the same pressure drop at the same flow rate in the exposure chamber. The aerosol flow rate provides for a residence time of about 3.5 minutes (15 air changes per hour).

CAPs Analysis: The ambient and chamber levels of fine particulate mass are determined gravimetrically by collecting particles onto pre-weighed 47 mm Savillex teflon filters sampled at 3 L/minute. Filters were gravimetrically analyzed using a Cahn 31 electrobalance in a temperature- and humidity-controlled room. The end filter weights, sampling time, and sampling flow rate were used to calculate the particle concentration in $\mu\text{g}/\text{m}^3$. In addition to the gravimetrically-determined fine mass concentrations, ambient air samples were drawn through a micro-orifice uniform deposit impactor (MOUDI; MSP Corporation, Minneapolis, MN) to determine the fine particle size distribution of the ambient aerosol. The MOUDI is a cascade impactor with micro-orifice nozzles that collect particles onto pre-weighed filters at a flow rate of 30 L/min for a known length of time. The weights (post-particle sampling) at each stage were used to determine the mass median particle diameter (MMAD) and geometric standard deviation (GSD).

Blood Analyses: Twenty-four hours following the last day of exposure, rats were euthanized with an overdose of sodium pentobarbital (65 mg ip, Anthony Products Company, Arcadia, CA). Blood was obtained by cardiac puncture. A one ml aliquot of whole blood was collected in a 1.5 ml EDTA-treated collection tube to prevent clotting. Total white blood cell counts (WBCC), differential profiles, and blood chemistry were assessed at the Tufts Veterinary Diagnostic Laboratory (Grafton, MA).

Bronchoalveolar Lavage: Bronchoalveolar lavage was performed through a tracheal incision using endotoxin-free Dulbecco's phosphate-buffered saline (PBS). Viability (> 95%) and total cell counts were determined by hemacytometer counts of small aliquots of the re-suspended BAL diluted in trypan blue solution. Cell type was determined from modified Wright-Giemsa-stained cytocentrifuge preparations, and 200 cells were counted per sample. Total BAL lactate dehydrogenase was measured within the acellular BAL supernatant from the first lavage as a marker of cytotoxicity.

Statistical Analyses: One-way analysis of variance (ANOVA) of means from blood and BAL parameters amongst the four experimental groups were performed and differences between groups were determined by Student-Newman-Keuls post hoc analysis. Differences were considered significant when $p < 0.05$.

Results

In the present study, animals were exposed to filtered air or CAPs for 6 hours/day for three consecutive days. Mean CAPs exposure levels were 70, 150, and 80 $\mu\text{g}/\text{m}^3$, on day 1, 2, and 3, respectively. The mass median diameter was 0.18 μm with a geometric standard deviation of 2.9 throughout the exposure.

Following exposure, animals were sacrificed, blood was taken by cardiac puncture, and bronchoalveolar lavage (BAL) was performed. Pulmonary inflammatory responses due both to CAPs exposure and the difference in age were observed. Figure 1A shows the mean BAL cell counts from the four treatment groups. Young animals exhibited significant increases in cell count following exposure to CAPs. In contrast, aged animals had no change in the total cell count. It was also observed that aged animals had significantly fewer pulmonary cells retrieved by bronchoalveolar lavage compared to younger animals.

Differences due to CAPs-exposure and age were also observed in the BAL differential cell profile. Both young and aged animals exhibited significant increases in pulmonary neutrophils following CAPs exposure (Figure 1B); young animals also exhibited significant increases in lymphocytes due to CAPs exposure. Aged animals had significantly fewer macrophages than younger animals regardless of exposure.

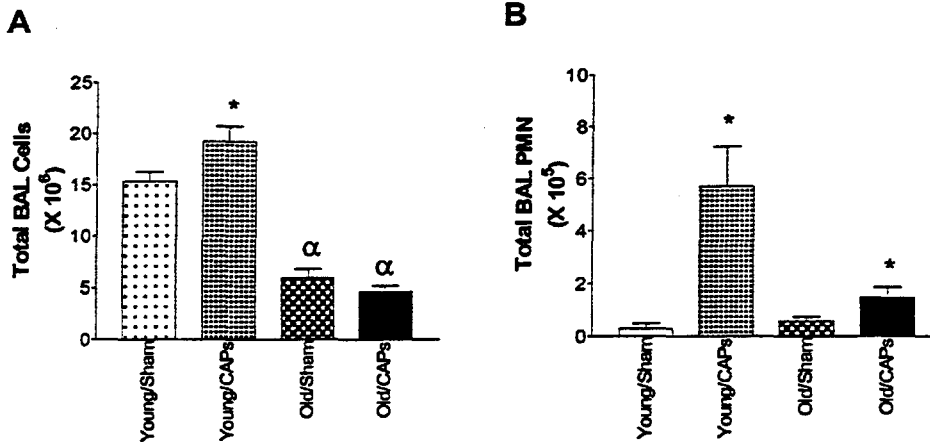


Figure 1A and B. Mean of A) total bronchoalveolar lavage (BAL) cell counts and B) polymorphonuclear leukocyte (PMN) cell counts following three days of filtered air- or CAPs-exposure in young and aged rats. Each value represents the mean \pm SE for each treatment group (6-10 animals per group). * = $p < 0.05$ versus CAPs; α = $p < 0.05$ versus age.

There was only one significant result due to CAPs exposure in any of the blood parameters assessed. Circulating eosinophils were increased in young and old animals following CAPs exposure. Total white blood cell (WBC) counts, monocytes, lymphocytes, neutrophils, and blood hemoglobin exhibited no CAPs-related changes. In contrast, age was associated with significant alterations in several parameters. Total WBC counts (Figure 2A), blood hemoglobin levels, and blood lymphocytes were all significantly lower in aged animals. Blood neutrophils were significantly increased in aged animals (Figure 2B).

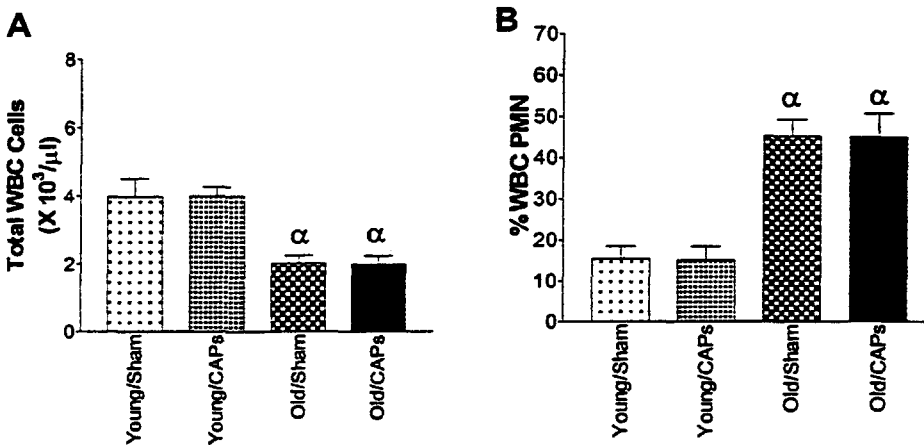


Figure 2A and B. Mean of A) peripheral blood white blood cell counts and B) the peripheral blood percentage of PMN following three days of filtered air- or CAPs-exposure in young and aged rats. Each value represents the mean \pm SE for each treatment group (6-10 animals per group). * = $p < 0.05$ versus CAPs; α = $p < 0.05$ versus age.

Discussion

The present study investigated the pulmonary and systemic effects of inhaled ambient urban air particulates in normal young and aged animals to find a link with increased morbidity and mortality observed in exposed human populations. Despite the large body of epidemiological evidence suggesting

an increased susceptibility to ambient particle exposure in elderly populations (Pope et al, 1995), the pathophysiological mechanism of these responses remains unknown.

The use of aged animals as a susceptible model to particle inhalation addresses an important population in the response to CAPs. As stated above, aged individuals exhibit higher morbidity and mortality following episodes of elevated ambient particle concentrations. Also, aged individuals generally have some degree of immunocompromise consistent with advancing age. Therefore, they exhibit greater incidence of pulmonary disease and respiratory infection (Zissel, 1999). The addition of inhaled particles may exacerbate these conditions leading to observed morbid and fatal responses.

The age of the animals used in the present study also represents a more appropriate model of advanced age. The previous study investigating age factors and concentrated ambient air particles employed animals that were six months old (Gordon et al, 1998). In the present study, seventeen month old rats were used; these rats were selected based on survival curves generated by Harlan Laboratories. Given that the potential lifespan of a Fisher rat can be over 3 years, seventeen months represents a better model of advanced age. However, the use even older rats might be the optimal model to define the role of age.

The decreased total cell numbers retrieved by bronchoalveolar lavage as well as the decreased numbers of white blood cells in aged animals suggest that these animals are experiencing immunocompromise. The lack of retrieval of pulmonary cells by BAL indicates that the lungs of these aged animals either have fewer pulmonary immune cells in their parenchyma, or that these cells are more adherent in the lung than in younger animals. Either way, the decreased cell numbers appear to be related to decreased pulmonary immunoresponsiveness. The decreased number of white blood cells provide evidence for the former: decreased pulmonary cells are retrieved because there are fewer marginating white blood cells due to age-related immunocompromise.

It is also appears that the observed decrease in immune response may have significant impact on cellular signaling pathways. Aged animals exhibit a significantly higher percentage of circulating neutrophils than their younger counterparts. It might therefore be expected that the acute inflammatory response in these animals would be more pronounced in these animals as has been previously observed in mice exposed to particles (Johnston et al, 1998). Although significant, the increase in BAL PMN in aged animals was small; this was especially true when compared to the large PMN influx observed in younger animals. This occurred despite the fact that aged animals had greater than 40% circulating neutrophils compared to 15% in young animals. Potential mechanisms for this difference include altered adhesion molecules, decreased chemokine signaling, and decreased ability of neutrophil deformation in aged animals.

This small pulmonary PMN influx does suggest that CAPs are a powerful stimulus upon inhalation. Previous work from our group has suggested that CAPs provided a significant stimulus on pulmonary function, even more so than the pre-existing chronic bronchitis in the test population (Clarke et al, 1999a). In the present work, it appears CAPs act as a very powerful stimulus able to elicit a significant response from an immunocompromised animal. Despite the low numbers of circulating white blood cells and pulmonary immune cells, CAPs inhalation induced significant PMN numbers to travel to the pulmonary region. Therefore, even if the signaling pathways necessary to generate this stimulus are impaired, as suggested above, CAPs provides a strong enough impetus to provoke some immune response.

This small pulmonary immune response and apparent general immunocompromise in the aged population provide a potential mechanism whereby pulmonary infection and disease would be

augmented in an elderly population. The young animals exhibit a significant increase in BAL cells and a large influx of PMN following inhalation of CAPs. This inflammatory response would generally be viewed as a positive result; the increased number of pulmonary immune cells allows for rapid and complete removal of inhaled matter as well as provides a surveillant response if infectious processes commenced. In contrast, the aged animals would not be able to respond as completely under the same conditions. Previous studies have clearly demonstrated immunosuppression due to inhalation of ambient particle surrogates (Zelikoff et al, 1994; Jakab et al, 1996). Also, inhalation of acid-coated carbon particles has been shown to exacerbate pulmonary infection (Clarke et al, 1999b). Therefore, inhalation of CAPs may predispose aged animals to increased incidence and severity of infection.

The significant inflammatory response of the younger animals suggest that strain specificity may be important in the response to inhaled particles. Previous work from our group had reported significant inflammation due to inhaled CAPs (Clarke et al, 1999a) in Sprague-Dawley rats. However, the exposure levels in that previous study averaged over 500 $\mu\text{g}/\text{m}^3$ over the three day exposure period. In the present study with Fisher rats, exposure levels averaged only 100 $\mu\text{g}/\text{m}^3$ over the three-days. Sprague-Dawley rats have not responded similarly at these modest CAPs levels (Clarke et al, 1999c). Therefore, Fisher rats may represent a more sensitive strain for the investigation of pathophysiological mechanisms caused by ambient particle inhalation.

In summary, the present work provided the first assessment of ambient particle effects in a model of advanced age. From the observed results, it does appear that age is a significant factor in the biological response to particles. Furthermore, these results suggest 1) young Fisher rats may represent a sensitive model for the examination of pulmonary inflammatory responses following CAPs exposure and 2) the lack of an inflammatory response in the aged rats, despite the presence of a higher percentage of circulating neutrophils, may reflect decreased sensitivity to inhaled particles and pathogens.

References

- Clarke, R.W., Catalano, P., Murthy, G.G., Koutrakis, P., Wolfson, M., Sioutas, C., and Godleski, J.J. 1999a. Pulmonary function and inflammatory response alterations following inhalation of concentrated urban air. *Inhal Tox* 11:101-120.
- Clarke, R.W., Hemenway, D.R., Frank, R., and Jakab, G.J. 1999b. Particle-bound sulfate: Aerosol conditions and alveolar macrophage phagocytic function. *Inhal Tox*, in press.
- Clarke, R.W., Rice, T., Reinisch, U., Catalano, P., Coull, B., Koutrakis, P., Krishna Murthy, G.G., Lovett, E., Paulauskis, J.D., and Godleski, J.J. 1999c. Dose- and composition-dependent pulmonary and hematological responses to inhaled concentrated ambient air particles (CAPs). Manuscript in preparation.
- Dockery, D.W., Pope, C.A., 3d, Xu, X., Spengler, J.D., Ware, J.H., Fay, M.E., Ferris, B.G., Jr, Speizer, F.E. 1993. An association between air pollution and mortality in six U.S. cities. *New Eng J Med* 329(24):1753-1759.
- Dockery, D.W. and Pope III, C.A. 1994. Acute respiratory effects of particulate air pollution. *Ann Rev Pub Health* 25:107-132.

Gordon T., Nadziejko C., Schlesinger R., Chen L.C. 1998. Pulmonary and cardiovascular effects of acute exposure to concentrated ambient particulate matter in rats. *Tox Lett* 96-7:285-288

Gyetko M.R., Toews G.B. 1993. Immunology of the aging lung. *Clin in Chest Med* 14(3):379-391.
Jakab, G.J., Clarke, R.W., Hemenway, D.R., Longphre, M.V., Kleeberger, S.R., Frank, R. 1996. Inhalation of acid coated carbon black particles impairs alveolar macrophage phagocytosis. *Tox Lett* 88(1-3), 243-248.

Johnston C.J., Finkelstein J.N., Gelein R., Oberdorster G. 1998. Pulmonary inflammatory responses and cytokine and antioxidant mRNA levels in the lungs of young and old C57bl/6 mice after exposure to teflon fumes. *Inhal Tox* 10(10):931-954.

Pope III, C.A., Dockery, D.W., Spengler, J.D., Raizenne, M.E., 1991. Respiratory health and PM10 pollution. A daily time series analysis. *Amer Rev of Respir Dis* 144(3 Pt 1):668-674.

Pope III, C.A., Dockery, D.W., Schwartz, J. 1995, Review of epidemiologic evidence of health effects of air pollution. *Inhal Tox* 7:1-18.

Saldiva, P.H.N., Pope III, C.A., Schwartz, J, Dockery, D.W., Lichtenfels, A.J., Salge, J.M., Barone, I., and Bohm, G.M. 1995. Air pollution and mortality in elderly people: A time-series study in Sao Paulo, Brazil. *Arch Environ Health* 50:159-163.

Schwartz, J. 1991. Particulate matter and daily mortality: A synthesis. *Pub Health Rev* 19:39-60.
Schwartz, J. and Dockery, D. 1992. Increased mortality in Philadelphia associated with daily air pollution concentrations. *Am Rev Resp Dis* 145:600-604.

Sioutas, C., Koutrakis, P., Burton, R.M. 1995. A technique to expose animals to concentrated fine ambient aerosols. *Environ Health Per* 103(2):172-177.

Zelikoff, J.T., Sisco, M.P., Yang, Z., Cohen, M.D., and Schlesinger, R.B. 1994. Immunotoxicity of sulfuric acid aerosol: Effects on pulmonary macrophage effector and functional activities critical for maintaining host resistance against infectious diseases. *Toxicology* 92:269-286.

Zissel G. Schlaak M. Muller-Quernheim J. 1999. Age-related decrease in accessory cell function of human alveolar macrophages. *J Invest Med* 47:51-56.

Corresponding Author

R.W. Clarke, Ph.D., Harvard School of Public Health, 665 Huntington Avenue, Boston, MA. 02115; Telephone: (617)-432-4966; Facsimile: (617)-432-0014; Internet: rwclarke@hsph.harvard.edu

**Endotoxin Priming Affects the Lung Response to Ultrafine Particles and Ozone
in Young and Old Rats**

Alison C.P. Elder¹, Robert Gelein¹, Jacob N. Finkelstein², Christopher Cox³, and Günter Oberdörster¹

Departments of Environmental Medicine¹, Pediatrics², and Biostatistics³

University of Rochester
575 Elmwood Ave., Box EHSC
Rochester, NY 14642

Correspondence may be sent to:

Alison Elder

Running title: Particle and ozone responses after endotoxin exposure

Suggested key words: lipopolysaccharide, endotoxin, ozone, ultrafine particles, age, species, reactive oxygen species, lung inflammation, rats, mice

Abstract

Epidemiological studies have demonstrated a correlation between low levels of ambient particles and morbidity, particularly in the elderly with existing cardiopulmonary disease. Such correlations have been challenged due to doubts as to whether particles act alone to cause these detrimental effects. We hypothesized that ambient carbonaceous ultrafine particles (part of the urban fine particle mode) and ozone (O_3) together would induce greater oxidative stress in the lung than when administered alone and that their effects would be amplified in the compromised, aging lung. We, therefore, exposed male F344 rats (10 wks, 20 months) to ultrafine carbon particles (count median diameter 25 nm, $100 \mu\text{g}/\text{m}^3$, equivalent to $50 \mu\text{g}/\text{m}^3$ inhaled by humans) and to O_3 (1 ppm) alone and in combination for 6 hrs. Low-dose endotoxin (LPS) priming by inhalation (70 endotoxin units estimated alveolar deposited dose) was used as a model of respiratory tract infection. Inflammatory parameters in bronchoalveolar lavage (BAL) fluid and oxidant release from BAL cells were assessed 24 hrs after exposure. A significant main effect of carbon, O_3 , and LPS on lung inflammation and a significant interaction between LPS and O_3 that resulted in lower inflammation was observed in young rats. In old rats, only LPS and O_3 had significant effects, but carbon and O_3 interacted and increased lung inflammation above the effect level for either component alone. Oxidant release by BAL cells generally corresponded with the PMN response; however, in young rats, the combination of LPS priming with carbon and O_3 exposure decreased oxidant release. In old rats, this combination increased oxidant release. These results are consistent with our hypothesis that urban ultrafine carbonaceous particles are involved in increased morbidity in sensitive populations. In addition, age and co-exposure with a high level of O_3 can significantly affect both lung inflammation and inflammatory cell activation such that the aged organism will experience increased oxidative stress in the lung. In both age groups, LPS enhanced the effects of particles and O_3 , thus allowing the observation of effects that would otherwise be masked.

Introduction

Epidemiological studies suggest that low mass levels of ambient particles are associated with morbidity and mortality in individuals with compromised cardiopulmonary systems (COPD, pneumonia, heart failure) (Peters *et al.*, 1997b; Schwartz *et al.*, 1999); however, the leap from statistical association to causality has been challenged by questions as to whether or not particles alone are responsible for decrements in human health. Ambient fine particles consist of both accumulation-mode (diameter = 0.1-1 μ m) and nucleation-mode (ultrafine; diameter <0.1 μ m) particles. Studies have shown that ultrafine particles are approximately 22,000 times greater in terms of number concentration as compared to accumulation-mode particles under normal conditions (Hughes *et al.*, 1998; Pekkanen *et al.*, 1997). Episodic higher concentrations have been recorded, though, increasing this difference in number concentration between the two modes by another factor of 10 (Brand *et al.*, 1992) and a mass concentration of ultrafine particles approaching 50 μ g/m³. Furthermore, theoretical models of particle deposition (ICRP, 1994) predict that ultrafine particles of about 20 nm have the greatest alveolar deposition compared to all other particle sizes.

Ozone (O₃) is a ubiquitous component of photochemical smog that induces free radical formation, lipid peroxidation, arachidonic acid release, alterations in epithelial permeability, epithelial proliferation, and the production and/or release of several cytokines, chemokines, and cell adhesion molecules (Bhalla *et al.*, 1992; Pendino *et al.*, 1994; Pryor *et al.*, 1995; Vincent and Adamson, 1995). Endotoxin (lipopolysaccharide, LPS) is a component of the gram-negative bacterial cell wall that is released during infection and such bacteria are commonly associated with the pathogenesis of pneumonia in COPD (Hamacher *et al.*, 1995; Klein and Cunha, 1997). LPS induces cytokine and chemokine expression and release (Johnston *et al.*, 1998; Ulich *et al.*, 1991a,b), increased respiratory burst activity of lavage inflammatory cells (Elder *et al.*, 1999), cell adhesion molecule expression (Albelda, 1991; Smith, 1990), and stress protein production (Carraway *et al.*, 1998) in the lung when inhaled or administered intratracheally.

During the normal aging process, several changes occur that can impact the lung's response to inhaled toxicants, including exaggerated response or injury following exposure to toxicants and alveolar antioxidant depletion. For example, an early study by Evans and colleagues (1977) showed that continuous exposure to an oxidant gas (NO₂) resulted in more epithelial damage and delayed tissue repair in old vs. young rats. Vincent and Adamson (1995) demonstrated that although young and old rats repair O₃-induced epithelial damage in a similar time frame, the proliferative response was higher in old rats. Our own studies revealed that lavage cells from old rats and mice have higher resting and activated respiratory burst activity than cells from young animals, suggesting greater lung oxidative stress in the old organism (Elder *et al.*, 1999). However, another group showed that lavage fluid and whole lung glutathione levels become depleted with age (Teramoto *et al.*, 1994); thus, older animals may not be able to appropriately respond to oxidant-induced lung injury.

We tested the hypothesis that ultrafine particles alone, based on their high number concentration in ambient air and the lung region in which they are most likely to deposit, would induce inflammation and oxidative stress in the lung. Since both ultrafine particles and O₃ are present in the environment, we also hypothesized that the particle effects would be enhanced by additional stress or injury caused by co-exposures with O₃. Furthermore, the effects of particles and O₃ may be exaggerated in the aged, compromised lung. LPS exposures were used to mimic the early phase of respiratory tract infection to investigate the impact of lung target cell priming on the response to particles and O₃.

Materials and Methods

Animals and General Study Design

Specific pathogen-free male Fischer 344 rats (8 wks or 20 mos of age) were housed in wire-bottom cages with free access to Purina rodent chow and water. Young rats were obtained from Harlan (Indianapolis, IN) and old rats (retired breeders) from the National Institute on Aging colony at Harlan. The animals were allowed to acclimate for at least one week prior to use in experimental protocols. Rats ($n = 3$ per

group) were exposed to all combinations of LPS, ultrafine particles, and O₃ and to each agent alone such that there were eight separate exposure groups for both the young and old animals.

Exposures to Endotoxin, Ultrafine Carbon Particles, and Ozone

Animals were exposed to LPS aerosols in a compartmentalized whole body chamber (31 L plastic tank). LPS from *P. aeruginosa* (Sigma Chemical Co., St. Louis, MO; lot 87F4009; 4 x 10⁶ endotoxin units (EU)/mg) was mixed with 4 ml sterile 0.9% saline and aerosolized using an Aerotech[®] II nebulizer (CIS-US, Inc., Bedford, MA). The aerosol concentration was monitored using a real-time aerosol sensor and its output was displayed on a chart recorder. The inhalation exposures lasted for about 12 mins, during which the animals were active. The estimated alveolar deposited dose of LPS (predicted from a deposition model that included particle size (MMAD=0.72 μm; GSD=1.61), body weight, and respiratory frequency (Schum and Yeh, 1980)) was determined to be 70 EU.

Ultrafine carbon particles (100 μg/m³, 6 hrs) were generated from two opposing ultrapure graphite electrodes *via* electric arc discharge in an argon-filled chamber (Palas Co., Germany). The generated particles typically had a count median diameter of 25 nm with a GSD of 1.6 (particle classifier; TSI, Inc., St. Paul, MN). Electrostatic charge was brought to Boltzman equilibrium by a ²¹⁰Po source. Available instrumentation monitored particle number and mass concentrations at regular intervals (condensation particle counter, TSI; TEOM, Rupprecht and Patashnik, Albany, NY). Diluting air was added with a small amount of O₂, monitored by a sensor in the chamber (Teledyne; Los Angeles, CA), to maintain normal pO₂. Animals were exposed in a compartmentalized, horizontal flow whole-body chamber (31L plastic tank).

Ozone (1.0 ppm) was generated by passing medical grade oxygen by a mercury arc lamp (Ultra-Violet Products, Inc.; San Gabriel, CA). It was directed into the compartmentalized exposure chamber by itself or after being mixed with ultrafine carbon particles; its concentration was measured at the breathing zone *via* UV absorption (Dasibi Environmental Corp., Glendale, CA). The ultrafine carbon and O₃ exposures began within 30 minutes after the LPS exposures; controls were unexposed.

Bronchoalveolar Lavage and Biochemical Parameters Measured in Lavage Fluid

Twenty-four hrs after LPS exposure, animals were killed with an overdose of sodium pentobarbital (IP, 50 mg/100 g BW). As detailed elsewhere (Elder et al., 1999), the lungs, trachea, and heart were removed *en bloc* and the lungs were lavaged with a fixed volume of sterile, pyrogen-free 0.9% saline (10 x 5 mls), separating the first 2 lavages for protein and enzymatic analyses. The cells were pooled from all fractions for viability determination (trypan blue exclusion), enumeration, differential analysis (Diff-Quik[®]; Baxter Scientific, Edison, NY), and chemiluminescence (an indicator of oxidant release; see below). Total protein concentration and lactate dehydrogenase (LDH) and β -glucuronidase activities were measured using commercially-available kits (Pierce Chemical Co., Rockford, IL; Sigma, St. Louis).

Chemiluminescence

Details of this assay are described elsewhere (Elder et al., 1999); reagents were purchased from Sigma (St. Louis). Briefly, in order to measure resting and activated respiratory burst activity, BAL cells were mixed with luminol (10^{-4} M) in Krebs's-Ringer-HEPES buffer with or without phorbol myristate acetate (PMA; 1.5×10^{-7} M) to activate the cells. Chemiluminescence was measured for 20 mins using a TD-20e luminometer (Turner Designs; Sunnyvale, CA) and a time-response curve for each sample was constructed to calculate the area under these curves (SigmaPlot, Jandel Scientific; San Rafael, CA) to quantitate respiratory burst activity.

Data Analyses

Results (%PMNs in lavage fluid; resting and activated respiratory burst activity) were analyzed for statistically significant main effects and interactions by three-way analysis of variance (ANOVA). Data were appropriately transformed if an analysis of residuals suggested deviations from the assumptions of normality and equal variance. The factors were the presence or absence of LPS, ultrafine carbon particles, and O₃. Effects were considered to be statistically significant when $p \leq 0.05$.

Results

The cellular and biochemical parameters assessed in this study are shown in Tables 1a (young rats) and 1b (old rats). In young rats, LPS, ultrafine carbon, and O₃ each had a significant impact on the degree of lung inflammation following exposure, as assessed by the percentage of PMNs in lavage fluid. Additionally, LPS and O₃ significantly interacted such that the combination of the two factors produced a greater response level than was expected for either factor alone (Table 2a). In old rats, LPS and O₃ had significant main effects on the PMN response; carbon interacted with O₃ as it did with LPS in young rats to enhance the inflammatory cell response (Table 2b).

The respiratory burst activity of PMA-stimulated BAL cells was different in young and old rats. Figures 1a, b, and c and 2a, b, and c show the percentage of PMNs in lavage fluid and the resting and PMA-stimulated respiratory burst activities of lavage cells from young and old rats, respectively. Respiratory burst activity followed quite closely the PMN response, as was expected (*i.e.* a fixed number of BAL cells is used in the assay, so the absolute number of PMNs can be determined from the percentage in BAL fluid). The exception to this was found in cells from young rats exposed to the combination of O₃ and ultrafine carbon particles with LPS priming: although this group had the highest percentage of BAL PMNs, the stimulated activity of reactive oxygen species (ROS) was at an intermediate level. This lower response, however, was not observed in cells from old rats. In general, the magnitude of the respiratory burst activity (resting and PMA-stimulated) of cells from old rats was higher than that of cells from young rats (compare ordinate labels in Fig. 1b,c with Fig. 2b,c). As was true for BAL neutrophils, LPS and O₃ significantly and independently affected the activated ROS activity by BAL cells; the impact of ultrafine carbon in young rats was marginally significant for this endpoint. Ozone significantly interacted with carbon in both young and old rats, but the direction of this effect is different in the two age groups. In young rats, O₃ also interacted with LPS to enhance response above what was expected for the two factors alone (Tables 2a,b).

For resting BAL cell ROS activity, all three factors again had a significant impact individually on this response in young rats; in old rats, O₃ and LPS had significant effects. In young rats, O₃ had the consistent effect of reducing basal ROS production by itself and when combined with either LPS or ultrafine carbon or both; in old rats, although carbon did not have a significant main effect, it interacted with both LPS and O₃ to produce higher-than-expected ROS activity (Tables 2a,b).

Conclusions

Low dose endotoxin priming, modeling a mild respiratory tract infection caused by gram-negative bacteria, can unmask the more subtle effects of common airborne pollutants, such as ultrafine carbonaceous particles and O₃, on neutrophilic inflammation and BAL cell oxidant generation. Our results show that combined exposures to ultrafine carbon particles and O₃ consistently produce the greatest inflammatory response in LPS-primed young and old rats. However, the result of this interaction in terms of inflammatory cell ROS release is different between age groups: although the magnitude of the PMN response is similar in both age groups, BAL cells from young rats had lower respiratory burst activity than expected (perhaps due to a suppressive interaction of particles and O₃), whereas BAL cells from old rats were stimulated and displayed ROS activity that was much higher than in young animals. These results suggest fundamental effects of ultrafine particles and O₃ on the function of BAL cells (*i.e.* respiratory burst activity) and that the control of ROS release or antioxidant defenses are different in young and old rats. They also indicate that sensitized old rats are at greater risk for oxidative lung damage caused by inhalation of low levels of ultrafine carbonaceous particles in combination with O₃ than young rats.

Old and young rats received the same estimated alveolar deposited dose of LPS (70 EU) through adjustment of the aerosolized exposure concentrations; thus, the magnitude of the PMN response in both age groups was 7-9% of the BAL cells. The exposure concentration of ultrafine carbon particles (100 µg/m³ for 6 hrs) corresponds to a number concentration of 13 x 10⁶ particles/cm³. Based on the ICRP model of particle deposition in humans (1994), the rat-specific particle deposition model of Yu and Xu

(1987), and the comparative lung surface area and ventilatory rate of humans vs. rats, one can derive that this mass concentration is equivalent in terms of lung dose to about $50 \mu\text{g}/\text{m}^3$ in humans. The particle concentration used in our studies was chosen to mimic the unusually high episodic hourly or daily excursions that have been recorded for ambient air (Brand *et al.*, 1992). As to O_3 , others have shown that there is no difference between young and old rats in terms of lung dosimetry (Vincent *et al.*, 1996). In our studies, although the effect of O_3 was consistently significant, the magnitude of response was not the same between the two age groups, suggesting different dose-response relationships. The concentration of O_3 used in these studies (1.0 ppm) is similar in terms of lung dose to an exposure to 0.25 ppm in an exercising human, as derived from the work of Hatch *et al.* (1994). The maximum one-hour O_3 concentration in many metropolitan areas is about 0.1 ppm, but concentrations 3 times higher have been recorded in some cities (EPA, 1996). Although an n of 3 per group in our study may seem relatively small, it should be pointed out that the multi-group design and three-way ANOVA with a total n of 24 gives it high statistical power. Nevertheless, further studies with lower concentrations of O_3 and larger group sizes should be performed to verify these results before they are applied to human risk assessment.

Since elderly individuals with COPD or pneumonia belong to the susceptible group for particle-induced morbidity and because gram-negative bacteria are common pathogens in these disease states, it is tempting to speculate that the priming effect of LPS described herein could occur in humans. A heightened responsiveness and increased oxidative stress could help to explain the susceptibility of the human populations defined in epidemiological studies. The underlying mechanisms of this susceptibility are not yet clear, however the link between the respiratory and cardiovascular systems cannot be ignored (Seaton *et al.*, 1995). A recent epidemiology study by Peters *et al.* (1997a) reported an association between total suspended particulate concentration in ambient air and increased plasma viscosity. This could be due to particle-induced oxidative stress in the lung and resulting systemic acute phase reactions and/or initiation of the blood coagulation cascade. Indeed, the results from our studies show that ultrafine carbonaceous particles, particularly in combination with O_3 , increased the respiratory burst activity of

alveolar inflammatory cells. LPS, which itself induces oxidative stress in the lungs, induces a procoagulant state (decreased circulating platelet number, thrombin generation, fibrinogen consumption) when administered systemically (Hara *et al.*, 1997; Jourdain *et al.*, 1997). It also decreases heart rate variability (Godin *et al.*, 1996), a condition associated with arrhythmia-induced mortality (Kleiger *et al.*, 1987). Ozone causes a decrease in heart rate in experimental animals (Watkinson *et al.*, 1995), but the effects of particles and O₃ on heart rate variability and blood coagulability *per se* need further investigation.

In summary, the results presented herein are consistent with the hypothesis that urban ultrafine carbonaceous particles are causally associated with lung inflammatory responses; however, other common pollutants (O₃) or existing stress in lung target cells (e.g., LPS priming, mimicking pneumonia or COPD) can significantly alter the response and function of pulmonary inflammatory cells.

Acknowledgments

The authors thank Nancy Corson, Kiem Nguyen, and Pamela Wade-Mercer for technical assistance. This work was supported by HEI contract #95-11-3, NIEHS Environmental Health Sciences Center grant (P30 ESO1247), NIH grant RO1 ESO4872, and an NIEHS training grant (ESO527873; A.C.P. Elder).

Figure Legends

Figure 1. Percentage of PMNs in bronchoalveolar lavage fluid (top) and respiratory burst activity (PMA-stimulated, middle; resting, bottom) of lavage cells from young rats exposed to combinations of carbon and ozone with LPS priming. Data are presented as means \pm SE; $n = 3$ rats per group.

Figure 2. Percentage of PMNs in bronchoalveolar lavage fluid (top) and respiratory burst activity (PMA-stimulated, middle; resting, bottom) of lavage cells from old rats exposed to combinations of carbon and ozone with LPS priming. Data are presented as means \pm SE; $n = 3$ rats per group.

Figure 1.

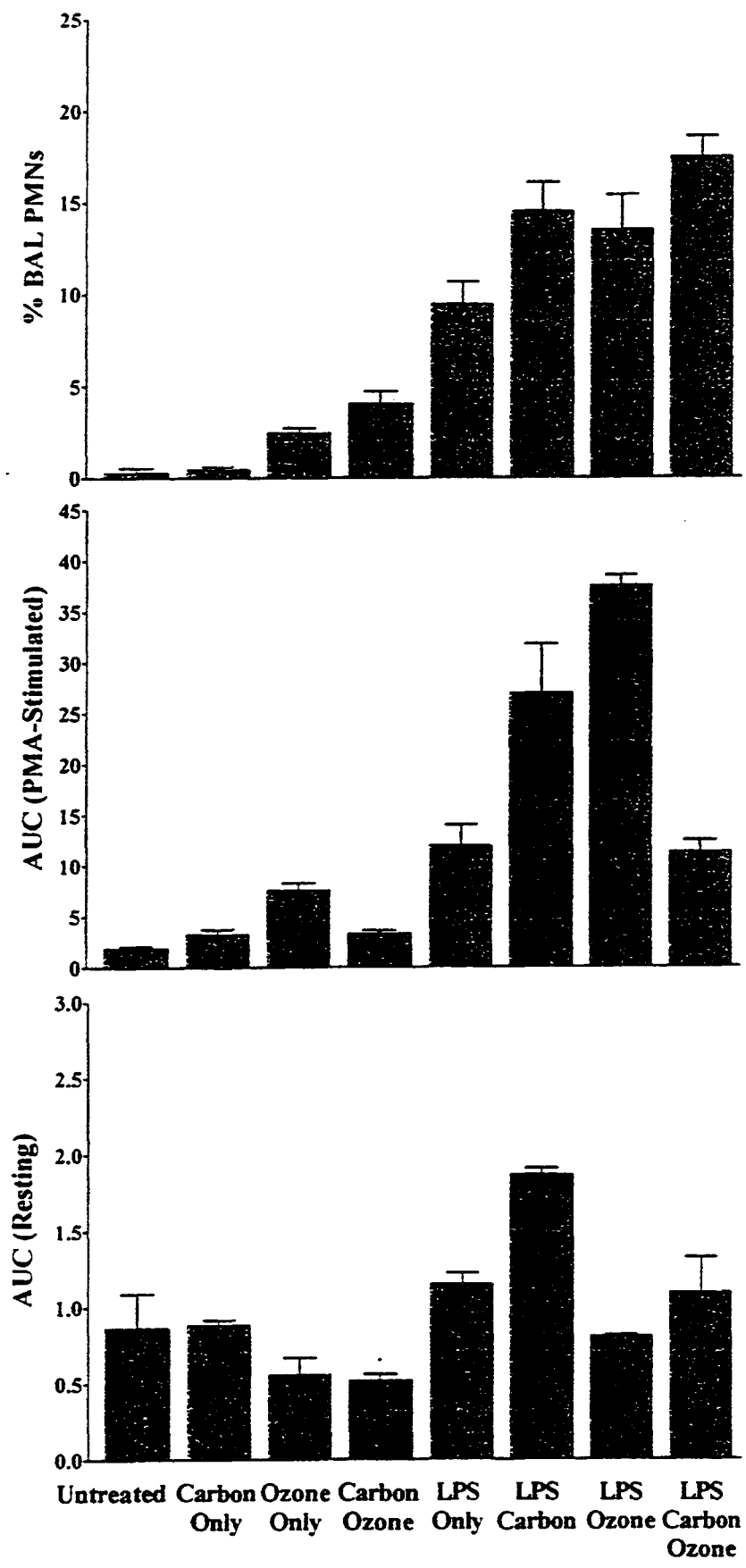


Figure 2.

